NTNU – Trondheim
Norwegian University of
Science and Technology

Design of heat recovery system in an aluminium cast house

Design av varmegjenvinningssystem i et
aluminium smelteverk

Daniel Albert

Master of Science in Engineering and ICT
Submission date: September 2012
Supervisor: Trygve Magne Eikevik, EPT

Norwegian University of Science and Technology
Department of Energy and Process Engineering

NTNU
Norwegian University of
Science and Technology

SINTEF

ESaK
EUROPÄISCHE
STUDIENAKADEMIE
KÄLTE-KLIMA-LÜFTUNG

Diploma Thesis

„Design of heat recovery systems in an aluminium cast house“

approved thesis in partial fulfilment of the requirements for the degree of
„Diplom-Ingenieur (BA) Kältesystemtechnik”
(Diploma-Engineer (BA) Refrigeration Technology)
at the European Academy
of Refrigeration and Air Conditioning
by

Daniel Albert
Matr.-No. 0913255701

Begin:	Mo. May 28th, 2012
End:	Fr. August 24th, 2012
Practical-partner:	SINTEF Energy Research Kolbjørn Hejes vei 1 A NO - 7456 Trondheim
Supervisor:	Dr.-Ing. Armin Hafner and M.Sc. Tom Ståle Nordtvedt SINTEF Energy Research
	Prof. Dr.-Ing. Dominik Cibis and Dr.-Ing. Rainer Jakobs European Academy of Refrigeration and Air Conditioning (ESaK)

Diploma Thesis for

Mr. Daniel Albert

Matr.-No. 0913255701

ESaK
EUROPÄISCHE
STUDIENAKADEMIE
KÄLTE-KLIMA-LÜFTUNG

Topic:

„Design of heat recovery system in an aluminium cast house “

The industry has a long tradition of self-improvement with respect to energy consumption. Transition from Søderberg technology to Pre-bake technology is an example of recent technological improvements that reduce the energy footprint. Moreover, recycling of Aluminium provides an additional advantage, as aluminium is energy packed in solid form. Most of the original energy input can be recovered: recycling and remelting requires only 5 % of the energy required for primary metal, saving thus 95 % relative to primary metal. Solid aluminium may be considered an everlasting "energy bank", where we only pay 5 % every time we borrow aluminium (energy). New technology has made it easier to control and optimize aluminium cast house production both in the primary and recycling industry. With transparent regulations and environmentally conscious and well-educated workers progress should be rapid in conserving energy and metal.

An important task is to determine the heat losses, i.e. recovery potential over the complete process line of liquid metal handling, scrap, hardeners, furnace tending, dross handling, casting, pit stripping and sawing. There will be a close cooperation with Norsk Hydro Sunndalsøra and several visits and measurement campaigns should be performed.

Main focus will be to evaluate various heat recovery solutions like ORC's and thereby determine the energy reduction/recovery potential at the end of the project over the complete process line. Most of the fluid flows are in a temperature range between +40 °C and +150 °C.

The following tasks are to be considered:

1. Literature review of the aluminium cast house energy flow, fluid properties and temperature levels
2. Overview of heat losses over the complete process line and propose possible heat recovery solution, either to enhance the process (internal use of heat for pre-heating) or power production (ORC)
3. Calculation of annual energy saving potential of the various recovery systems
4. Prepare a draft scientific paper from the results of the thesis
5. Make proposals for further work

All supervisors are to be contacted at regular intervals to report about the work’s current progress.

Begin:	Mo. May 28, 2012
End:	Fr. August 24, 2012
Restriction Note:	**no**
Supervisors:	**Tom Ståle Nordtvedt and Armin Hafner (SINTEF Energy Research)**
	Dr.-Ing. Rainer M. Jakobs (ESaK)

Prof. Dr.-Ing. Dominik Cibis
Head of ESaK

NTNU
Det skapende universitet

MASTERKONTRAKT
- uttak av masteroppgave

1. Studentens personalia

Etternavn, fornavn **Albert, Daniel**	Fødselsdato **18. feb 1989**
E-post **daniealb@stud.ntnu.no**	Telefon **+4917660835541**

2. Studieopplysninger

Fakultet **Fakultet for Ingeniørvitenskap og teknologi**	
Institutt **Institutt for energi- og prosessteknikk**	
Studieprogram **Master i ingeniørvitenskap og IKT**	Studieretning **Energi- og prosessteknikk**

3. Masteroppgave

Oppstartsdato **28. mai 2012**	Innleveringsfrist **15. okt 2012**
Oppgavens (foreløpige) tittel **Design of heat recovery system in an aluminium cast house** **Design av varmegjenvinningssystem i et aluminium smelteverk**	
Oppgavetekst/Problembeskrivelse Background and objective The industry has a long tradition of self-improvement with respect to energy consumption. Transition from Søderberg technology to Pre-bake technology is an example of recent technological improvements that reduce the energy footprint. Moreover, recycling of Aluminium provides an additional advantage, as aluminium is energy packed in solid form. Most of the original energy input can be recovered: recycling and remelting requires only 5% of the energy required for primary metal, saving thus 95% relative to primary metal. Solid aluminium may be considered an everlasting "energy bank", where we only pay 5% every time we borrow aluminium (energy). New technology has made it easier to control and optimize aluminium cast house production both in the primary and recycling industry. With transparent regulations and environmentally conscious and well-educated workers progress should be rapid in conserving energy and metal. An important task is to determine the heat losses, i.e. recovery potential over the complete process line of liquid metal handling, scrap, hardeners, furnace tending, dross handling, casting, pit stripping, sawing. There will be a close coop...	
Hovedveileder ved institutt **Professor Trygve Magne Eikevik**	Medveileder(e) ved institutt
Merknader	

4. Underskrift

Student: Jeg erklærer herved at jeg har satt meg inn i gjeldende bestemmelser for mastergradsstudiet og at jeg oppfyller kravene for adgang til å påbegynne oppgaven, herunder eventuelle praksiskrav.

Partene er gjort kjent med avtalens vilkår, samt kapitlene i studiehåndboken om generelle regler og aktuell studieplan for masterstudiet.

Trondheim, May 29th 2012
Sted og dato

Student

Hovedveileder

Originalen lagres i NTNUs elektroniske arkiv. Kopi av avtalen sendes til instituttet og studenten.

STATEMENT OF AUTHORSHIP

I hereby certify that this diploma thesis has been composed by myself, and describes my own work, unless otherwise acknowledged in the text. All references and verbatim extracts have been quoted, and all sources of information have been specifically acknowledged. This diploma thesis has not been accepted in any previous application for a degree.

Trondheim, August 24th 2012

_____

Daniel Albert

ACKNOWLEDGEMENT

At first, I would like to express my gratitude to Dr.-Ing. Armin Hafner. He gave me the opportunity to write my diploma thesis at SINTEF-Energy Research in Trondheim.
Furthermore, I would like to thank Tom Ståle Nordtvedt for the encouraged and serene team work, as well as the confidence that has been placed in me in the CastAl project.
Similarly, I would like to thank Dr. Yves Ladam for his essential support, guidance and advice during my diploma thesis.
Further thanks go to Dr.-Ing. Rainer Jakobs, who was willing to supervise me on the part of the European Academy for Refrigeration and Air Conditioning (ESaK).
Cordial thanks to the BFS/ESaK-Foundation for their financial support during my stay in Norway.
In addition, I would like to thank my BASF colleagues, especially Thomas Köhler, Michael Heeger and Heinrich Ochs, for their benevolently and fruitful team work during my study.

Finally, but ranked first, I would like to thank my family, especially my mother Birgit Albert, sister Sina Albert and uncle Dieter Gramsch, who have marked the path of my own life and to whom I owe a deep debt of gratitude.

SUMMARY

In this diploma thesis, the possibilities to enhance the process production and energy efficiency as well as the energy recovery potential of PFA 2 at Hydro-Sunndalsøra have been determined.

To identify the potentials for energy recovery, it has been conducted energy balances. The results from the balances give an overview of the waste heat sources and their total energy content, together with the temperatures at which they are available. The total energy in the waste heat sources for PFA 2 was found to be 17.8 GWh/year. The largest waste heat sources were localised in connection to the cooling agent of the casting ingot machine. Here disappears 12.32 GWh/year through cooling water within a temperature range of 10 to 30°C as well as convection and radiation to surrounding. The cooling water section one was determined as the most promising heat recovery potential with 7.47 GWh/year. Furthermore the initialisation of liquid aluminium alloy was revealed as a waste heat source with 5.48 GWh/year. Here disappears 3.34 GWh/year through the flue gas of the furnace within a temperature range of 288 to 1,100°C and creates the most promising heat recovery potential at the furnace.

The energy saving potential is divided into three groups: energy saving by existing equipment, optimising of equipment and waste heat recovery. Here energy saving by existing equipment reveals 26.4 MWh/year for an improved control quality of the melt temperature. The greatest potential for energy saving by optimisation of the equipment was found to be 1.98 GWh/year for the implementation of regenerative burner. Furthermore effects an installation of a furnace pressure control system 689.14 MWh/year less energy consumption due to the avoided false air. The greatest energy saving potential for waste heat recovery was estimated to 1.65 GWh/year for the preheating of charged metals to 300°C, instead of 20°C. The preheating also leads to improved safety, because of the elimination of moist metal in the furnaces, and increases the process production, as a consequence of larger melt capacity. Furthermore, heat to power solutions revealed the use of favourable electricity production by the generation of waste heat. Here the greatest generation potential was found to be in the flue gas from the furnace. A common Rankine cycle, with a direct heat recovery design and water as working fluid, was estimated with a recovery potential of 1.1 GWh/year. With the use of an organic Rankine cycle the potential can be recovered to 489.8 MWh/year for an indirect heat recovery design and pentane as working fluid. There are still some challenges associated with flue gas heat exchangers (dust) and operation of such power generation plants at alternating heat loads, but the technology is under rapid development. The waste heat generation potential for the casting ingot machine was determined with 411.3 MWh/year for an ideal organic Rankine cycle heat recovery design, within a temperature range of 58 to 90°C and R 134a as working fluid. An alternative ideal organic flash cycle layout revealed 253.4 MWh/year ($\eta_{expander} = 0.6$) respectively 416.5 MWh/year ($\eta_{expander} = 0.6$), within a temperature range of 36 to 90°C and butane as working fluid. These considerations have lower efficiencies compared to the furnace layouts caused by the low application temperatures ($T_{Boiler} < 90°C$).

TABLE OF CONTENT

LIST OF FIGURES

LIST OF TABLES

LIST OF ABBREVIATIONS

ENOVA	Norwegian National Energy Agency owned by the Royal Norwegian Ministry of Petroleum and Energy. Enova SF, Professor Brochsgt. 2, NO-7030 Trondheim Access on July 12th, 2012: http://www.enova.no/about-enova/259/0
CastAl	Project name, consortium of the project participants Hydro, SAPA, NTNU and SINTEF
Hydro	Norwegian aluminium and renewable energy company Norsk Hydro ASA, Drammensveien 260, NO-0283 Oslo Access on July 12th, 2012: http://www.hydro.com/
SAPA	Swedish aluminium profile, building system and heat transfer solution company SAPA AB, Humlegårdsgatan 17, SE-11485 Stockholm Access on July 12th, 2012: http://www.sapagroup.com/
NTNU	Norges Teknisk-Naturvitenskapelige Universitet (Norwegian University of Science and Technology) NTNU, O. S. Bragstads plass 3, NO-7491 Trondheim Access on July 12th, 2012: http://www.ntnu.edu/
SINTEF	Stiftelsen for Industriell og Teknisk Forskning (Foundation for Scientific and Industrial Research), Scandinavian research organisation SINTEF Energy Research, Kolbjørn Hejes vei 1 A, NO - 7456 Trondheim Access on July 12th, 2012: http://www.sintef.no/home/
PFA 2	Production Line 2, Foundry Alloy Cast House, Hydro, Sunndalsøra
OAE	Other Alloy Elements
OFC	Organic Flash Cycle
ORC	Organic Rankine Cycle
IPN	Innovation Project for the Industrial Sector
ODP	Ozone Depletion Potential
GWP	Global Warming Potential
ALT	Atmospheric Life Time
CIM	Casting Ingot Machine
ORMAT	Company name of Ormat Technologies Inc., Reno, Nevada, USA

NOMENCLATURE

μ	-	Friction factor
m	kg	Mass
$\dot{m}$	kg/s	Mass flow
c_{p}	kJ/(kgK)	Isobaric heat capacity
c	kJ/(kgK)	Heat capacity
T	°C	Temperature
α	W/(m²K)	Heat convective coefficient
L	m³	Air volume
H	kJ	Enthalpy
h	kJ/kg	Specific enthalpy
$\dot{Q}$	W	Heat power
Q	kJ	Heat
q	kJ/kg	Specific heat
p	Pa	Pressure
S	kJ/K	Entropy
δ	-	Differential
x	kg/kg	Vapour content
η	-	Efficiency
V	m³	Volume
$\dot{V}$	m³/h	Volume flow
v	m/s	Velocity
ρ	kg/m³	Density
λ	-	Excess air ratio
R	m³	Combustion gas
ϕ	(m/s)/ (m/s)	Ratio of exhaust flow rate
ψ	Pa/Pa	Ratio of pressure
A	m²	Area
ε	-	Emissivity
σ	W/(m²K)	Boltzman constant
P	W	Power
t	s	Time
κ	-	Adiabatic exponent
W	kJ	Work
w	kJ/kg	Specific work
f	-	Factor
β	(kg/m³)/(kg/m³)	Ratio of densities

1. Introduction

1.1. Background

The Norwegian industry´s potential to reduce energy consumption was investigated by ENOVA in 2009. This study was initiated as a result of an increased awareness for conserving resources and more effective energy use. It is noted that the aluminium industry was the largest energy consumer with a consumption of 22 TWh a year in 2007 [ENOVA 09]. Hence production of aluminium requires vast investment of capital and high operating costs due to the high energy consumption. It is important for the industry to use not more energy than required, to reharvest energy by reusing, recycling and remelting. This will obviously make the industry sector more sustainable, but it also gives the aluminium industry an economic advantage, as energy expenses are a determining factor in the cost price. In the primary aluminium industry up to 2 % of these previous noted 22 TWh (440 GWh per year) are used in cast houses and a considerable part can be saved by technology and operation improvements.
The CastAl project as a consortium between Hydro, SAPA, NTNU and SINTEF, where this diploma thesis is placed in, therefore aims to reduce energy consumption in aluminium cast houses, both primary and re-melt. This will be achieved by consuming less energy per ton produced aluminium than the benchmark 500 kWh/ton [Hydro 12.1]. CastAl in this application seeks to overcome the barriers for energy improvements in the primary and recycling by development of technology, increasing consciousness and knowledge of energy consumption. The CastAl project is an IPN project financed by the research council of Norway.
However, this disquisition will focus on quantifying heat losses within the casting process of alloying ingots as an initial step in the CastAl project. It translates these to operational optimisation, detect useful heat recovery technology and obtain areas for further research.

1.2. Objective and Execution

At present many cast houses do not calculate an energy balance of their production. This is also the current state at PFA 2. Prediction of the energy needed from the burners to bring a full charge to a targeted temperature is used. This is done by accounting for heat loss (generally from the whole furnace) and using a kind of system efficiency, typically estimated of heat loss and the efficiency to be around 50 % [Hydro 12.1]. Recent studies at NTNU did also neither quantify or at most assumed like [Tabuk 08] the heat in the exhaust gas nor the heat exchange from the cooling water in the cast house. This is caused by the focus of the aluminium industry, which primary consider at first the hugest cost-usage effect like as at the aluminium electrolysis [Ladam 11]. This is now beginning to change and energy considerations are extending in further segments of the aluminium value chain, caused by ecological image and prospective cost challenges.
For a total energy balance of the considered production line, heat loss in the furnace, launder, cooling water and dross processing is studied and partly verified by measurements. The temperature in the flue gas varies between 280 and 1100°C. The volume rate varies between 50 and 7500

m^3/h. The flow rate of cooling water used in the cast house is 25 m^3/h for water section 2, and 65 m^3/h for water section 1, within a temperature range of 10°C up to 35°C for each section. To be most energy efficient, the complete process line of liquid metal handling, scrap, dross handling and casting must be fully integrated, which is the aim of this study.
Increased energy efficiency at Foundry Alloy Cast House will give Hydro both financial savings and strengthen their image as an environmentally conscious company.
The resulting objective of this diploma thesis is thereby an energy mapping and audit of PFA 2 in the Foundry Alloy Cast House at Sunndalsøra, Hydro ASA. This means determining and depicting possible solutions for decreased energy consumption in this production line. The result, after an evaluation of various heat recovery solutions, leads to a proposal of various heat recovery systems to enhance the process efficiency and presents a calculation of an annual energy saving potential.

1.3. Structure of Thesis

The **first** chapter gives an introduction of the scope of work and forms background knowledge for a better understanding of this disquisition. The **second** chapter provides a description of PFA 2 and gives an insight of existing plant, understanding of dimensions and process sequences. The **third** chapter aims the determination and depiction of mapped energies through an energy balance. Simplified theoretical aspects for setting an energy balance are described for the furnace and casting ingot machine. The **fourth** chapter concerns itself with improved energy efficiency and links the results from chapter 3 with recommendations to enhance the efficiency. A calculation of the determined most promising heat recovery solutions indicates annual energy saving potentials. The **fifth** and last chapter proposes and indicates approaches for further work.

The literature review is linked as comparable reference information in each subchapter and thereby leads to comprehensible statements.

2. Foundry Alloy Cast House

Before aluminium alloys can be used for extrusion, rolling or subsequently for other forming operations, they are usually cast into ingots of suitable size and shape [Wang 09], which is carried out at the foundry alloy cast house in Sunndalsøra. Small quantities of other metals can be added to the liquid aluminium to produce foundry alloys of different durability and tensile strengths [Hydro 12.2]. Typically produced alloys are used for producing castings or fabricating wrought products, e.g. in the automobile industry or heat exchanger as illustrated in *figure 2.1*. A value chain in *figure 2.2* illustrates an overview of an aluminium life cycle.

The aluminium used as a raw material for casting operations, is purchased and tapped from nearby pots and transported to the foundry alloy casting plants in a molten state. Usually, however, purchased aluminium ingots are charged together with alloying elements into melting furnaces at the casting plant. Several types of furnaces can be used, but reverberatory furnaces are the most common [BCS 08] and these are implemented as existing heat supply technology at the foundry alloy cast house in Sunndalsøra.

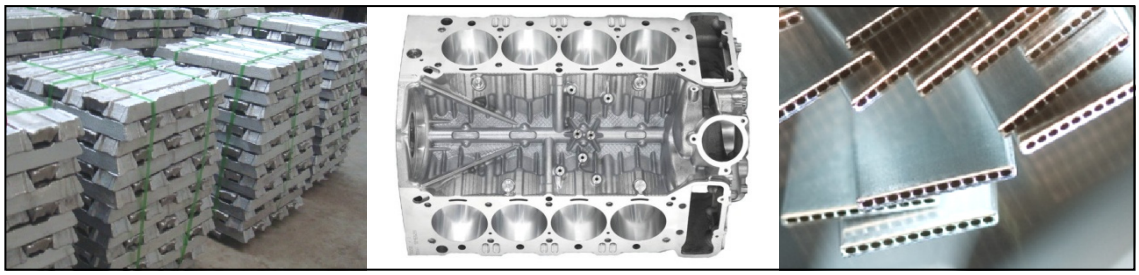

Figure 2.1: Typical bundle and ingot billet as a product of foundry alloy cast house at Sunndalsøra (left) and products like a motor block (mid) [XTC 06] or extruded heat exchanger elements (right) [Meltech 11].

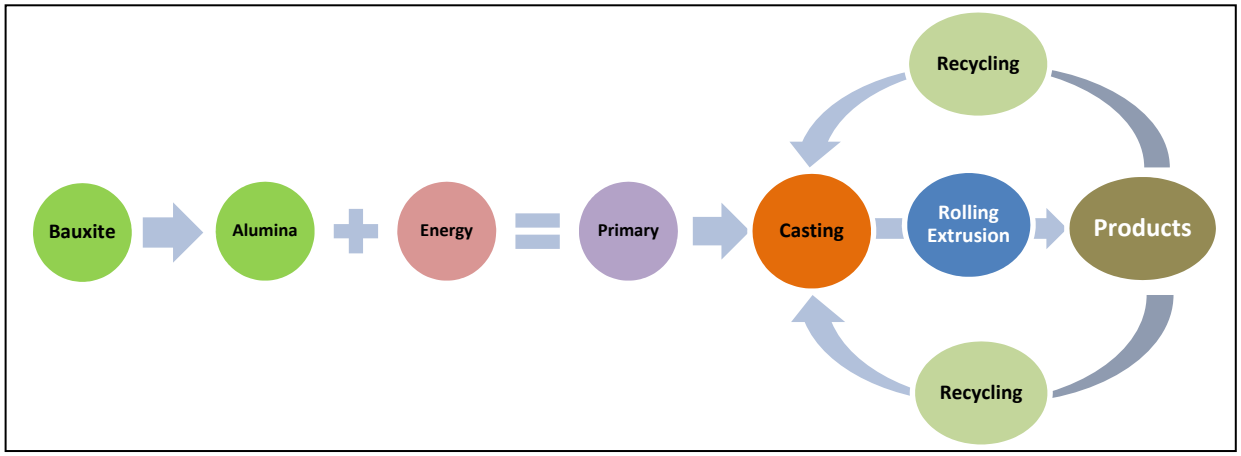

Figure 2.2: Value chain of aluminium at a foundry alloy plant. Illustration of casting as a connector between raw material and finished products, bypassed through the recycling chain [Hydro 12.2].

2.1. Construction of Process Line PFA 2

The process line PFA 2, which has to be considered (see *figure 2.3*), consists mainly of two furnaces called “Ovn 9 and 10” (furnace 9 framed with red dashed line), a launder system (B to C), filter system (between B and C), casting ingot machine (C to D), two cooling sections (D and E) and one attached packing station (F) for finishing casted ingots.

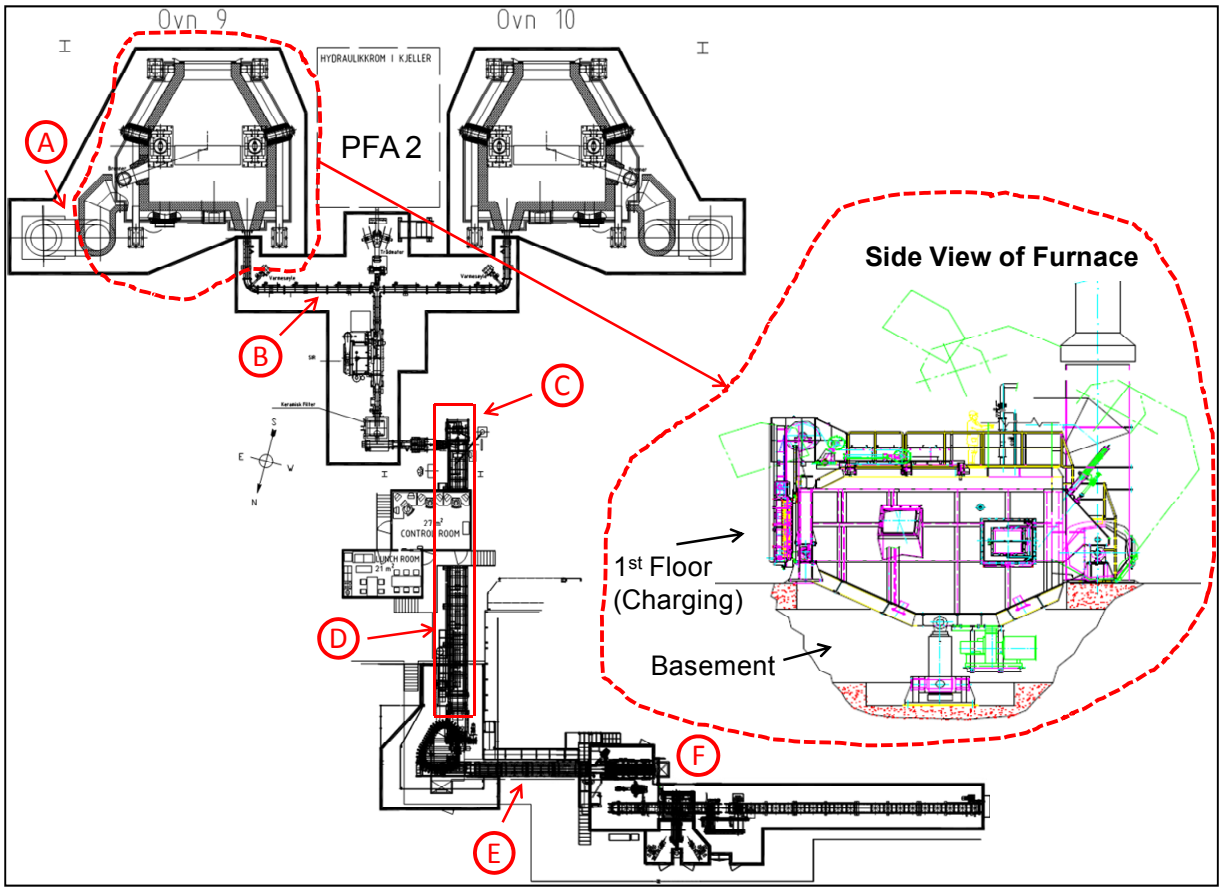

Figure 2.3: Total view of PFA 2. On top are both furnaces (furnace 9 red dashes framed) illustrated which are connected by launder (B) with casting ingot machine (C to D). (D) and (E) indicate cooling section one and two. (F) indicates the packing and finishing section. (A) indicates the location of flue flow rate and temperature measurement [Hydro 08.1], [Hydro 08.2], [Maerz 06].

2.1.1. Furnace

The reverberatory furnaces are fuelled by natural gas. Combustion air serves as oxidizer and is sucked into a ventilating system in the basement under the furnace and streams into the furnace chamber while the burner is running. Also furnace types fuelled by natural gas and pure oxygen are known and used for casting procedures [Memo 11]. *Figure 2.4* illustrates useful parameters for getting to know the operation behaviour of the considered furnace 9. The existing furnaces are alternately charged, caused by the needed amount of liquid alloy for the attached casting ingot machine. This means to two furnaces operate in batch to supply the continuous casting ingot machine. PFA 2 therefore operates at an alternating modus. This means that after e.g. furnace 9 is discharged and tilted to the maximum angle (approximately 31° in *figure 2.4* and side view

furnace, green line, *figure 2.3*), the second furnace 10 is automatically tilt up and the cast session continuous. This is essential for a continuous casting procedure like at PFA 2. Every session starts with charging the furnace chamber by loader, with held alloying billets and silicon. This is indicated in *figure 2.4* by the opened main door and inexistent gas flow. Temperatures cool down and indicate a heat discharge in the furnace. After a while of holding the furnace at stand-by, caused by the frequented operating and requested energy saving, preheating by burner begins. The gas flow reaches now a maximum and temperatures rise. Charged elements begin to change phase from solid to liquid. If the furnace roof temperature reaches a typically practical defined limit, liquid aluminium from pot rooms is tapped through small ports. During this procedure the burner is still running but temperatures decrease. A mixing procedure and magnetic stirring ensure a good homogenisation of molten alloy composition after this procedure. The temperatures decrease furthermore until a feasible casting temperature is reached. Subsequently, the liquid aluminium alloy is held as long as needed, while the other furnace is going to discharge. Depending on the logged temperatures the burner is switched on and off during this time. If the other furnace is discharged and going to tilt down, the opposite furnace tilts up and serves the alloy for a continuous casting procedure. This is indicated by the successive increasing angle in *figure 2.4*. These molten liquid aluminium alloy streams from the tilting furnace through the launder (B) into the moulds of the casting ingot machine (C). It should be noted that the heat transfer from burners to the charge is reached by three main heat transfer mechanisms: Convection, Radiation (indirect through walls) and flame radiation (direct radiation). The mechanism that is highly important during the initial stages of the melting cycle is the heat transfer by convection [Migchielsen 05]. Another important indication takes place in *figure 2.5*. This figure indicates detailed pressure behaviour in the furnace chamber during the whole casting cycle. Therefore it is a necessary explanation for the following influences by the stack effect, which is caused by a density difference between furnace atmosphere and chimney outlet atmosphere, at the energy balance model. The maximum pressure is logged at +23 Pa compared to atmospheric reference pressure. This positive peak is reached while the burner runs at maximum power (100%) in the preheating phase, indicated by the gas flow in *figure 2.5*. This affects an escape of combustion gas to the surrounding atmosphere. In the opposite direction the minimum negative pressure peak is reached several times shortly after the burner is shut down and is logged at -50 Pa. This physical condition thus effects a sucking of atmospheric air into the furnace. This is confirmed by the pressure trend after these negative peaks (see holding session while burner is tilt up in *figure 2.5*), which shows a positive gradient. This positive gradient is an indication of pressure compensation by leaking ports anywhere at the furnace. These pressure values are common for such types of furnaces [Migchielsen 09]. After an evaluation an arising arithmetic averaged relative pressure for the total process cycle results with -26 Pa and thereby indicates that the furnace runs at a negative pressure most of the time. An ideal pressure of ±0 Pa is stated at [Migchielsen 09]. But it should be noted that this aimed target is just to solve with an expensive controlling system and therefore a slightly positive pressure is tolerated. This slightly positive pressure avoids an undesired heat discharge by sucked in atmosphere air, for the whole process time. This subject takes place at the furnace energy balance.

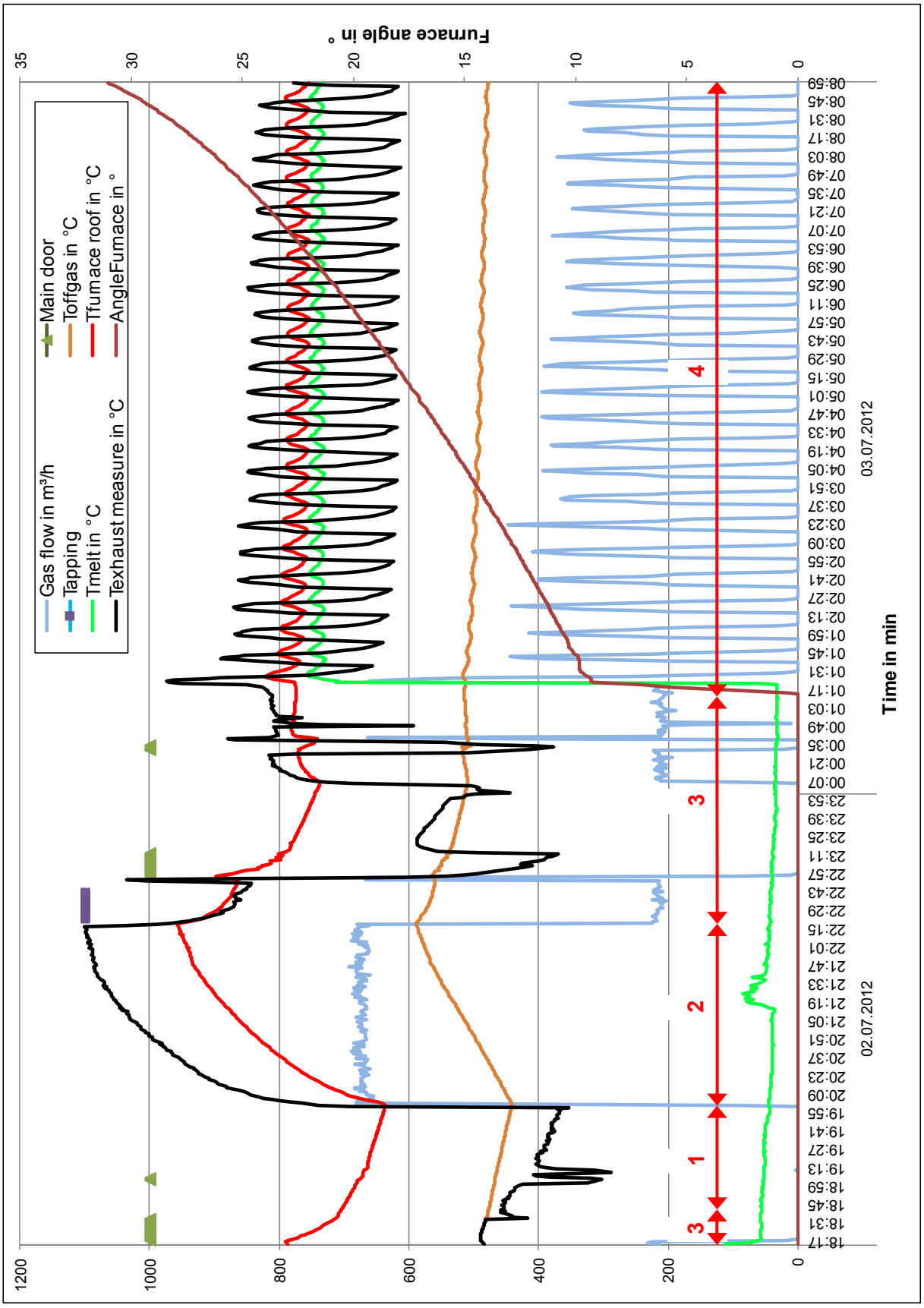

Figure 2.4: Logged process parameter for a total charging (1), melting (2), holding (3) and casting (4) procedure at furnace 9, Charge 67801.

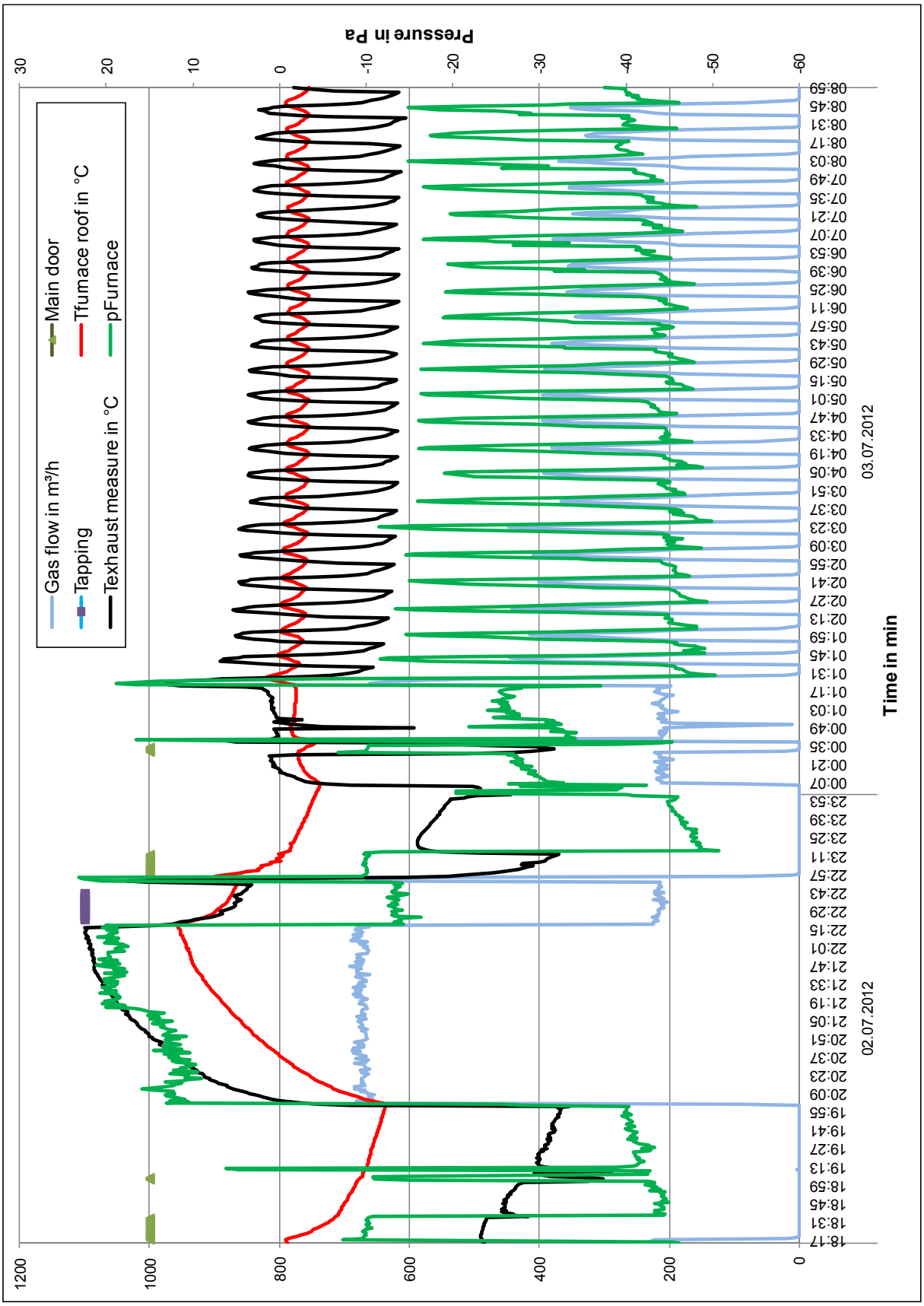

Figure 2.5: Additional logged pressure data for a complete process cycle at furnace 9, Charge 67801.

2.1.2. Casting Ingot Machine

After charging, melting and holding in the furnace the composited alloy supplies the casting ingot machine. This machine is an oversized horizontal chain hoist (*figure 2.6*) with moulds and transports the filled in liquid alloy continuously above a previously opened water cooling section, *figure 2.3* (D). During this cycled transport procedure cooling water absorbs heat from the aluminium alloy. Heat is also emitted to the atmosphere by the surface of aluminium. The enclosed air ventilating system (D) and *figure 2.6* additionally leads to heat dissipation. This is delberated in this process section and after a dwell in the mould the alloy has changed phase and is solid. After a converting section between (D) and (E), at the end of the casting ingot machine, the casted ingots fall out of the mould and are becoming transported to another second water cooling section (E). An automated packing and finishing station completes the process line (F).

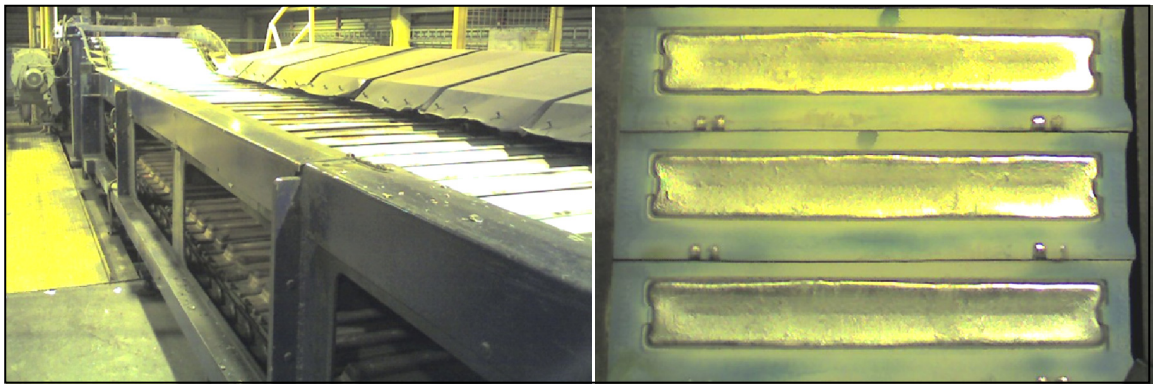

Figure 2.6: Side view of casting ingot machine (left) and top view of filled casting moulds (right).

2.2. Conclusion

A description of PFA 2 provides an insight of the existing plant and therefore gives an understanding of the dimensions and process sequences. A short constructive and operational description of both most important process sectors at PFA 2, regarding energy intensity and heat recovery potential, the furnace and casting ingot machine, is given. *Figure 2.4* and *Figure 2.5* contain the necessary information and explanation for the following energy balance and tasks.

3. Energy Balance

The challenge is to enhance PFA 2 thus reducing or rather reusing of waste heat energy. The most promising way to do this is the compilation of energy flows in the process line. Exposing these build the basis for getting an energy balance and making visible the potential for a heat recovery system and process optimisation. The energy balance is meant to be the first step on the way to make a priority list of further measures or considerations for improved energy efficiency at PFA 2. A system energy balance exposes an overview of the in and out coming energies regarding defined system borders.

3.1. Furnace

Enthalpy differences between ingoing and outgoing materials depend on the temperature difference between ingoing and outgoing materials. Enthalpies related to phase transitions, such as melting, must be included. In addition, there are also enthalpies of mixing and reaction. The major enthalpy of mixing is the heat that is released or consumed when e.g. two metals are mixed. Heats of reaction are for example these which are formed while dross is produced (burning of aluminium) or gas is burned [Rosenkilde 10]. However, there are further points which have to be considered for the energy balance of furnace 9. There are additionally waste heat sources like losses caused by convection and radiation from its outer surface or open ports. A detailed description of energy flows is given in the following and listed in *table 3.1*. The system borders are defined as the shell of the furnace 9. The reference temperature is set to 25°C.

The **liquid aluminium** is considered at first. The mass was given from Hydro for this special Charge 67801 and is fixed for one cycle, but varies from charge to charge and alloying campaign to alloying campaign. This is caused by different compositions of alloys which are requested by the consumer. The temperature of this tapped metal varies between 800 and 860°C. It depends on several parameters, e.g. crucial transport time or initial temperature of crucial (transport vehicle). It should be noted that this temperature of liquid metal is not logged or measured before tapping from Hydro. Therefore an assumed value was substituted by 840°C. This means that the tapped metal is a heat emitting position in the energy balance. Section now only one point is open for this energy balance, the furnace temperature of charge while tapping. This temperature is also not logged and measured. Therefore a temperature is substituted from [Memo 11] with 750°C. The metal temperature in the furnace is just measured shortly before and during discharging procedure. *Equation 3.1* therefore leads to a heat amount of -3,797 MJ as illustrated in *table 3.1*.

$$Q_{\text{liquid alu}} = m_{\text{liquid}} \cdot c_{\text{p,liquid}} \cdot \left(T_{\text{in liquid}} - T_{\text{casting}}\right) \tag{3.1}$$

The next point, **silicon,** describes the complete amount of silicon which is charged (including percentage of internal scrap) and is a heat consumer section. Silicon is the most important single alloying ingredient in the vast majority of aluminium casting alloys [Apelian 09]. It is always added as a solid and always ends up dissolved in the molten alloy [Rosenkilde 10]. The silicon charge depends on the enquired alloy composition and varies from 5 to 11% of total charged

mass. This position describes the relatively most energy intensive section of charged metals. Silicon requires more energy than aluminium for heating and melting [Rosenkilde 10]. The energy needed for silicon is expressed in *equation 3.2*.

$$Q_{\text{silicon}} = m_{\text{silicon}} \cdot \Delta h_{\text{silicon 20 to 750°C}} \quad (3.2)$$

Here [Memo 11] states $\Delta h_{\text{silicon 20 to 750°C}}$ with 2,088 kJ/kg. This means that for one kilogram silicon, which is added at 20°C, 2,088 kJ are needed for heating, melting and mixing to the casting temperature of 750°C.

Table 3.1: Energy balance table of furnace 9, Charge 67801.

Magnitude	Mass in kg	Volume in m³	Temperature in °C	c_p in kJ/(kg·K)	Density kg/m³	MJ
Liquid Aluminium	35,836	-	840	1.177	-	- 4,640
Silicon	3,725.5	-	20	-	-	7,779
Ingot (99,7 % Al)	11,000	-	20	-	-	12,700
Scrap (internal)	1,641.5	-	20	-	-	1,895
Other Alloy Element	1,055	-	20	-	-	1,218
Heel	2,000	-	670	-	-	141
Dross extracted	552.6	-	900	0.9	-	438
Theoretical combustion gas	-	31,888.7	1,025	1.1	0.73	26,102
False Air	-	14,028	600	1.06	0.8	6,797
Radiation Loss	-	-	750	-	-	605
Convective Loss	-	-	80	-	-	20,662
Combustion of Natural Gas	-	2,950	25	-	0.84	-69,886
Dross Reaction	55,258	-	-	-	-	- 2,751
					Input:	-77,278
					Output:	78,338
					Σ	**1,060**

The charged **ingot** (billet) has a purity of 99.7 % and is computed as pure aluminium. The mass was given by Hydro. Used heat capacities are listed in *appendix*. The initial temperature of the metal was measured in the cast house and substituted with 20°C. It should be noted that there is no preheating before charging the metal. For an evaluation of this heat amount the phase change has to be considered, which leads to *equation 3.3*.

$$Q_{\text{ingot}} = m_{\text{liquid}} \cdot \left(\left(c_{\text{solid}} \cdot \left(T_{\text{fusion}} - T_{20°\text{C}} \right) + c_{\text{liquid}} \cdot \left(T_{\text{casting}} - T_{\text{fusion}} \right) + \cdot \Delta h_{\text{fusion}} \right) \right) \quad (3.3)$$

Equation 3.3 is also used for the following next two points of the energy balance model: **scrap** and **other alloy elements**. Scrap describes the internal amount of aluminium which is remelted during this cycle. Other alloy elements describe different ingredients for the correct composition

of the alloy. It is also assumed as pure aluminium and confirmed by Hydro that necessary material properties differ marginally against aluminium [Sivertsen 12].
Heel describes the amount (given by Hydro) of metal which is already in the furnace from an upstream connected cycle and must be heated up from a higher assumed initial temperature of 670°C. Without phase change while heating up *equation 3.4* results for assumed pure aluminium.

$$Q_{\text{heel}} = m_{\text{heel}} \cdot c_{\text{liquid}} \cdot \left(T_{\text{casting}} - T_{670°\text{C}}\right) \tag{3.4}$$

The **dross** which is extracted before casting is considered as a fixed ratio to the total mass of charged metal (indicated at dross reaction). This fixed value is stated in [Memo 11] with 1 % of the total mass. The temperature of the dross is substituted with 900°C and for the heat capacity 0.9 kJ/(kg K) is used. The result is expressed in *equation 3.5*.

$$Q_{\text{dross}} = m_{\text{total}} \cdot f_{1\%} \cdot c_{\text{dross}} \cdot \left(T_{\text{dross}} - T_{25°\text{C}}\right) \tag{3.5}$$

The **combustion gas** is a theoretical computed parameter of the energy balance and results from the stoichiometrical rate of needed air and natural gas. A theoretical assumption was chosen due to presently unavailable logged data. But it should be noted that measurement equipment for the flow rate of combustion air already exists. It was confirmed that the rate from combustion air to natural gas is proofed yearly by Hydro and has a steady condition while running the burner [Sivertsen 12]. This was the reason for assuming the amount with an excess air value of 3 % as stated in [Rosenkilde 10]. This leads to a theoretical combustion air flow rate by the following *equations 3.6* to *3.8* which are used for the energy balance.

$$1\ \mathrm{CH_4} + 2\ \mathrm{O_2} + 2\frac{0.79}{0.21}\ \mathrm{N_2} = 1\ \mathrm{CO_2} + 2\ \mathrm{H_2O} + 2\frac{0.79}{0.21}\ \mathrm{N_2} \tag{3.6}$$

$$L_{\text{min air}} = \left(\frac{V_{\text{air}}}{V_{\text{CH4}}}\right) = \frac{2}{0.21} = 9.524\ \text{m}^3 \tag{3.7}$$

$$L_{\text{air}} = \lambda \cdot L_{\text{min air}} = 1.03 \cdot L_{\text{min air}} = 9.81\ \text{m}^3 \tag{3.8}$$

$L_{\text{min air}}$ is thereby the minimal needed air volume for a stoichiometrical combustion of 1 m³ methane and λ the excess air amount. It is necessary to know that this magnitude has a sensitive impact on the resulting heat consumption (heat up inert gases) and flame temperature (decreases at increasing excess air, *figure 3.2*). The temperature is evaluated from the available logged data and is substituted with an integrated average value of 1,025°C. Density and heat capacity are chosen from air as an average value between 25 to 1,025°C (see *table 3.1*). But it should be noted that this magnitude is computed and results by the integration of each state in an EXCEL matrix. *Equation 3.9* expresses the magnitude of the combustion gas.

$$Q_{\text{off gas}} = V_{\text{off gas}} \cdot c_{\text{off gas}} \cdot \rho_{\text{off gas}} \cdot \left(T_{\text{average off gas}} - T_{25°\text{C}}\right) \tag{3.9}$$

The **false air** in the energy balance is the magnitude with most surprising results. This magnitude is caused by the temporary negative pressure in the furnace (see *chapter 2.1.1*) which results from different densities in the furnace (T = 1,025°C and ρ_{air}= 0.2 kg/m³) and atmosphere (T = 25°C and ρ_{air}= 1.2 kg/m³). This physical phenomenon is also known as stack effect. This high value of false air is caused by no regulation of the exhaust outlet and pressure control in the fur-

nace. When the main door is opened or any other leakage supplies false air, the furnace sucks these into the burning chamber, heats the air up and discharges the air as hot exhaust gas, or so called flue, out of the furnace. During this procedure a huge insert heat amount is wasted (8.7 %). The correct magnitude of this section could be only evaluated while the exhaust gas (flue) is steadily measured, logged and integrated [De Monte 03] in a process controlling system. Such information is important to define plant running conditions from a thermal point of view. Simultaneously the amount of natural gas and combustion air is necessary. For getting a first impression of how big the magnitude of false air flow rate is, experimental velocity measures in the exhaust line are executed and documented in *table 3.2*. The exhaust flow rate was measured with a handheld Pitot tube [Testo 11] during essential running states of furnace 9. The measure location is illustrated in *figure 2.3* (A) and *figure 3.1*. *Table 3.2* indicate relatively high velocity values while the burner is off. That leads to the assumption that the false air must be significant (especially at burner off state) and has to be considered more accurately for the following energy balance considerations at the CastAl project. It should also be noted that the measure location at *figure 3.1* is unfortunate for an accurate measure result of the exhaust gas velocity. This is caused by an unsteady gradient of the stream profile for one point in this area, which is a result of constructed and existing exhaust gas pipe layout. For an accurate measure of velocity a laminar or at least defined turbulent streaming profile is necessary which requires a defined inlet and outlet distance at the measure point.

Table 3.2: Results of exhaust flow rate measurement at furnace 9 as a verification of energy balance.

Date	Operation state	Time	v in m/s	T in °C	$\dot{V}$ in m³/h
02.07.2012	burner off	19:30	1.5	390	6,107.3
	burner on	20:05	4	850	16,286
	burner on	20:35	5	930	20,357.5
03.07.2012	burner off	08:55	1.5	640	6,107.3
	burner on	09:00	3.5	750	14,250.3

For further, more detailed and accurate evaluation of a furnace energy balance, a location with a sufficient inlet and outlet distance has to be chosen, so that a constant streaming profile could be build and measurement equipment could work sufficiently. The section between measured location and bypassed atmosphere air in the exhaust line could be an applicable place for more accurate velocity measure results (see *appendix-B*). It should be noted that this will lead to invasive handling of measurement equipment in the exhaust pipe, which was at present not necessary and possible for such an initial consideration. The exhaust flow rate (flue) is a function of minimal needed combustion air, excess air and natural gas as illustrated in *equation 3.10* and *3.11*.

$$R_{\text{flue,min}} = \frac{V_{CO_2}+V_{H_2O}+V_{N_2}}{V_{CH_4}} = 10.524 \text{ m}^3 \tag{3.10}$$

$$R_{\text{flue}} = R_{\text{flue,min}} + (\lambda - 1) \cdot L_{\text{min air}} = 10.81 \text{ m}^3 \tag{3.11}$$

This means that for 1 m³ methane 10.81 m³ flue ($R_{\text{off gas}}$) are resulting at an excess air rate of $\lambda = 1.03$. Assumed the ratio ϕ of exhaust flow rate is correct, despite the unfortunate measure location, the following magnitude results in *equation 3.12* for measured velocity in *table 3.2*.

$$\phi = \frac{v_{\text{burner off}}}{v_{\text{burner on}}} = \frac{1.5\ m/s}{5\ m/s} = 0.3 \tag{3.12}$$

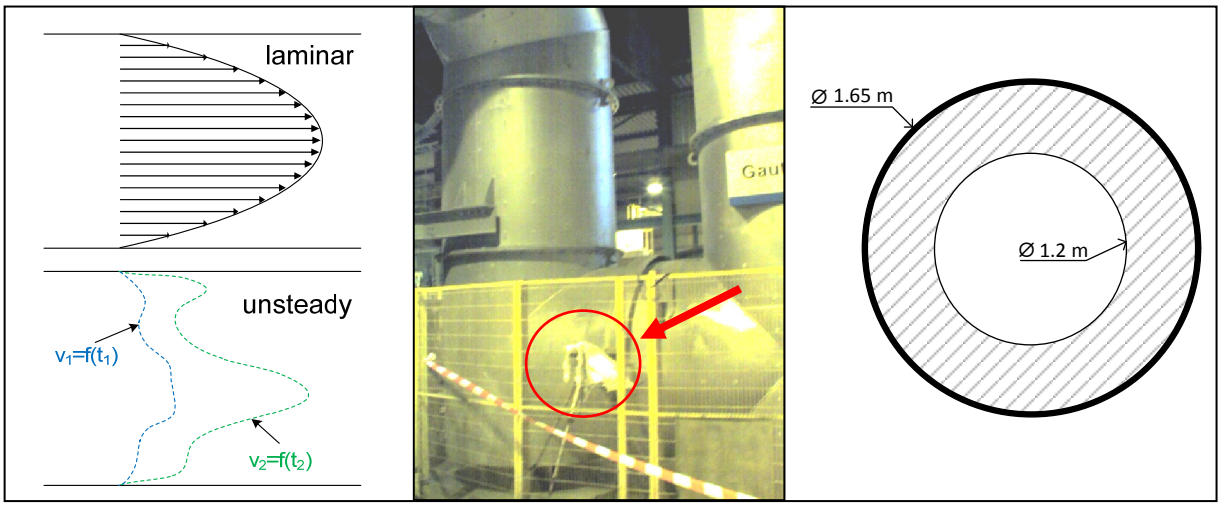

Figure 3.1: Illustration of desirable laminar and existing unsteady flow profile of the exhaust gas (left). The measure location of flow rate and temperature is indicated in the middle. A cross-section of the existing exhaust pipe clarifies the dimension (right).

This means that while the burner is off, the exhaust gas flow rate is about 30 % of the maximal measured exhaust gas flow rate (while the burner is running, which is relative accurate), caused by false air that has been drawn into the system. This magnitude of maximal exhaust gas flow rate is assumed with the theoretical combustion air value and natural gas amount, which is plausibly caused by the positive pressure in the furnace during this time (see *figure 2.6*). No false air is sucked into the exhaust and furnace during this defined period. This assumption sets the value for the ratio of maximal exhaust rate amount (measured with $v_{\text{burner on}} = 5\ \text{m/s}$) while the burner is on and exhaust rate caused by stack effect while the burner is off (measured with $v_{\text{burner on}} = 1.5\ \text{m/s}$). This means that while running the burner, the exhaust flow rate is assumed as a function of theoretical combustion air and natural gas amount. And while the burner is shut down, the flow rate of exhaust gas is a function of 30 % of the maximal exhaust flow rate and is therefore constant. This assumed result is also checked and confirmed with another theoretical approach for the stack effect. The assumed integrated false air leads therewith to the heat loss of false air and is expressed in *equation 3.13*.

$$Q_{\text{false air}} = V_{\text{false air}} \cdot c_{\text{off gas}} \cdot \rho_{\text{off gas}} \cdot \left(T_{\text{exhaust average}} - T_{\text{cast house,25°C}}\right) \tag{3.13}$$

The next position and considered magnitude is the heat loss caused by **radiation**. Therefore an emissivity of 0.95, $\sigma = 5.76 \cdot 10^{-8}$ W/(m²K), $T_{\text{in furnace}} = 700$°C, $A_{\text{port}} = 0.7$ m², $A_{\text{main door}} = 3.5$m², $t_{\text{tapping}} = 21$ min and $t_{\text{main}} = 45$ min door was chosen.

$$Q_{\text{radiation}} = \varepsilon \cdot \sigma \cdot \left(T_{\text{in furnace}}^{\ 4} - T_{\text{cast house}}^{\ 4}\right) \cdot A \cdot t \tag{3.14}$$

The loss caused by **convection** should be also noted as a significant magnitude of such furnace energy balances (26.38 %). This magnitude is a function of the furnace surface $A_{\text{furnace}} = 1{,}500\ \text{m}^2$, the heat convective coefficient $\alpha_{\text{furnace}} = 5\ \text{W}/(\text{m}^2\text{K})$, total cycle duration $t_{\text{total}} = 14\ \text{h}\ 45\ \text{min}$, surface $T_{\text{surface}} = 80°\text{C}$ and ambient temperature $T_{\text{cast house}} = 25°\text{C}$ as described in the following *equation 3.15*.

$$Q_{\text{convection}} = \alpha_{\text{furnace}} \cdot (T_{\text{cast house}} - T_{\text{surface}}) \cdot A_{\text{furnace}} \cdot t_{\text{total}} \tag{3.15}$$

The position **natural gas** is the main heat supplier for this energy balance and is thereby essential for the energy balance. The hot combustion gas gives off heat to the charge and leaves the furnace at a lower temperature than the flame temperature. The *figure 3.2* illustrates the adiabatic flame temperatures for combustion of methane and propane with air, as a function of the fuel to air ratio. The amount of heat given off is simply the difference between the enthalpy of combustion gas at the adiabatic flame temperature and the enthalpy of the same gas at the exhaust temperature, as expressed in *equation 3.16* for burner efficiency.

$$\eta_{Burner} = \frac{H_{T,flame} - H_{T,exhaust}}{H_{T,flame} - H_{T,ambient}} \tag{3.16}$$

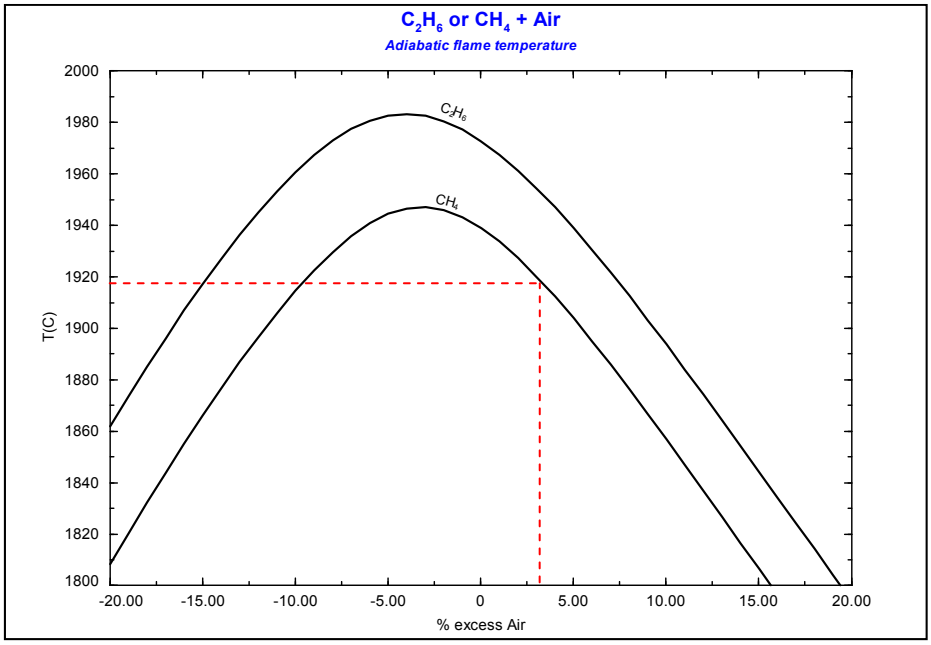

Figure 3.2: Adiabatic flame temperature for the combustion of methane as function of excess air [FactSage 12].

Figure 3.3 illustrates the burner efficiency and combustion enthalpy of methane as function of the exhaust gas temperature, which is chosen for the integration of charged heat by natural gas. The temperature $T_{\text{exhaust gas}}$ was logged during the measure campaign and is integrated in the function shown in *figure 3.3*. Natural gas consumption is hereby given. The specific enthalpy of the natural gas depends on the exhaust gas temperature $T_{\text{exhaust gas}}$ and natural gas factor f_{NG} of 0.97.

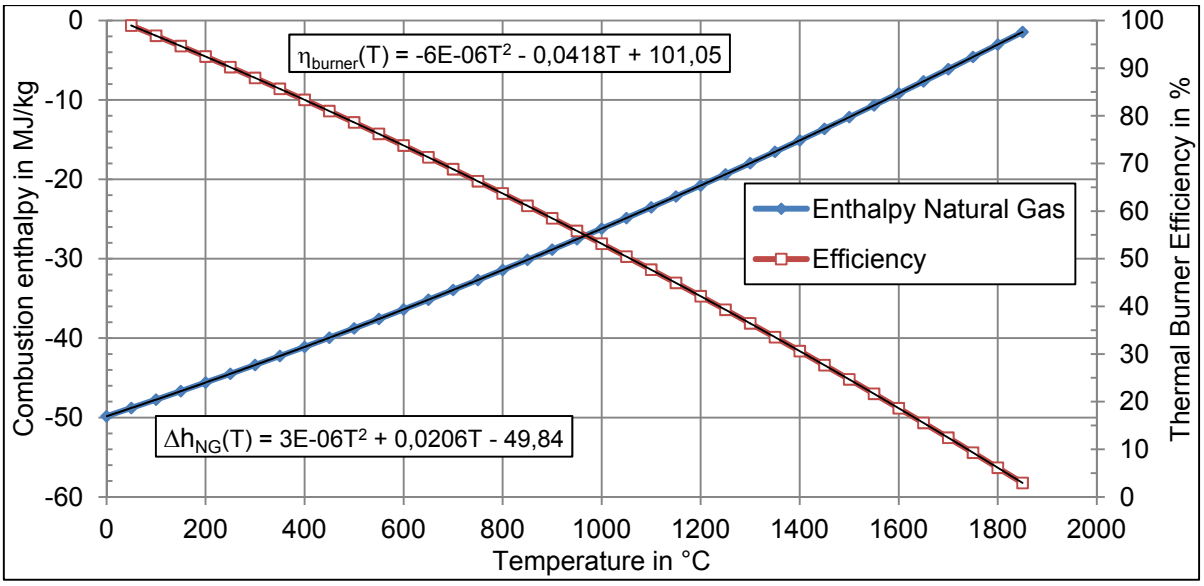

Figure 3.3: Combustion enthalpy of natural gas at 3% excess air and thermal burner efficiency as a function of the exhaust gas temperature.

The natural gas factor describes the deviation to pure methane caused by e.g. contained inert gases. The result is expressed in [Memo 11] with *equation 3.17*.

$$\Delta h_{CH4} = f_{NG} \cdot \left(3 \cdot 10^{-6} \cdot T_{exhaust\,gas}{}^{2} + 0.0206 \cdot T_{exhaust\,gas} - 49.84\right) \qquad (3.17)$$

After the integration for each specific enthalpy Δh_{CH4}, the heat amount caused by combustion of natural gas is computed with *equation 3.18*.

$$Q_{natural\,gas} = \Delta h_{CH4} \cdot \rho_{NG} \cdot V_{NG} \qquad (3.18)$$

The density ρ_{NG} is chosen at 1.3 bar absolute and 25°C with 0.84 kg/m³ for pure methane. The integration of each time step leads to -69,886 MJ.
The last section of the energy balance, **dross reaction**, describes a chemical reaction which is exothermic as noted in [Rosenkilde 10] and expressed in *equation 3.19*.

$$2\,Al\,(l) + 1.5\,O_2(g) = Al_2\,O_3 \qquad (3.19)$$

[Memo 11] sets $\Delta h_{Dross} = -16{,}596$ kJ/kg therefore a value of. This means that for one kilogram Al_2O_3, which reacts with oxygen, -16,596 kJ are emitted and heat is given off. Another factor f_{oxide} is set to 0.3 and describes the fraction of oxide in dross formed by reaction in the furnace [Memo 11]. The parameter f_{dross} describes the relative amount of dross for each charge and s set to 0.1. That leads to *equation 3.20* and completes the furnace energy balance.

$$Q_{Dross\,reaction} = m_{total} \cdot \Delta h_{Dross} \cdot f_{oxide} \cdot f_{dross} \qquad (3.20)$$

3.2. Casting Ingot Machine

The system borders for the energy balance (listed at *table 3.3*) are set on the beginning of the casting procedure (after the moulds are filled with liquid alloy) and at the end of water section 2 (before packaging unit). Within these borders the surrounding completes the border shell of the considered energy system.

Table 3.3: Energy balance table of water section one (CIM) and water section two, Charge 67801.

Magnitude	Mass in kg	Volume in m³	Temperature in °C	c_p in kJ/(kg K)	Density kg/m³	MJ
Casting Metal (Alloy)	55,258	-	688	-	-	60,775
Air System	-	67,425	40	1.007	1.3	1,324
Water Section 1	-	440	10	4.185	1,000	36,828
Water Section 2	-	240	10	4.185	1,000	20,088
Radiation	-	-	450	-	-	238
Convective	-	-	350	-	-	208
					Input:	-60,775
					Output:	58,686
					Σ	**- 2,089**

At first the **casting metal** has to be considered and computed with *equation 3.21*. The temperature of liquid metal, which is filled into the casting moulds, is measured by Hydro and chosen from the control centre (688°C) at PFA 2. The mass is given from consideration before (55,258 kg). The heat capacities and fusion are chosen for pure aluminium.

$$Q_{\text{casting}} = m_{\text{metal}} \cdot \left(\left(c_{\text{solid}} \cdot \left(T_{\text{fusion}} - T_{25°\text{C}} \right) + c_{\text{liquid}} \cdot \left(T_{688°\text{C}} - T_{\text{fusion}} \right) + \Delta h_{\text{fusion}} \right) \right) \quad (3.21)$$

The **air system** section describes the cooling system by the forced ventilating cooling section one (shown in *figure 2.6*, left). The surface of casted ingot is cooled down in this section. The air flow rate is chosen from manufacturer data and temperature was measured (40°C). This leads to *equation 3.22*.

$$Q_{\text{air system}} = V_{\text{air}} \cdot c_{\text{air}} \cdot \rho_{\text{air}} \cdot \left(T_{\text{air out}} - T_{\text{cast house}} \right) \quad (3.22)$$

Water section 1 and **water section 2** are evaluated with measured water flow rates (ultrasonic clamp on flow meter [GE 97]) in each section, as a verification of installed equipment as well as in- and outlet temperatures (10 and 30°C). *Equation 3.23* expresses the heat amount of both sections.

$$Q_{\text{water}} = V_{\text{water}} \cdot c_{\text{water}} \cdot \rho_{\text{water}} \cdot \left(T_{\text{out}} - T_{\text{in}} \right) \quad (3.23)$$

It should be noted that water section 2 works with a spray water concept and is simplified assumed as a conventional cooling section (like water section 1, liquid and single phase). This

leads furthermore to the noted fact that this section will not be useful for a heat recovery concept, caused by the open system type and spray water application.
For heat loss by **radiation** an average temperature of 450°C is assumed, which is plausible after a temperature measure with an infrared camera [FLIR 12] all over the casting ingot machine and furnace (see *appendix*). *Equation 3.14* is therefore used.
Convective loss is computed with *equation 3.15*. For the convective area of mould $A_{\mathrm{mould}} = 0.7\ \mathrm{m}^2$ and a heat transfer coefficient $\alpha_{\mathrm{ingot}} = 40\ \mathrm{W/(m^2K)}$ are chosen. The cycle duration is set to $t_{\mathrm{casting}} = 80\ \mathrm{s}$.

3.3. Conclusion and Discussion

Simplified theoretical aspects for setting an energy balance are described. They built the basis for a good understanding of scope and detailed analysis for improved energy efficiency. The determination and depiction of mapped energies conclude this section. These initial simplified energy balances indicate the order of magnitude and expose further steps for getting a more accurate balance, if necessary in the CastAl project.
The energy balance of furnace 9 demonstrates that only 30 % of consumed energy is used for primary target: Preheating, liquefying and initialisation of aluminium alloy. The residual 70 % of insert energies are wasted as illustrated in *figure 3.4*. These statements correspond approximately with the statements in [BCS 08] which contains a fuel input efficiency of 34 %, at the same reference temperature for aluminium reverberatory furnaces.

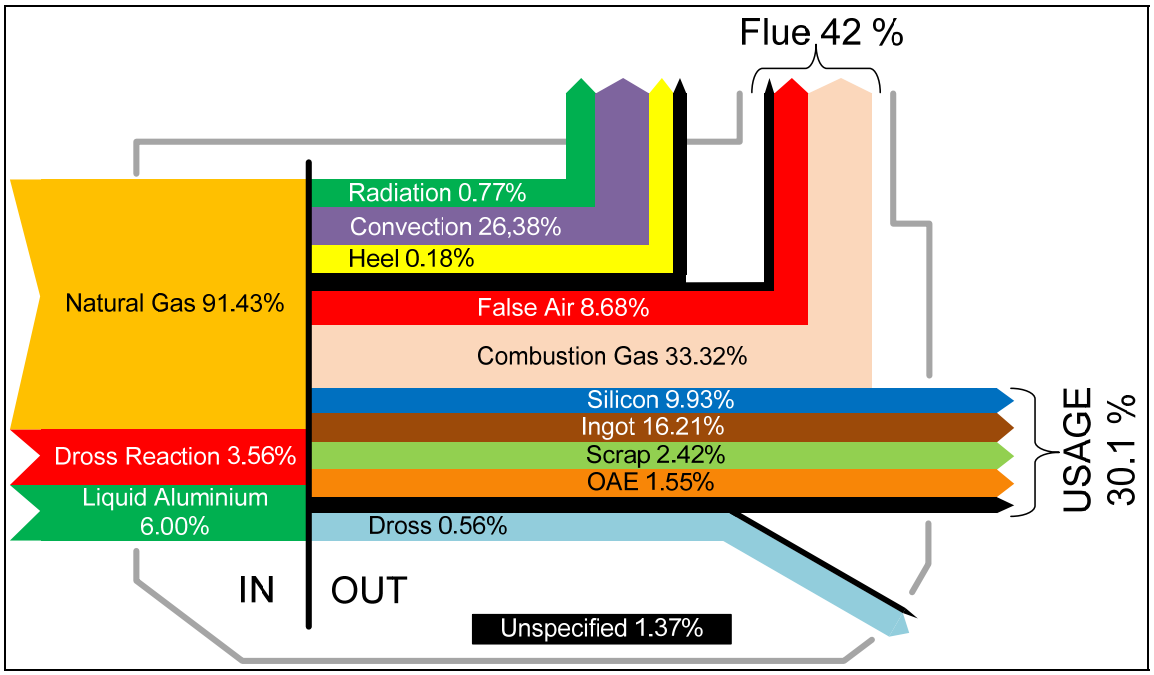

Figure 3.4: Sankey diagram of furnace 9 illustrates the incoming and outgoing energies and therefore the order of magnitudes for the heat recovery potentials.

This indicates a slightly higher waste energy amount (4 %) for the existing furnace 9 at PFA 2, regarding the benchmark stated at [BCS 08]. Expressed as an energy amount, 3,091 MJ more is consumed for the considered Charge 67801, compared to benchmark. Of course it is not that

easy to compare it with the benchmark given at [BCS 08], caused by different parameters like charge composition (5 to 11 % silicon), but it is an indication and states need for acting. This slightly negative competitive advantage is mainly caused by the energy loss through false air (8.68 %). Wasted energy can be distinguished between easily avoidable and extensive improvable heat losses. False air is an easily avoidable magnitude. The false air is sucked from the cast house atmosphere into the furnace chamber due to negative pressure (stack effect) and is heated up from +25°C to an integrated temperature (between 400 and 1100°C). Controlling pressure in the furnace by adding a valve in the exhaust pipe (see *chapter 4.1.*), closed while burner off and/or main door or tapping ports are open, would be therefore a first step of improvement. Equally a preheating system is possible which could be realised for the combustion air and charged ingot. This leads directly to less consumption of natural gas and thereby effects an increase of the total cycle efficiency. *Table 3.4* gives magnitudes of increased efficiency by preheating combustion air for reverberatory furnaces [BCS 08].

Table 3.4: Improvement of furnace efficiency by preheating of combustion air, based on a natural gas furnace with 10% excess air [BCS 08].

Furnace Outlet Temperature in °C	Combustion Air Preheat Temperature				
	204°C	316°C	427°C	538°C	649°C
1,427	22%	30%	37%	43%	48%
1,316	18%	26%	33%	38%	43%
1,204	16%	23%	29%	34%	39%
1,093	14%	20%	26%	31%	36%
982	13%	19%	24%	29%	33%
871	11%	17%	22%	26%	30%
760	10%	16%	20%	25%	28%

Aluminium reverberatory furnaces lose approximately 13.7 TJ/a via exhaust gases [BCS 08] and thus effect a huge potential for heat recovery systems in aluminium cast houses.

An extensively improvable heat loss is an improved insulation, which leads to decreased heat losses through convection (26.38 %).

Other magnitudes like dross, radiation, heel and combustion gas are operational parameters and have to be considered in further project steps.

The indication of sum balance (-1,060 MJ) is not zero which is accounted by unspecified energies (1.37 %) in *figure 3.4*. This differs to ideal theoretical results of zero and reveals that such a complex system cannot be described exactly, caused by the sensitivity of each parameter chosen for the model. In this case too much heat is consumed and the system is not balanced. The result of this consideration would lead to a system which is getting colder and colder. However, in reality, this of course is not the case.

The energy balance for the casting ingot machine (depict in *figure 3.6*) illustrates the distribution of the heat amount during the cooling procedure of aluminium in this process line. Both water sections are the main consumer of absorbed heat with 93.65 %. The water outlet temperatures are very low (30°C) and the water flow rates with 56.8 m³/h in section 1 and 31 m³/h in section 2 are high. Changing the splitting of water strings like in *figure 3.6* here lead to a higher potential of using accrue waste heat and decreases consumed water. The only limitation that has to be considered is the ingot temperature after water section 1. A maximal limit of 120°C there is con-

firmed by Hydro. One water loop will give in this section better heat demands for possible heat recovery systems and decreases the running costs of the casting ingot machine. Only 2 % is utilised by the air ventilating system. After an enquiry in the Hydro control centre it has been confir-

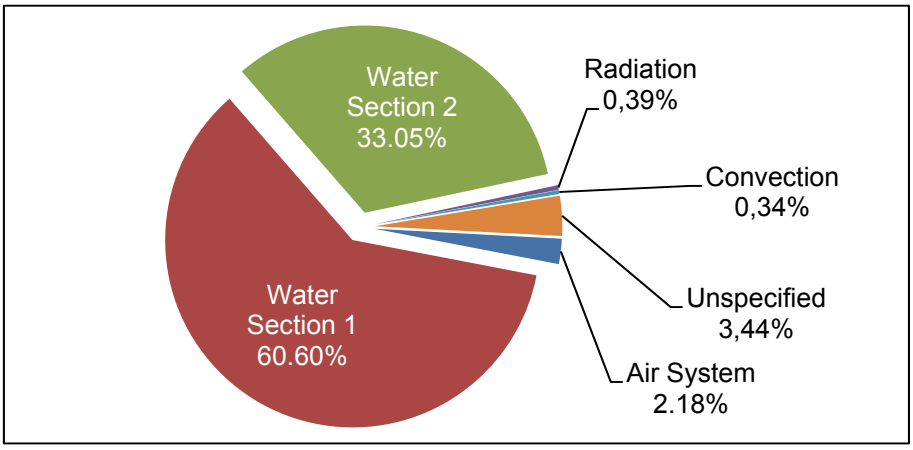

Figure 3.5: Heat discharge distribution of liquid alloy for each cooling section at the CIM.

med that the system was installed after the casting ingot machine was already installed, due to the varying amount of silicon (5 to 11 %) in the alloy. A selective shut down of the air ventilating system during charges with a low silicon amount at this point leads here to a decrease of energy consumption. The unbalanced sum (-2,089 MJ) reveals furthermore for the casting ingot machine that this is just a theoretical consideration. In reality the sum must be zero. This is caused by deviation from reality and indicates furthermore the sensitivity of parameters for these models.

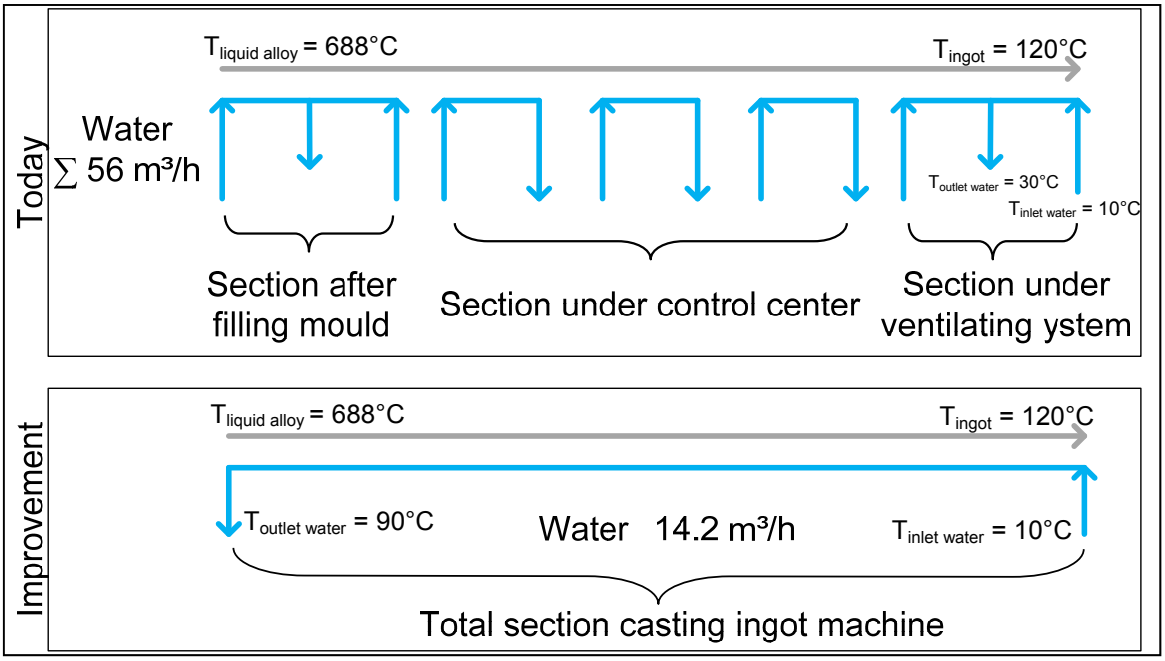

Figure 3.6: Existing cooling concept at water cooling section 1 with seven inlet loops (each 8 m³/h) on the top. Improved future cooling concept with one loop, increased water outlet temperature and decreased water flow rate.

4. Improvement of Energy Efficiency

4.1. Principle

The current fuel price development, the pursuit of sustainability and competitive advantage in the aluminium industry gives new impulses to further development of waste heat recovery solutions in aluminium cast houses. It has to be differentiated between two main tasks of improving energy efficiency: reduction and conservation of energy by increasing the efficiency. To reduce the input of energy is the prior target of energy efficiency considerations. If e.g. fuel consumption can be economised by just operational measurements that do not involve investment, each percentage gain will automatically lead to improved business performance. When investment is involved, the cost has to be carefully balanced with the saving. This tends to be also the most decisive factor of the conservation of energy. Conservation of waste energy is therefore an add-on and can be differentiated in three sub stages:

a) Saving energy by existing equipment
b) Optimising of equipment (modifications and adjustments)
c) Active waste heat recovery

These sub stages are elucidated in the following subchapters and present or rather propose possibilities to enhance the process by energy saving and heat recovery solutions. The explanation focuses on the furnace and most promising process section regarding improvement of energy efficiency at PFA 2.

4.1.1. Energy saving by existing equipment

The first step in energy saving is saving energy with the existing production facilities. Optimising production will lead to minimising cost and energy consumption with little or no investment. Long-time experience with melting furnaces teaches the importance of the correct **charging sequence** on the melt rate and the metal recovery. Straightforward rules like charging the lighter scrap first and the heaviest pieces last have noticeable effect on the performance and energy consumption [Migchielsen 09].
Furthermore, operating the furnace with minimum **door opening time** has positive effects of the production, energy consumption and metal loss. Saving energy is continuing with the optimisation of the production process. A furnace that is holding, uses fuel, but does not produce. Based on the energy balance each minute 23.4 MJ (390 kW) are wasted by convection, which is the second largest waste heat consumer. The result would therefore be a minimum time for pre and cast holding, because the time is an essential factor for this waste energy source (see *equation 3.15*).
Shortening the **process** or at least **holding time**s for each casting session must therefore be a target and will create an essential efficiency factor for the Foundry Alloy Cast House in Sunndalsøra.

Figure 2.4 indicates also an energy saving potential which can be exploited by existing equipment. The alternating melt temperature (T_{melt}) of the alloy charge is depicted there during the casting procedure in between a temperature range of 706 to 758°C. Assumed that an average temperature of 732°C is targeted, by controlling the cast temperature of 690°C before filling the moulds, the alloy temperature in the furnace is temporarily too high. This means for the considered Charge 67801, during a casting duration (furnace angle 0 to 31° in *figure 2.4*) of 466 min, the furnace creates approximately a temperature level which is too high half the time (233 min). This temperature can be stated at 745°C as an arithmetic average temperature between the alternating temperature of 758°C and set average temperature of 732°C. That leads to the statement that the alloy temperature (T_{melt}) while cast holding is averaged 13°C higher than needed, for 233 min and has a control quality of ± 26°C for each casting session. This constitution leads to an additionally unneeded increase of fuel consumption, caused by *equation 3.1*

$$Q_{\text{temperature peak}} = \frac{m_{\text{total}}}{2} \cdot c_{\text{p,Al.,liquid}} \cdot (T_{745°\text{C}} - T_{732°\text{C}}) = 423\ \text{MJ/casting session}$$

and states at least the heat amount for heating up the averaged alloy charge during casting. The total mass m_{total} is reduced to an arithmetic average mass caused by the tilting up and discharging of the furnace. It should be noted that based on this simplified consideration a feasible temperature **control quality** of ± 10°C has to be targeted, while holding the furnace content at casting procedure. This improvement of operation behaviour leads to 61.5 % (26.4 MWh/a for 365 casting sessions per year for furnace 9) less energy consumption during casting for those temperature peaks and reduces also metal loss in the furnace (high molten metal temperatures cause excessive hydrogen pick up as well as excessive dross formation). This can be achieved by operating at part load with the existing burner or with a second part load burner, which requires a second burner implementation.

Comparing the average fuel **consumption per unit of production** with the specific fuel consumption associated with the furnace, demonstrates the opportunity in optimising production or rather burner operation.

Adjusting the **burner**s to the most optimum setting should not be a once in a lifetime or yearly event, but must be repeated on a regular basis as an integral part of maintenance. Due to wear and ageing of components, the settings may change with higher fuel consumption and unnecessary environmental pollution results. Operating burners at a too high air-fuel ratio has a negative effect on the fuel consumption [Migchielsen 05]. The efficiency of the furnace reduces (see *figure 4.1*) as the temperature decreases (see *figure 3.2*) and the amount of flue gas increases.

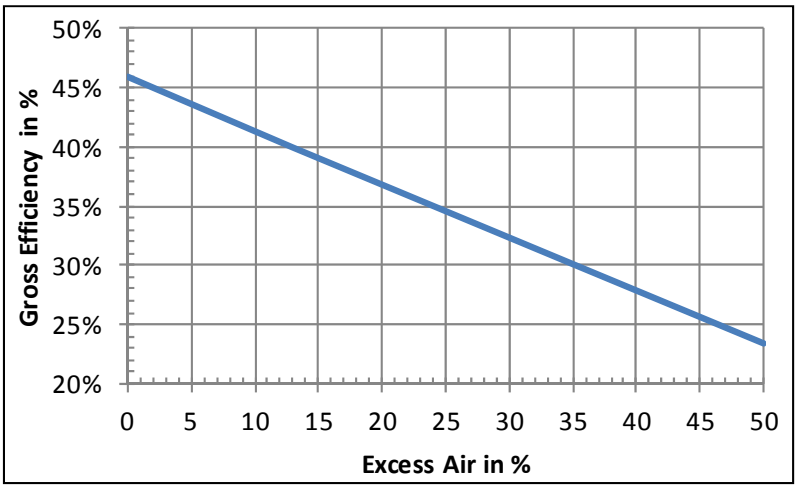

Figure 4.1: Simplified relation between excess air and burner efficiency of an ambient air burner [Migchielsen 05].

Another measure in the field of maintenance is to keep the sealing of doors and hatches in an optimum shape. Together with an effective furnace pressure control system (see chapter 4.1.2.) these prevent ingress of air into the furnace and reduce unnecessary stack loss. Air leakage does not only increase the amount of flue gas and thus the stack loss, but it also introduces local high oxygen levels in the furnace, causing unnecessary metal loss [Migchielsen 05].

4.1.2. Optimising of Equipment

Figure 4.1 illustrates that the efficiency of the burner can be increased by reducing the excess air ratio. The reason for this fact is, that with a lower excess air ratio, less flue gas is produced per amount of fuel. But it should be noted that a certain amount of excess air is desirable (3-10 %), caused by less environmental pollution (nitrogen oxide and carbon monoxide) and targeted at complete combustion of insert fuel (avoid unburned hydrocarbons, less dross formation). However, the amount of heat loss by flue gas is the largest waste heat source at the furnace (42 %, see *figure 3.4*). By just fixing the excess air level to 10 %, the flue gas, in general meets the environmental requirements in all operating cases. Full combustion is not only determined by the excess air ratio only, but by the furnace temperature as well. At a higher furnace temperature, a lower excess air will give full combustion as well. With modern electronically governed **air-fuel control systems**, the excess air ratio can be adjusted to follow the furnace box temperature via the PLC control. In this way, few lines of programming save an approximate one percent of fuel [Migchielsen 05]. A further option in the control of the excess air ratio is using a continuous **oxygen level monitoring** in the flue gas that leaves the furnace. The lowest possible oxygen level is desired, this does not only save energy but reduces dross formation as well.
A positive pressure inside the furnace does prevent ambient air, as suggested before, from entering into the furnace through gaps around doors and does increase dwelling time of the products of combustion in the furnace. A proper furnace **pressure control system** regulates the heat lost through the stack and thereby does the fuel consumption decrease, by up to 10%, as stated in [Migchielsen 10] and shown in *figure 4.2*. For Charge 67801 would be 6,797 MJ saved, which means 689.14 MWh/a for 365 equal sessions per year. Generally the pressure is set in such a

way, that at the main door has still atmosphere or just positive pressure predominate, preventing ambient air being drawn in at the same time preventing hot gas flow from blowing out of the

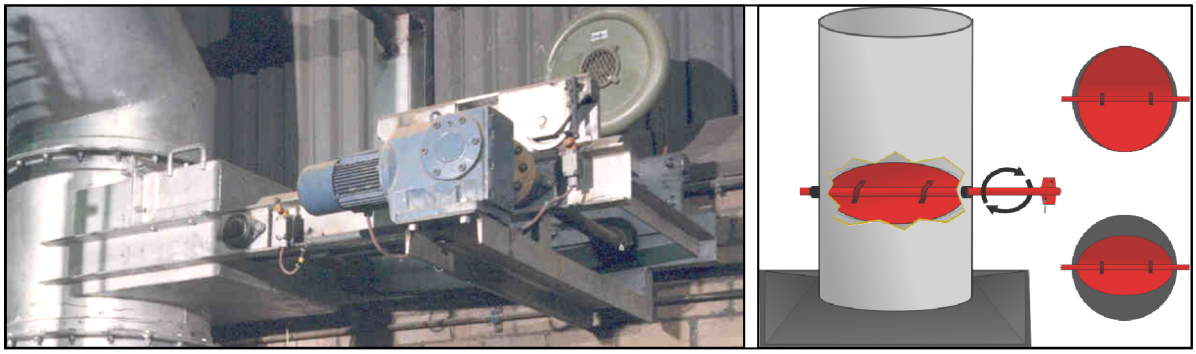

Figure 4.2: Horizontal arrangement (left) [Migchielsen 10] and a schematic construction (right) of a furnace pressure control damper system [Wiki 09].

furnace too vigorously. The graph below in *figure 4.3* illustrates how much ambient air is drawn into a furnace, if a gap of 2 mm exists around the main door with a size of 2 x 2 m and how much extra fuel is consumed on an annual basis. It should be noted that this function and derivation of **leakage air** is not applicable for the considered energy balance of furnace 9, caused by unknown gaps, gap sizes or other leaking areas. But it can be used as comparison of resulting waste heat for false air in *table 3.1*. Furthermore was a pressure test of the existing equipment for identifying the leak area was not operable without a shutdown of furnace 9. Those tests can determine the leak area. The knowledge of the leak area in combination with e.g. *equation 4.1* leads to the given throughput of leakage air into the furnace as a function of the furnace pressure.

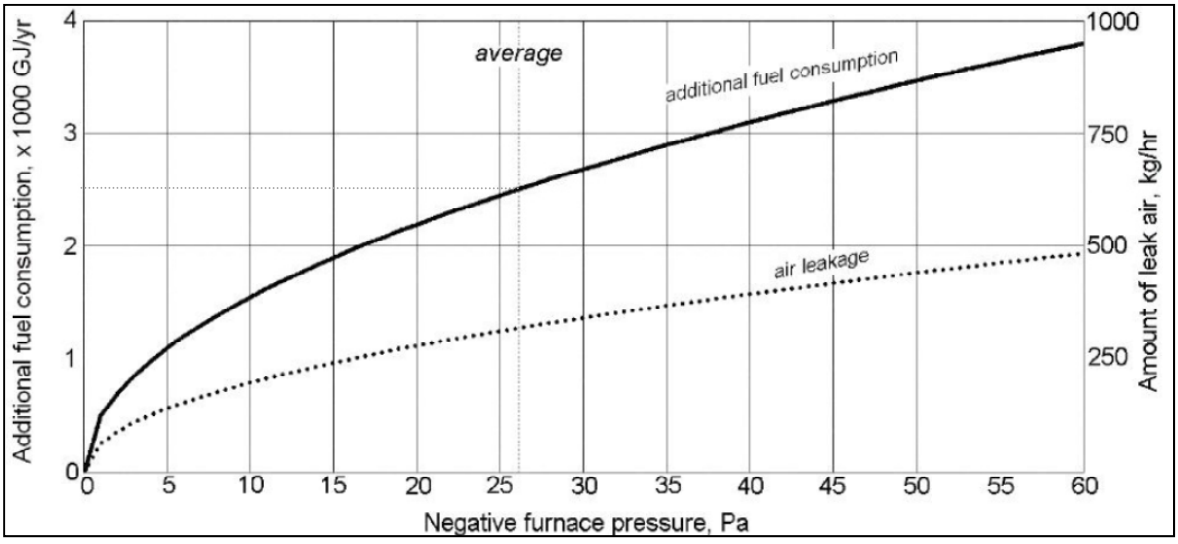

Figure 4.3: Amount of leakage air and waste heat as a function of furnace pressure [Migchielsen 10]. Dashed average furnace pressure line match with average furnace pressure for Charge 67801 at 26 Pa.

Equation 4.1 is valid for the throughput of a compressible fluid (gas) through a leak in a pressurised vessel [Steck 12] like a furnace.

$$\dot{m} = \mu \cdot A \cdot \sqrt{\left|\frac{\kappa}{\kappa-1} \cdot \left[\left(\frac{p_{out}}{p_{in}}\right)^{\frac{2}{\kappa}} - \left(\frac{p_{out}}{p_{in}}\right)^{\frac{\kappa+1}{\kappa}}\right]\right|} \cdot \sqrt{2 \cdot p_{out} \cdot \rho_{out}} \qquad (4.1)$$

A is thereby the leak area of port, μ is the coefficient of friction (in reality $\mu < 1$), κ the adiabatic exponent for air drawn into the furnace, p_{in} the varying pressure inside the furnace, p_{out} the atmosphere pressure and ρ_{out} the density outside the furnace. It can be stated that the negative average pressure in *figure 4.3* equals those of Charge 67801 (-26 Pa). A comparison of the resulting additional waste heat in *figure 4.3* (with 2,500 GJ/a and a process time of 14 h 43 min for Charge 67801 results in a waste heat amount of 4,209 MJ/session) and the determined waste heat by false air in *table 3.1* (6,797 MJ/session) furthermore supports the evaluated results for the energy balance in *table 3.1* for furnace 9. The deviation is caused by the balance assumptions and a more extensive leak area in reality compared to the assumed area above. Therefore the consideration above states comprehensible that leakage air must be avoided by a proper pressure control system.

Modern **refractory design** can help reducing the operational cost of a furnace. Whereas in most cases for the bath area of a melting or holding furnace, priority is given to maintaining the freeze plane in the hot face layer for security reasons, upper walls, doors and roofs can be looked at with the aim to improve insulating properties and hence, achieve lower shell temperatures and lower energy consumption by convection (see *table 3.1*). Using modular roof sections allow the use of higher insulating designs compared to more conventional suspended roof designs with hanger bricks as *figure 4.5* illustrates.

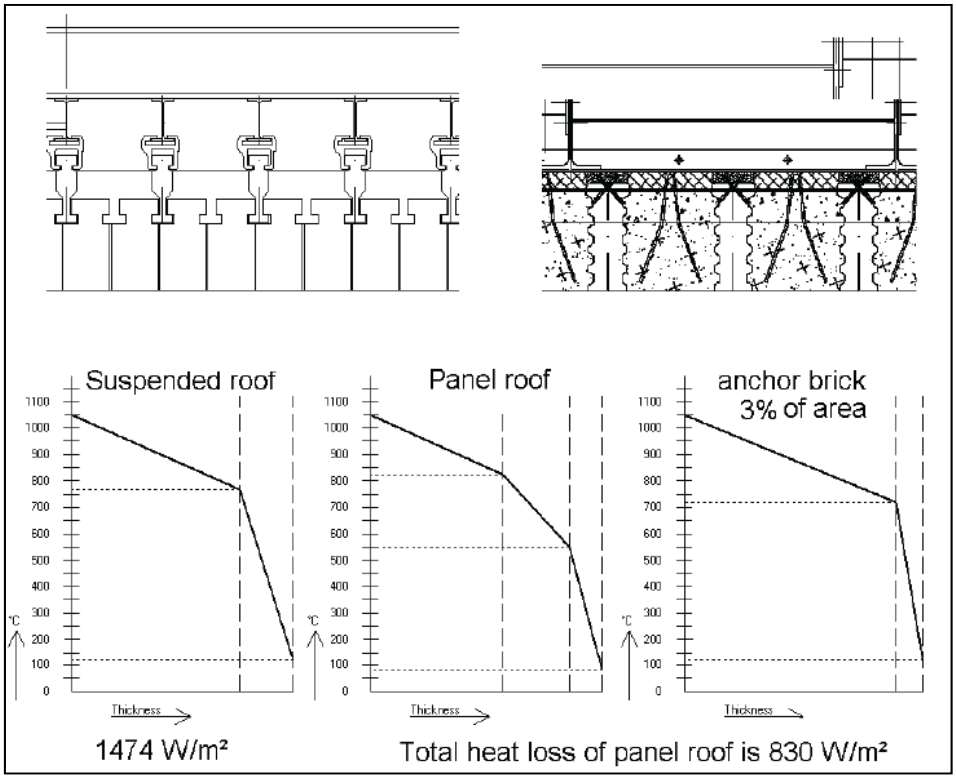

Figure 4.4: Comparison of insulating designs between conventional suspended with hanger bricks, roof and modular roof sections [Migchielsen 10].

Using appropriate materials in the bath area does benefit furnace lining life and does reduce dross built up which in turn leads to cleaner metal. It is worthwhile to consider using the relatively new ion-bonded refractory materials on places like the belly band and areas under very heavy use such as charging ramps. As these materials have excellent non-wetting properties resulting in very little dross built up and have very high CCS (Cold Crushing Strength) values,

making them very suitable to be used in areas where abrasion is high. These new materials are expensive to buy but are cost effective because of the many benefits they do bring about [Migchielsen 10].

Before considering the recovery of waste heat from flue gas, the amount of waste heat in the flue gas must be minimised. This can be achieved by using highly efficient **regenerative burner**s instead of existing ambient air burner. Regenerative burners have a thermal efficiency of around 70 %. With optimum burner adjustment this efficiency can be stretched to a maximum of 72 % [Migchielsen 09]. Approximately 80% from these 72 % percent are effectively used for melting metal. The result of the overall efficiency of a modern furnace is thereby at 58 % [Migchielsen 09] instead of 30 % as it the case presently. This means 28 % needed energy is saved and equals 1.98 GWh/a, when the heat amount of natural gas (69,886 MJ) at Charge 67801 is the basis for 365 session per year. The extent of flue gas heat recovery is determined by economic factors. The flue gas exhaust temperature is still on such level that some additional energy recovery is promising. For higher efficiency, higher heat recovery is required, resulting in a higher air preheat temperature as stated in *table 3.4*. Operating the burner at high average air preheat temperature and low average flue gas temperature requires frequent switching over of the burners. For larger burner sizes it is important to correctly control the burner output during switching over. This prevents high levels of excess air, consequential energy loss and peaks in the NOx (nitrogen oxygen) production. Developments in the burner technology that are currently being investigated are flameless oxidation. By creating more even temperature distributions inside the furnace, it is believed that the heat transfer can be increased. In combination with a new generation of regenerative burners, this is a promising development [Migchielsen 09]. When holding takes place for any length of time, it is generally recommendable to use a dedicated **holding burner**, much better sized to the heat input requirement during holding than large melting burners ever can be [Migchielsen 10]. Also, when extended holding times does occur, a small burner (carefully matched in size to the heat input requirement) does play a role in keeping hydrogen levels down compared to using a larger one. For holding purposes an oversized burner (while turned down) does not have a very efficient combustion because it has not been specifically designed to work frequently at such minimum input levels. The configuration of burners at the furnace is very important. Melting burners are generally medium velocity burners to give the best results both regarding radiant and convective heat transfer, also the burners will be angled down towards (as illustrated in *figure 4.5*) the charge pile to give the best heat transfer on to the charge and with that the fastest melt down of the material (remember that dross formation is not only a factor of temperature but also of exposure time), where as holding burners are under a more shallow angle and should have the highest possible exhaust velocity to create a homogenised temperature pattern of the flue gas above the bath to prevent local hot spots in the metal bath [Migchielsen 10].

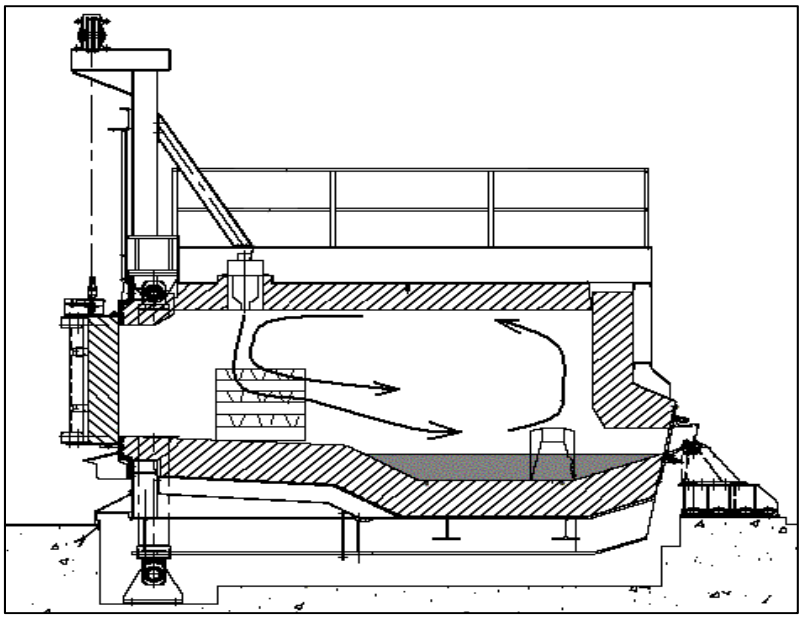

Figure 4.5: Gross section of a typical furnace and indication of heat transfer [Migchielsen 05].

4.1.3. Waste Heat Recovery

The last step in energy conservation is to actively recover heat from waste heat streams. A major source of waste heat is the flue gas from furnace 9, as depicted in *figure 3.4* (false air and combustion gas). Heat from wasted flue gas can be applied as one option, for **preheating charge** materials at melting furnaces. Apart from energy recovery, this has several additional advantages:

1. After preheating less heat is required for melting (melting process will be faster or increased production).
2. During preheating water inclusion is reduced, improving the safety of the melting process.
3. Drying of the metal gives less oxidation in the melt, so increased recovery, as moist reacts with liquid aluminium to form dross.

It must be emphasised that reducing metal loss also reduces energy consumption and CO_2 production as every kilogram of aluminium that is getting lost in the production process, eventually, has to be supplemented by primary aluminium, made in an energy intensive electrolyse process. Aluminium remelt plants produce a large amount of flue gas that contains sufficient waste heat for preheating the aluminium charge materials. Getting the heat from the flue gas to the charge materials in an economically justified way is not an easy task. The charge material has to be loaded into a preheating chamber for exposure to the hot flue gas from the flues. The flue gas can only transfer part of its heat to the load, as there must be always a temperature difference as a driving force to transfer heat from the flue gas to the charge load. Model calculations show that heat transfer to the charge material take a considerable time. Preheating a charge takes approximately the same time as melting in a melting furnace [Migchielsen 10]. In this way a full load for a melting furnace can be preheated with the flue gas that is released during melting of the previ-

ous load. Looking at the energy flow from furnace 9, the heat flow in the flue gas is an extensive waste heat. When using this, hot flue gas (400 to 1100°C), a huge amount of heat can be retrieved. When using waste flue gas as a heat source, the condensate has to be considered: As the dew point of flue is approximately 55 °C, some condensate may occur during the start of the drying cycle. *Figure 4.6* illustrates such a schematic installation of a preheating chamber. *Figure 4.7* gives the order of magnitude depicted as Sankey diagram for such a waste energy application and show an implemented application.

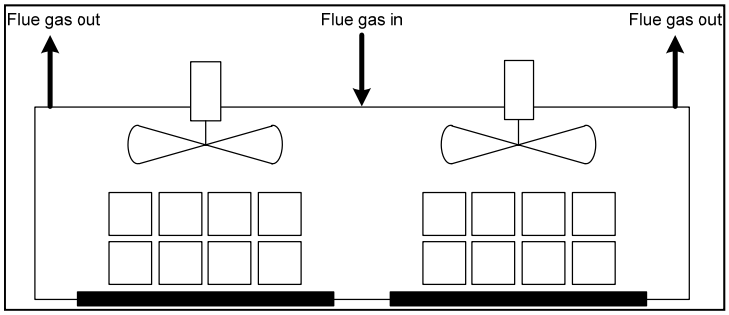

Figure 4.6: Scheme of a typical preheating chamber.

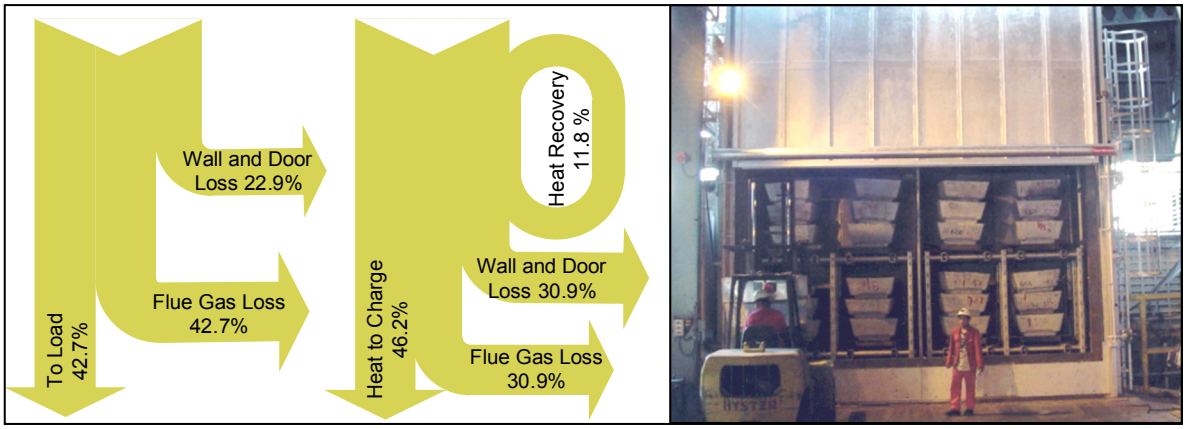

Figure 4.7: Simplified Sankey diagram show the typical effect of a preheating chamber which operates on waste flue gas (left) and a installed construction of a preheating chamber (right) [Migchielsen 06].

Preheating by waste heat seems promising, but considering the required investment and additional handling the high fuel prices do not justify this way of preheating. Additional justification is required for installing such preheating installation such as CO_2 trading off, safety features regarding the charge materials and subsidies for energy conservation or rather reduction of greenhouse gasses. Determining the optimal preheat temperature of charge is one of the most important design definitions of the preheat installation. Assumed that the metals (m = 55,258 kg) are charged at a temperature of 300°C instead of 20°C, 1.65 GWh/a less energy would be needed for the initialisation of the alloy if considering 365 sessions per year.

A second option and promising way of improved energy efficiency by using flue waste heat, is the heat to power conversion. This method is, described in detail in the following *chapter 4.2* and creates an alternative compared to the explicated concepts above.

4.2. Heat to Power

Thermal energy represents the most favourable energy form and provides the basis of the potential for a heat recovery solution in this disquisition. This energy is produced through tapping of hot liquid metal, the combustion of natural gas and exothermic chemical reaction of aluminium and oxygen in the furnace as depicted in *table 3.1*. After the evaluation of energy balances and listed improvement of energy efficiency above arises a further alternative of heat recovery solution, the conversion of thermal energy to electrical power. This is feasible by heat transforming applications which generates heat into work and finally electricity. The conversion is realised through a thermodynamical cycle. Other heat recovery solutions e.g. upgrading by heat pumps, the use of an internal or external heat district and the conversion by the Brayton or Kalina cycle are not at scope, caused by less promising implementation probability and seminal potential for PFA 2. The scope of calculations for a more economical and well known heat recovery technology is therefore positioned by the application of a Rankine, Organic Rankine and Organic Flash Cycle. These cycle types are considered in the following sub chapters and give the basis for a calculation of the annual energy saving or rather recovery potential.

4.2.1. Principle

One way to rate the conversion possibilities of thermodynamical cycles can be expressed by the definition of exergy destruction. This exergy destruction has a relative huge influence at low grade and a relative marginal influence at high grade waste heat conversion. The efficiency of a thermal process must be judged not only by the amount of thermal energy converted but also by how well exergy is conserved. Exergy is the part of energy which can be used for heat to power conversion and is therefore directly related to an economic value. In sum with anergy, which represents the energy of the surrounding and cannot be used for generating work, it defines energy. Energy is best utilised when exergy is managed most effectively. Processes requiring only low exergy should use thermal energy with low exergy where available and save thermal energy with high exergy for little need for exergy. It can be satisfied with thermal energy whose high exergy has been used first for energy conversion, as in the heat to power plant. The exergy potential can be stated with the calculation of a comparative Carnot cycle (see *figure 4.9*). It should be noted that the conversion can be only incomplete based on the second thermodynamical law and is connected therefore with losses. The unusable thermal energy becomes waste heat and must be dissipated to the surrounding, which is an inevitable thermodynamical procedure. Another important thing is in which kind of state the heat transforming fluid is available: Solid, liquid or gaseous. This influence the thermodynamical possibilities of heat conversion as illustrated in *figure 4.8*. In an ideal thermodynamical process for a given heat source, heat would be transferred from the source to the thermodynamic cycle at an infinitesimal temperature difference. The ideal thermodynamic processes are obviously impossible in reality, but they serve as benchmarks for all the thermodynamic processes working between the same heat source and sink conditions and are important tools in the performance analysis, comparison and development of actual thermodynamic systems.

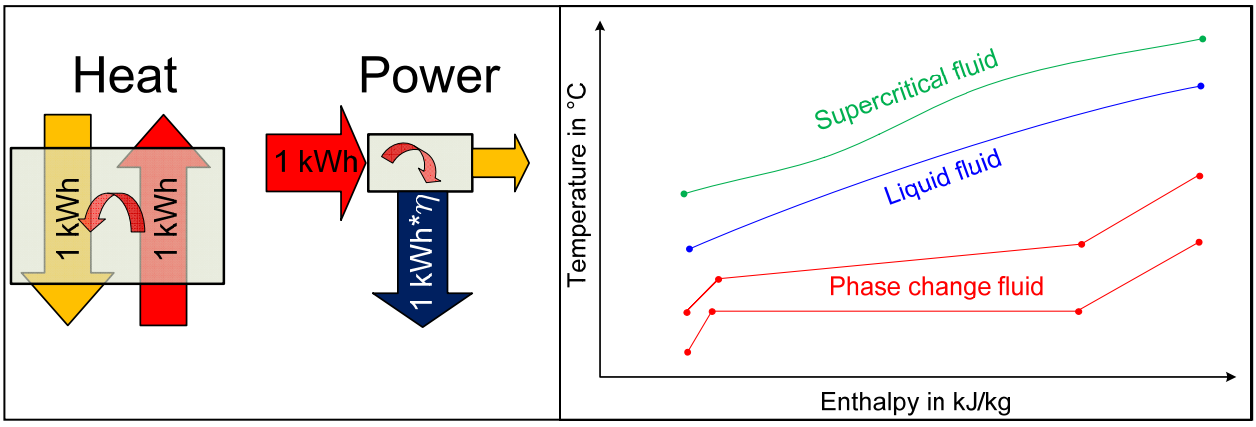

Figure 4.8: Clarification of heat conversion processes (left) and temperature profiles of heat transforming fluids (right).

The types of ideal thermodynamical processes are typically the Carnot Cycle but also the Lorenz or triangular cycle.

The **Carnot cycle** has been recognised as the most efficient thermodynamic cycle capable of converting thermal energy into work between two isothermally temperatures [Huijuan 10], as shown in *figure 4.9*.

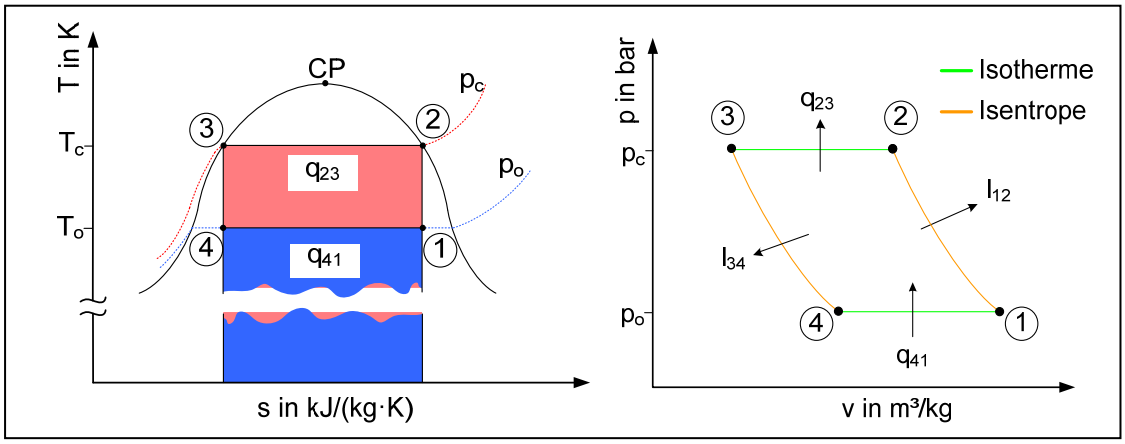

Figure 4.9: Carnot cycle in a T,s-diagram (left) and p,v-diagram (right) for phase change fluid.

The total thermal energy transferred from a reservoir to the system is:

$$Q_{\text{carnot}} = T_{\text{c}} \cdot (S_2 - S_3) \tag{4.2}$$

The amount of energy converted to work and the conversion efficiency of the Carnot cycle are:

$$W_{\text{carnot}} = \oint p \cdot \delta V = (T_{\text{c}} - T_{\text{o}}) \cdot (S_2 - S_3) \tag{4.3}$$

$$\eta_{\text{carnot,thermal}} = \frac{W_{\text{carnot}}}{Q_{\text{carnot}}} = 1 - \frac{T_{\text{o}}}{T_{\text{c}}} \tag{4.4}$$

In a Carnot cycle, the heat source has infinite heat capacity or size so that its temperature profile perfectly matches the isothermal vaporisation and condensation processes of the working fluid. However, in reality, the heat sources and sinks have finite heat capacities and sizes, so that their temperatures change during the heat exchange process in the boiler and the condenser. This is in *equation 4.5* accounted and *figure 4.10* depicted.

$$\eta_{\text{carnot,thermal gliding}} = 1 - \frac{T_o \cdot \ln\left(\frac{T_c}{T_o}\right)}{T_c - T_o} \quad (4.5)$$

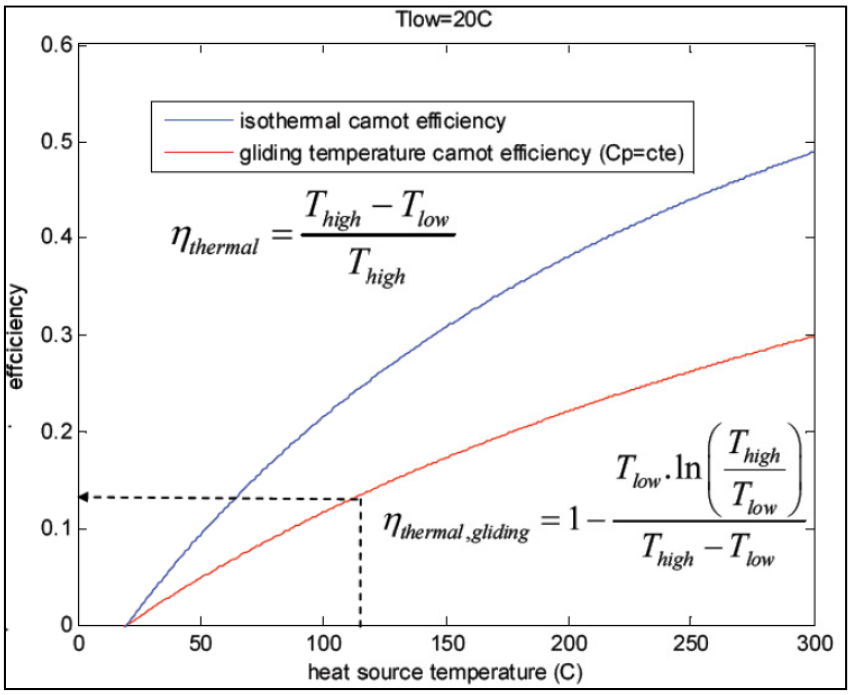

Figure 4.10: Illustration of achievable Carnot efficiencies [Nekså 09].

In the Carnot cycle, the heat addition and dissipation only happen at vaporisation and condensation processes. If a working fluid is heated from the condensation temperature to the heat source temperature, a **triangular cycle** (see *figure 4.12*) has to be chosen as the ideal cycle [Huijuan 10]. A supercritical Rankine cycle is usually the practical approximation of a triangular cycle, as shown in figure 3.

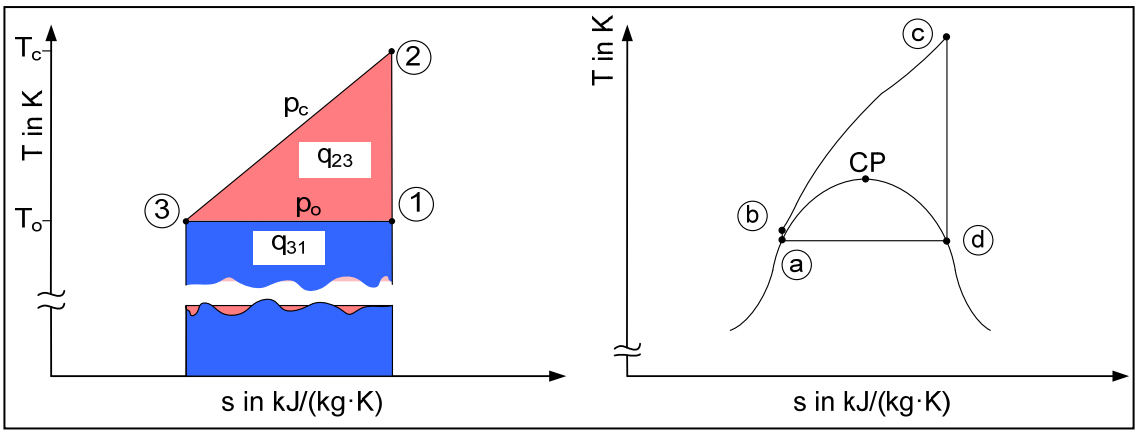

Figure 4.11: Triangular cycle (left) and supercritical cycle (right) in a T,s-diagram.

For a triangular cycle, the total heat input and net work output yield:

$$Q_{\text{triangular}} = \int_{S_3}^{S_2} T \cdot \delta S = \frac{(T_c - T_o)\cdot(S_2 - S_3)}{2} + T_o \cdot (S_2 - S_3) \quad (4.6)$$

$$W_{\text{triangular}} = \oint p \cdot \delta V = \frac{(T_c - T_o)\cdot(S_2 - S_3)}{2} \quad (4.7)$$

The efficiency of the triangular cycle can be expressed as:

$$\eta_{\text{triangular}} = \frac{W_{\text{triangular}}}{Q_{\text{triangular}}} = \frac{(T_c - T_o)\cdot(S_2 - S_3)}{2\cdot\left(\frac{(T_c - T_o)\cdot(S_2 - S_3)}{2} + T_o\cdot(S_2 - S_3)\right)} = 1 - \frac{2\cdot T_o}{T_c + T_o} \quad (4.8)$$

4.2.2. Organic Rankine Cycle

The Organic Rankine Cycle (ORC) applies the principle of the well known and common steam Rankine Cycle, but uses organic working fluids with low boiling points to recover waste heat from lower temperature heat sources. It should be noted that waste heat can be also feasible converted into electricity at high temperature and relative low net power output ranges $P_{el.} < 5$ MW by ORC (stated in [Nekså 09] and depict in *figure 4.13*). In comparison with water vapour, the

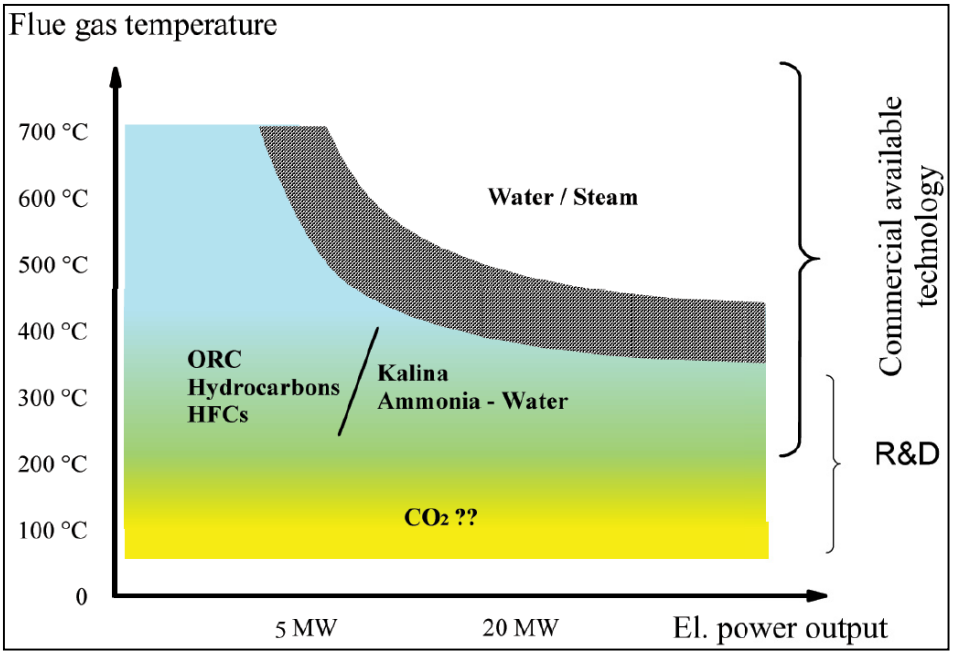

Figure 4.12: Depiction of waste heat power plant application ranges [Nekså 09].

working fluids used at ORC have a higher molecular mass, enabling compact designs, higher mass flow, and higher turbine efficiencies (as high as 80 up to 90%) [Duffy 05]. However, since the cycle functions at lower temperatures, the overall efficiency is only around 10 to 20 %, depending on the temperature of the condenser and boiler. While this efficiency is much lower than a high temperature steam power plant (30 to 40%), it is important to remember that low temperature cycles are inherently less efficient than high temperature cycles. Limits on efficiency can be expressed according to Carnot efficiency (see *figure 4.10*). A Carnot engine operating with a heat source at 150°C and rejecting it at 25ºC is only about 30% efficient. In this light, an efficiency of 10 to 20% is a substantial percentage of theoretical efficiency, especially in comparison to other low temperature options, such as piezoelectric generation for example, which are only 1% efficient. ORC technology is not particularly new. At least 30 commercial plants worldwide were employing the cycle before 1984 [STOWA 07] and further applications are noted in [Tchanche 11] from 1999 to 2010. Its applications include power generation from solar, geothermal, and waste heat sources. ORC is most useful for waste heat recovery among these three applications [Duffy 05]. Waste heat recovery can be applied to a variety of low to medium temperature heat streams. An example of a recent successful installation is in Germany, where a

cement plant installed an ORC to recover waste heat from its clinker cooler, whose exhaust gas is at about 500°C. The ORC provided 12% of the plant's electricity requirements and reduced CO_2 emissions by approximately 7,000 tons [Heidelberg 07]. Although the economics of ORC heat recovery need to be carefully analysed for any given application, it will be a particularly useful option in industries that have no in house use for additional process heat or no neighbouring plants that could make economic use of the heat. This is indeed the case for the following calculation in *chapter 4.3* and *4.4*.

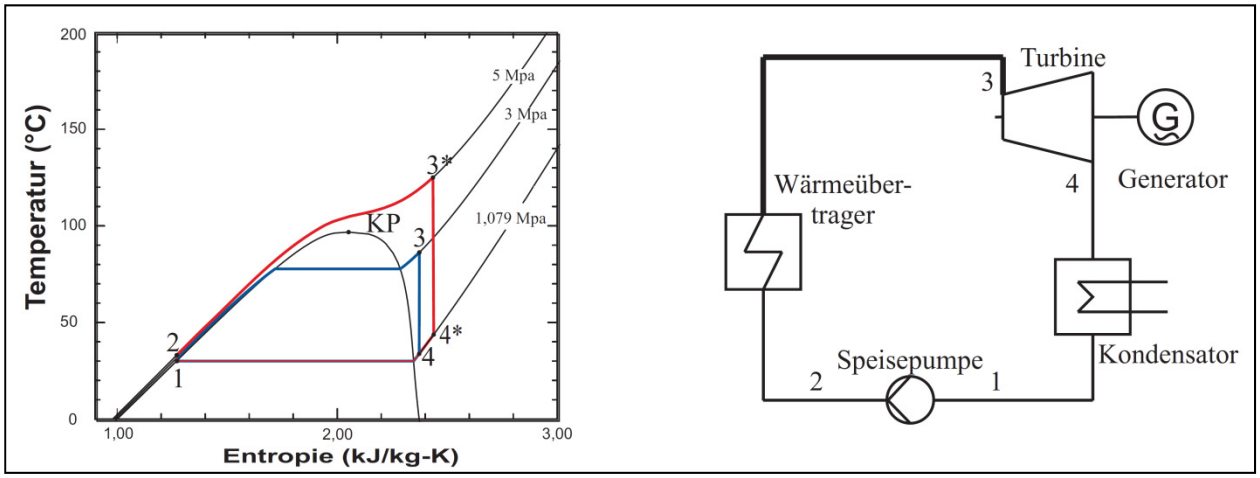

Figure 4.13: ORC at a T,s-diagram (left, sub- and supercritical) and scheme (right) [Vetter 11].

Figure 4.13 illustrates a typical ORC. From state 1 the working fluid is sucked into a pump and compressed to state 2. The working fluid is now sub cooled and streams through a boiler. Within this boiler waste heat is absorbed and leads to an isobaric pre-heating, phase change by evaporation and superheating of the working fluid until state 3 is reached. Then follows the expansion through a turbine and ends in state 4. In between these both states, 3 and 4, mechanical power is produced, which is generated by an attached generator into electricity. The isobaric condensation of the working fluid closes the thermodynamical cycle and liquefies the working fluid until state 1 is reached. Depending on the pressure, the heat charge proceeds at subcritical (blue line in *figure 4.13*) or supercritical (red line in *figure 4.13*) state in the boiler. The state of critical point (KP) depends on the type of working fluid and is an indication of usability regarding application temperature ranges.

Within the depicted states the enthalpy differences enable the calculation of specific energies of each attachment.

$$w_{\text{pump}} = h_2 - h_1 \tag{4.10}$$

$$q_{\text{charge}} = h_3 - h_2 \tag{4.11}$$

$$w_{\text{turbine}} = h_4 - h_3 \tag{4.12}$$

$$q_{\text{discharge}} = h_4 - h_1 \tag{4.13}$$

Here w_{pump} and w_{turbine} are the specific work of pump and turbine or rather q_{charge} and $q_{\text{discharge}}$ are the specific heat of boiler and condenser. With these equations the thermal efficiency of an ORC can be expressed by *equation 4.14*.

$$\eta_{\mathrm{ORC,thermal}} = \frac{|l_{\mathrm{turbine}}+l_{\mathrm{pump}}|}{q_{\mathrm{charge}}} = \frac{|(h_4-h_3)+(h_2-h_1)|}{h_3-h_2} \tag{4.14}$$

This description demonstrates an ideal cycle. But in reality pressure drops in pipes and attachments as well as further insert or loss of heat to the surrounding exists. Equally the pump and turbine does have losses caused by irreversibility. This is expressed as η_{pump} and η_{turbine}, the efficiencies of pump and turbine. Here, the indices *s* describes the resulting isentropic state.

$$\eta_{\mathrm{pump}} = \frac{h_{2s}-h_1}{h_2-h_1} \tag{4.15}$$

$$\eta_{\mathrm{turbine}} = \frac{h_3-h_4}{h_3-h_{4s}} \tag{4.16}$$

Significant advantages of ORC plants, especially for the conversion of waste heat at low temperature ranges, compared to the common water vapour driven Rankine Cycle are

1. Relatively high vapour pressure (above atmosphere pressure in condenser),
2. Increase of heat conversion efficiency due to less latent heat (better matching at heat transfer) and
3. Increase of handling the heat gradient per turbine stage which decrease the size and simplifies the turbine and makes it more economical [Vetter 11].

The application and choice of working fluid depends on thermo-physical properties like

a) Type of working fluid (see *figure 4.14* for wet, dry or isentropic fluids)

b) Latent heat, density, heat conductivity and specific heat

c) Effectiveness and conversion efficiency by superheating

d) Critical Point

but also parameters such as

e) Stability of the fluid and compatibility with materials in contact

f) Environmental aspects (OPD, GWP and ALT)

g) Safety (non-corrosive, non-flammable and non-toxic)

a) Availability and cost.

It should be noted that the gradient and shape of saturation curve is the most important property after the thermal matching with the heat transfer fluid regarding the calculation for such ORC. Depending on the gradient of the saturated vapour line it has to be distinguished between wet, dry and isentropic fluids as depicted in *figure 4.14*. Wet fluids have to be superheated due to the constructive limitation by the vapour content ($x > 0.9$) after the expansion in the turbine. However, dry fluids feature no challenges regarding superheating in boiler and less droplet in the turbine because the two phase area cannot be reached due to the positive gradient of the saturated vapour line and isotropes. But those possess a more superheated state after expansion at the condenser inlet. Economical factors, like a small scale of condenser (require low deheating section in condenser) and more efficient heat charge, therefore leads to the usage of recuperation. This

heat exchanger realises the heat discharge by deheating and uses the recovered heat for preheating of the working fluid before it streams into the boiler as depicted in *figure 4.14*.

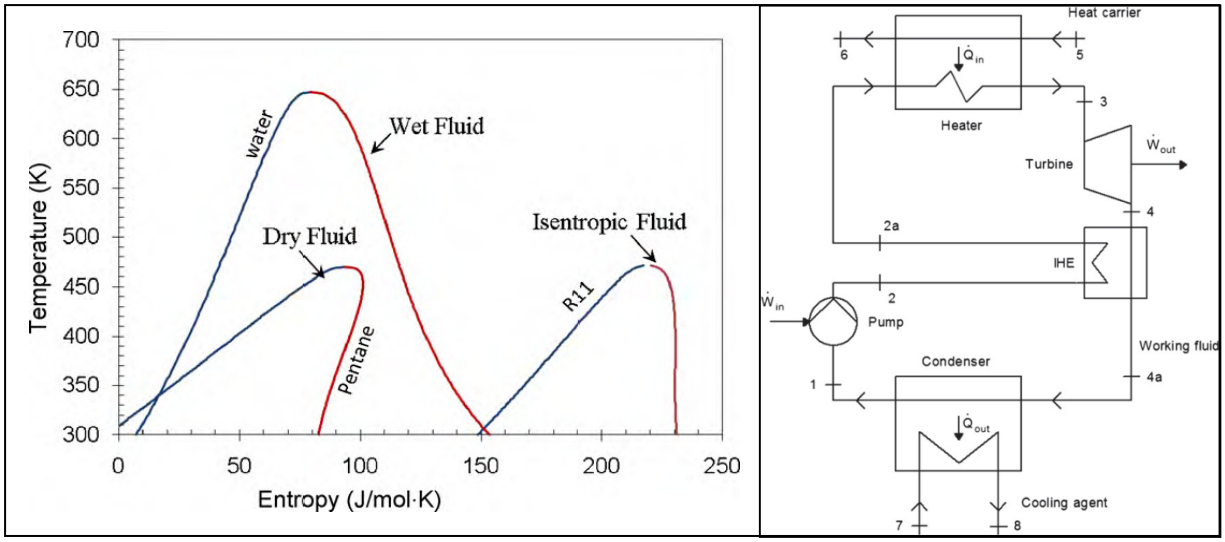

Figure 4.14: Types of working fluids (left) [Chen 10] and configuration of an ORC with recuperation (IHE, right) [Fischer 11].

A high specific work of turbine is reached when expanding to condensation temperature. [Förster 06] states that an increased averaged temperature at the heat charge and decreased averaged temperature at the heat discharge can be achieved by wet fluids compared to dry fluids. According to Carnot this leads to an increased thermal efficiency of the system (see *equation 4.4*).

4.2.3. Organic Flash Cycle

The OFC, also known as triangular or trilateral flash cycle, is still in a state of technical development and less known and is therefore described in a more detail than the ORC. This type of flash cycle is common in geothermal plants with water as working fluid. As OFC´s are less similar to Carnot cycles than Rankine cycles one expects OFC to have a smaller thermal efficiency than ORC at the same cycle temperatures. The advantage of the OFC, however, is the more efficient heat transfer from the heat carrier to the working fluid at low temperatures. Here, an organic fluid serves likewise as working fluid. The heat for an OFC (depicted in *figure 4.15*) is supplied from the heat carrier and removed by the cooling agent like the ORC. An OFC plant consists of a pump, a heater, a two-phase expander and a condenser. A schematic representation of the OFC in a T,s-diagram is also shown in *figure 4.15*, where CP is the critical point of the working fluid and the curve connecting points 1, 3, and CP is the boiling curve. At state 1 the working fluid is saturated liquid water at T_1 and the corresponding vapour pressure p_1, where T_1 is the minimum temperature and p_1 is the minimum pressure in the OFC. By adiabatic compression to p_2 which is the maximum pressure in the OFC, the state 2 is reached in the homogeneous sub cooled liquid at temperature T_2. The hypothetical state 2' (not shown in *figure 4.15*) lies on the isobar p_2 and has the same entropy as state 1 ($S_2' = S_1$). From state 2 the liquid working fluid flows isobarically through the heater till it arrives at its boiling temperature at state 3. The temperature T_3 is the maximum temperature in the OFC. During that process the working fluid takes

up the specific heat q_{23}. At state 3 the working fluid enters the expander where it undergoes a flash expansion till it arrives at state 4 in the wet vapour region with pressure p_1, temperature T_1 and the vapour content x. During that expansion the specific work w_{34} is delivered from the expander with the isentropic expander efficiency η_{expander}. The hypothetical state 4' lies on the isobar p_1 and has the same entropy as state 3. At state 4 the working fluid enters the condenser in which it returns isobarically to state 1 by releasing the specific heat q_{41} to the cooling agent.

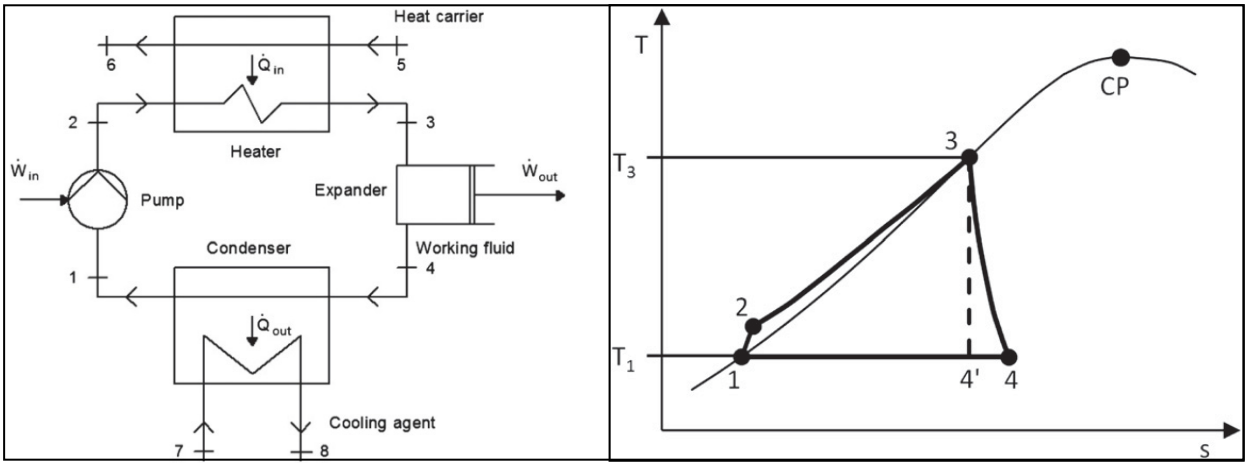

Figure 4.15: Configuration (left) and characteristics at a T,s-Diagram (right) of a typical OFC [Fischer 11].

Summarising, for the OFC the net specific work is

$$w = |w_{12} + w_{34}| = |(h_2 - h_1) + (h_4 - h_3)| \tag{4.17}$$

and the supplied specific heat is

$$q_{23} = (h_3 - h_2). \tag{4.18}$$

Then the thermal efficiency of the cycle is

$$\eta_{\text{OFC,thermal}} = \frac{w}{q_{23}} = \frac{|w_{12}+w_{34}|}{q_{23}} = \frac{|(h_2-h_1)+(h_4-h_3)|}{(h_3-h_2)}. \tag{4.19}$$

[Fischer 11] stated that an OFC has an efficiency which is 50 up to 100 % higher than those of an ORC. Model calculations for comparison of OFC and ORC have been published in [Zamfirescu 08]. They found that the exergy efficiency for power production, being the ratio of the net power output to the incoming exergy flow of the heat carrier, is about 2 up to 3 times larger for the OFC than for the ORC. [Fischer 11] stated that the exergy efficiency is between 14 and 20 % (for inlet temperature boiler T_5 at *figure 4.14* between 220 and 350°C) higher for the OFC than for the ORC and for T_5 = 150°C an additional advantage by 29 % for the OFC. The total exergy efficiency is slightly larger for the ORC than for the OFC for the case 62 to 280°C, in the other cases OFC is better between 1% and 9%. For a change of T_5 the exergy efficiencies of ORC do not change in a systematic way as optimal results are obtained from different organic working fluids and/or different cycle types. High exergy efficiency is desirable due to explanations in *chapter 4.2.1*. Therefore these results state a promising and at least equivalent heat recovery potential for OFC compared to ORC.

It should be noted that the two-phase expander is the technically most challenging component and can be e.g. a turbine, a scroll expander, a screw expander or a reciprocating engine. Recent developments are described for a screw-type engine in [Kliem 05] and for a reciprocating engine in [Löffler 07].

4.3. Potential of Casting Ingot Machine

The first promising heat source for a waste heat recovery system by ORC or rather OFC is the described water section one at the casting ingot machine. This heat source has a steady heat charge which is generally favourable for waste heat recovery solutions. Two layouts are considered and calculated. The short term heat recovery design, depicted in *figure 3.6* as well as in *figure 4.16*, is realisable without huge investment and further equipment regarding the heat transfer system. The subsequent ideal heat recovery design, depicted in *figure 4.23*, is driven by a pump in a closed heat transfer fluid (water) loop and thus differs from the short term heat recovery design.

4.3.1. Short Term Heat Recovery Design

A steady flow rate of water (56 m³/h), during the whole Charge 67801, absorbs 36,828 MJ at the casting ingot machine. This means that for running the casting ingot machine 7 h and 45 min a constant recoverable thermal power of 1,320 kW results, which has to be converted into electricity. It should be noted that the existing low water outlet temperature potential of 30°C challenges heat recovery solutions and therefore a higher water outlet temperature of 90°C would be preferable, as suggested in *figure 3.6*. This can be realised by combining the several water loop as described in *chapter 3.3* and therefore built the basis for the calculations within a temperature of 10 to 90°C. Additionally the consumption of water decreases down to 14.2 m³/h by changing loops and therefore creates an economical and environmental benefit. *Table 4.1* states the input data

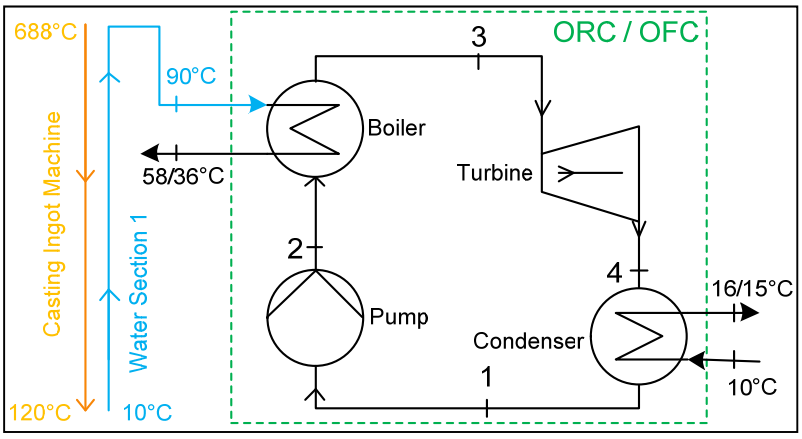

Figure 4.16: Design of the short term heat recovery system, CIM.

Table 4.1: Data input of calculation for the heat transfer fluid.

Casting:	465	min
p_{water}:	0,101325	MPa
$T_{water\ inlet}$:	10	°C
$h_{water\ inlet}$:	42,1188952	kJ/kg
$T_{water\ outlet}$:	90	°C
$h_{water\ outlet}$:	377,063487	kJ/kg
Q_{CIM}:	36828	MJ
Availability:	Constant	
$\dot{Q}_{thermal}$:	1320	kW
$\dot{m}_{water}$:	3,94095033	kg/s

for the heat transfer fluid and heat source. The starting point of calculation is the question about the maximal resulting net power output $P_{\max\,output}$. As working fluid for both low grade waste heat recovery solutions are chosen R134a, water and butane. R 134a is chosen as a well known

and most promising solution. It features a good thermo-physical match at the given heat source temperatures and has advantages regarding safety and availability compared to butane. Butane (R 600) is considered as a sustainable alternative working fluid due to its low GWP (GWP = 20) compared to R134a (GWP = 1300). As a further comparative working fluid water is chosen, which indicates concrete disadvantages regarding specific design parameters compared to both already mentioned fluids.

Calculation of the Organic Rankine Cycle

The following calculation procedure is described by a flow scheme in *figure 4.18*. It starts with setting the specifications of water as a heat transfer fluid and each chosen working fluid (R 134a, butane or water). The efficiencies are fixed values as well as the necessary pinches and temperature spread at the condenser, which are stated in *table 4.2*. The minimal condensation tempera-

Table 4.2: Input data for ORC the calculation procedure, CIM.

Working Fluid:	R 134a, butane or water
Heat Transfer Fluid:	Water
η_{pump} :	0.75
$\eta_{expander}$:	0.9
$\eta_{generator}$:	0.8
Pinch Heat Source :	10 K
$\Delta T_{heat\ sink}$:	5 K
Pinch Heat Sink :	10 K

ture is set to T_c = 25 °C by the given pinch of 10K for the heat sink, which describes the temperature difference between the temperature at the saturated vapour curve and cooling water at the same enthalpies (see *figure 4.17*), and a temperature spread of 5K at the equivalent state.

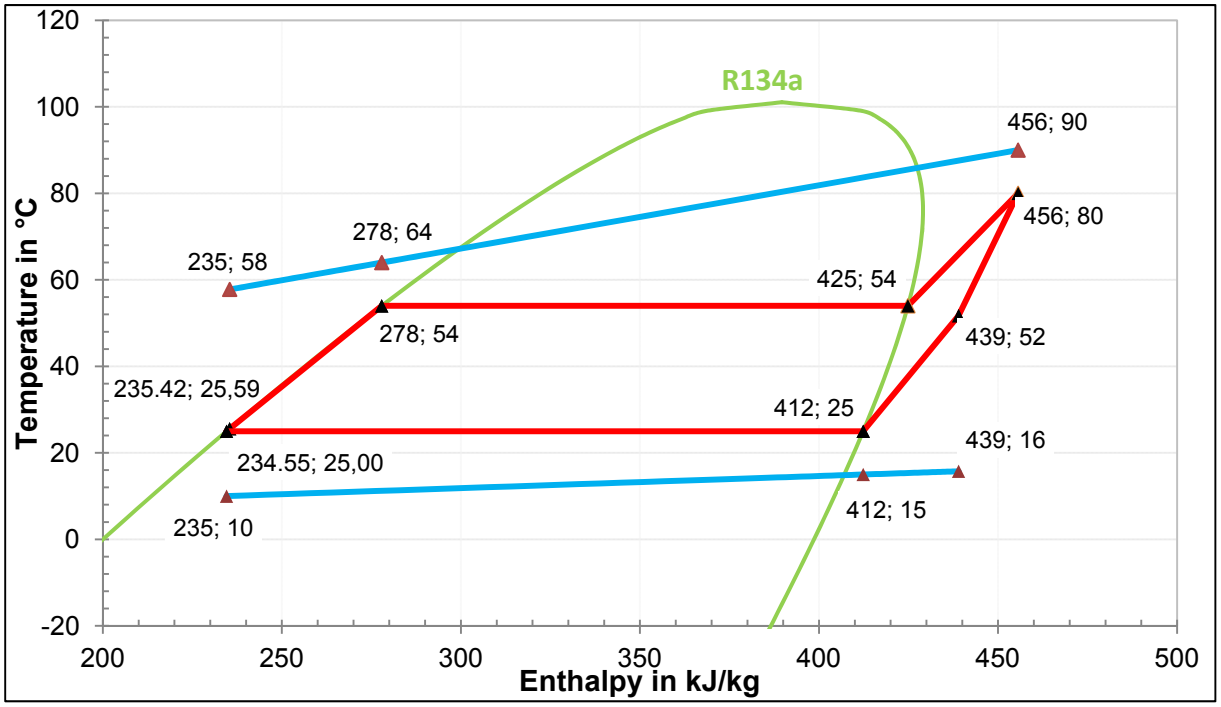

Figure 4.17: T,h-diagram of the short term heat recovery design with R134a as working fluid.

For this purpose the gradient of the heat transfer fluid has to be simplified as a linear function and set the downer limit of the thermodynamic cycle. The condenser effects no sub cooling of working fluid and the water outlet temperature in the condenser depends on the enthalpy state of turbine outlet. The upper cycle limit is generally set by the maximal heat source temperature (+90°C) and pinches of heat source (10K). These pinches are set at two points of the thermody-

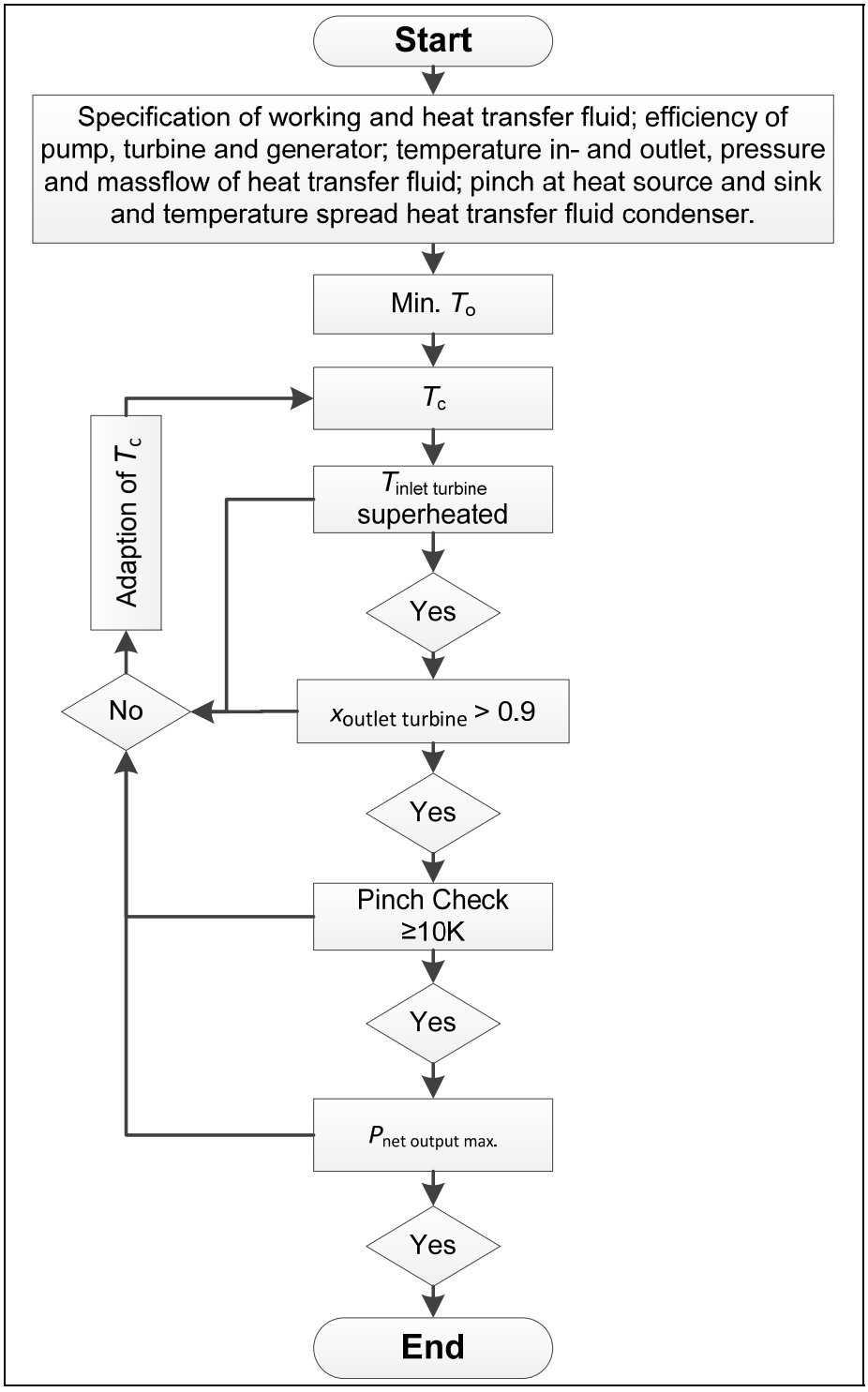

Figure 4.18: Simplified flow scheme of the ORC calculation procedure, CIM.

namical cycle. At first it is applied at the variable saturated liquid state of boiling temperature T_o and additionally at the fixed superheated inlet temperature state of turbine (+80°C). Therefore T_o

dictates the heat charge into the ORC and the outlet temperature of the heat charging fluid at the fixed state of enthalpy after the compression of the working fluid. The calculation procedure runs in 2K steps of boiling temperature T_o within the temperature range of +40 to +76°C. During this procedure three parameters are cross checked:

1. The state of superheat at the inlet of turbine ($T_{SH} > T_o$), attend hazard of droplets,
2. vapour content of the working fluid ($x > 0.9$), as turbine limitation, and
3. pinch check of ≥ 10K for the given sink and source of heat, so that the thermodynamic laws are attended.

In conclusion, it should be generally noted that pressure drops in the pipes and apparatuses as well as heat charge and discharge by surrounding is not accounted in those heat to power calculations at this disquisition.

Figure 4.19 depicts the results of the calculation procedure for the short term heat recovery design. $P_{max\ output}$ is detected at +54°C for R 134a and butane. R 134a with $P_{max\ output}$ = 30.5 kW is hereby identified as the best fluid solution regarding $P_{max\ output}$ in this comparison. Butane with $P_{max\ output}$ = 29.2 kW and water with $P_{max\ output}$ = 28.4 kW has slightly less $P_{max\ output}$ than R 134a. Furthermore is depict that controlling $T_{c,max}$ as high as possible will be most efficient, but that not most sufficient regarding the net power output. The most economical benefit

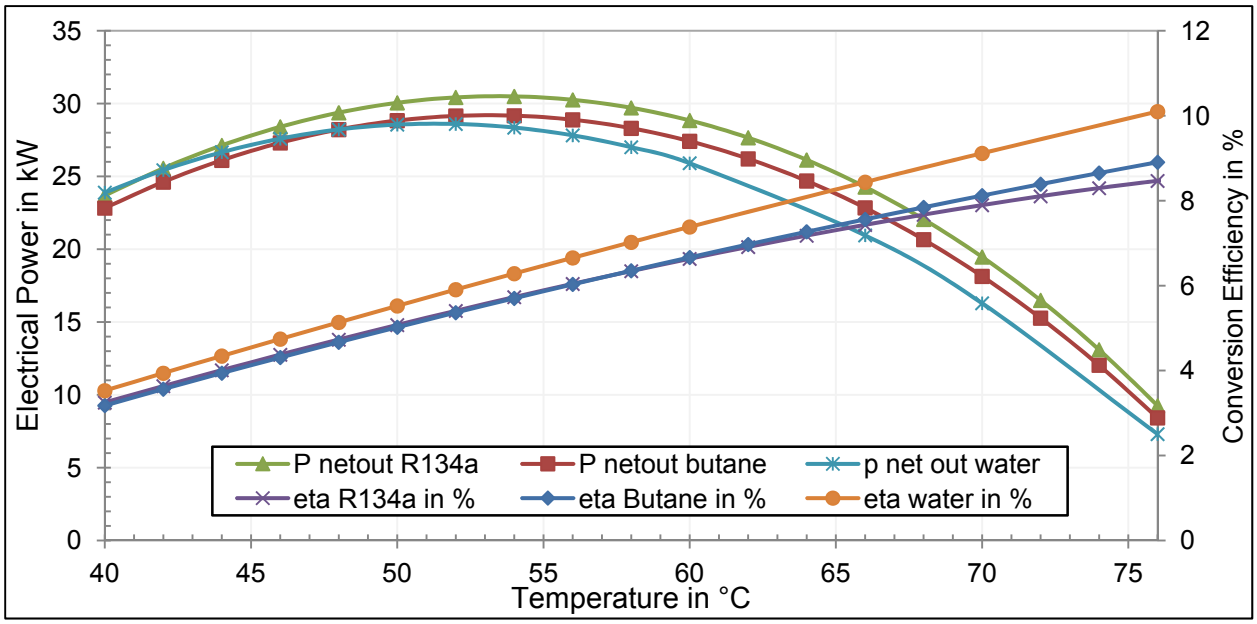

Figure 4.19: Net power output $P_{max\ output}$ and system efficiency η_{ORC} of the short term ORC design as a function of the boiling temperature T_o.

is therefore described with the most net power output for an ORC system which is mainly influenced by the heat charge and pressure drop above the expander. Controlling these states, by boiling temperature (54°C) or boiling pressure respectively, leads to the most usage and conversion of heat into power. The magnitudes in *figure 4.19* are expressed in *equation 4.20* and *4.21*. An overview of ORC energies is given in *figure 4.20*.

$$P_{max\ output} = \eta_{generator} \cdot \dot{m}_{R134a} \cdot \left(|h_4 - h_3| \cdot \eta_{expander} - (h_2 - h_1) \cdot \eta_{pump} \right) \quad (4.20)$$

$$\eta_{ORC} = \frac{P_{max\,output}}{\dot{Q}_{23}} = \frac{\eta_{generator} \cdot \left(|h_4 - h_3| \cdot \eta_{expander} - (h_2 - h_1) \cdot \eta_{pump} \right)}{h_3 - h_2} \quad (4.21)$$

Table 4.3 lists the resulting and distinctive parameters for each working fluid at the maximal net power output and therefore a comparison of the chosen fluids for this application. It is shown

Table 4.3: Resulting cycle parameter at $P_{max\,output}$ and T_c = 54 °C for the short term ORC design.

	R134a	Butane	Water
$\dot{Q}_{heat\ source}$ in kW:	532.3	511.6	451.3
$P_{turbine}$ in kW:	40.2	37.3	35.5
P_{pump} in kW:	2.1	0.8	0.01
$P_{net\ output}$ in kW:	30.5	29.2	28.4
$\eta_{power\ cyle}$ in %:	5.7	5.7	6.3
$\rho_{inlet\ turbine}$ in kg/m³:	61.7	12.1	0.1
$\rho_{outlet\ turbine}$ in kg/m³:	28.1	5.4	0.02
x_6 in kg/kg:	1.150	1.169	0.960
$\dot{V}_{outlet\ turbine}$ in m³/h:	309.7	747.4	26,572.2
$\beta_{ratio\ \rho 6/\rho 5}$ in (kg/m³)/(kg/m³):	0.456	0.449	0.260
$\dot{V}_{inlet\ pump}$ in m³/h:	7.2	7.1	0.6
p_{HP} in MPa:	1.455	0.550	0.015
p_{LP} in MPa:	0.665	0.243	0.003
$\psi_{ratio\ pHP/pLP}$ in MPa/MPa:	2.187	2.259	4.739
$\Delta p_{HP\text{-}LP}$ in MPa:	0.790	0.306	0.012
$\dot{Q}_{recuperator}$ in kW:	64.375	68.515	-
$\dot{m}_{working\ fluid}$ in kg/s:	2.418	1.125	0.177

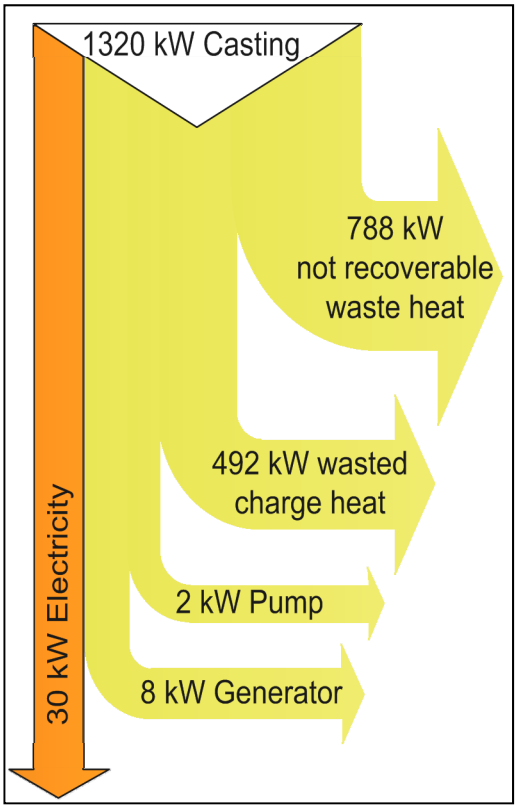

Figure 4.20: Sankey diagram of the short term ORC design with R 134a as working fluid.

that R 134a has the hugest heat load (532.3 kW). This is caused by the best thermo-physical match (latent heat and CP) and a sufficient requirement for heat to power conversion. But it should also be noted that R 134a has the largest pump energy consumption (2.1 kW) caused by the relative high mass flow (2.4 kg/s). Water indicates that ORC cannot be rated just by conversion efficiency, because water has here the best results (6.3 %) but the lowest net power output (28.4 kW). The densities and volume flow rates at the turbine are parameters of size. High densities and low volume flow rate are promising parameters for a feasible and economical implementation of an ORC. Here, water indicates huge flow rates (26,572 m³/h) caused by low densities (0.02 kg/m³). A further undesirable parameter of water is the pressure. Both, high and low pressures of the ORC are lower than the atmospheric pressure. Therefore leakage causes a contamination of the system by air and leads to corrosion at the interior of the equipment. R 134a and butane possess higher pressure levels which are above the atmospheric pressure but at manageable pressure levels. Another parameter x indicates the vapour content of the working fluid in the outlet of the turbine. Less than one indicates an expansion into the two-phase area and greater one means superheated state. As mentioned before superheated states after the turbine are undesirable. The range between the saturated vapour state and $x > 0.9$ has to be targeted, because this leads in most of the cases to an increase of generated power [Fischer 11]. Therefore $\dot{Q}_{recuperator}$

is an indicator for wasted heat charge and should be as small as possible ($\dot{Q}_{\text{opt. recuperator}}$ = 0 kW) for getting $P_{\text{max output}}$.

Calculation of the Organic Flash Cycle

The OFC calculation uses equal data inputs as the ORC calculation before. The efficiency for a two-phase expander is at present generally lower than those for a single phase expander. This is accounted for calculations with an adaption of η_{OFC} = 0.6, as stated in *table 4.4*. Research and development for those applications continue and promise a further increase of the expander efficiency (0.6 < η_{OFC} < 0.85) [Kliem 05]. The expander inlet state of T_0 = 80°C results at the heat source pinch of 10K as well as the boiler outlet temperature of 35.52 °C of the heat charging fluid at the given enthalpies of the OFC. Within the temperature range of 25.52 and 80°C, the saturated liquid curve is simplified as a linear function which leads to a slightly underrun of the pinch. But this underrun is marginal and theoretical. In reality the laws of thermodynamic are respected. Therefore the boiling isobar runs along the saturated liquid curve and is masked by these. The condensing states of the working fluid and the heat sink temperatures results as described at the ORC application. *Figure 4.21* depicts the calculation results of the OFC for butane and shows the advantage of the OFC, the thermal matching. Considerably more heat can be

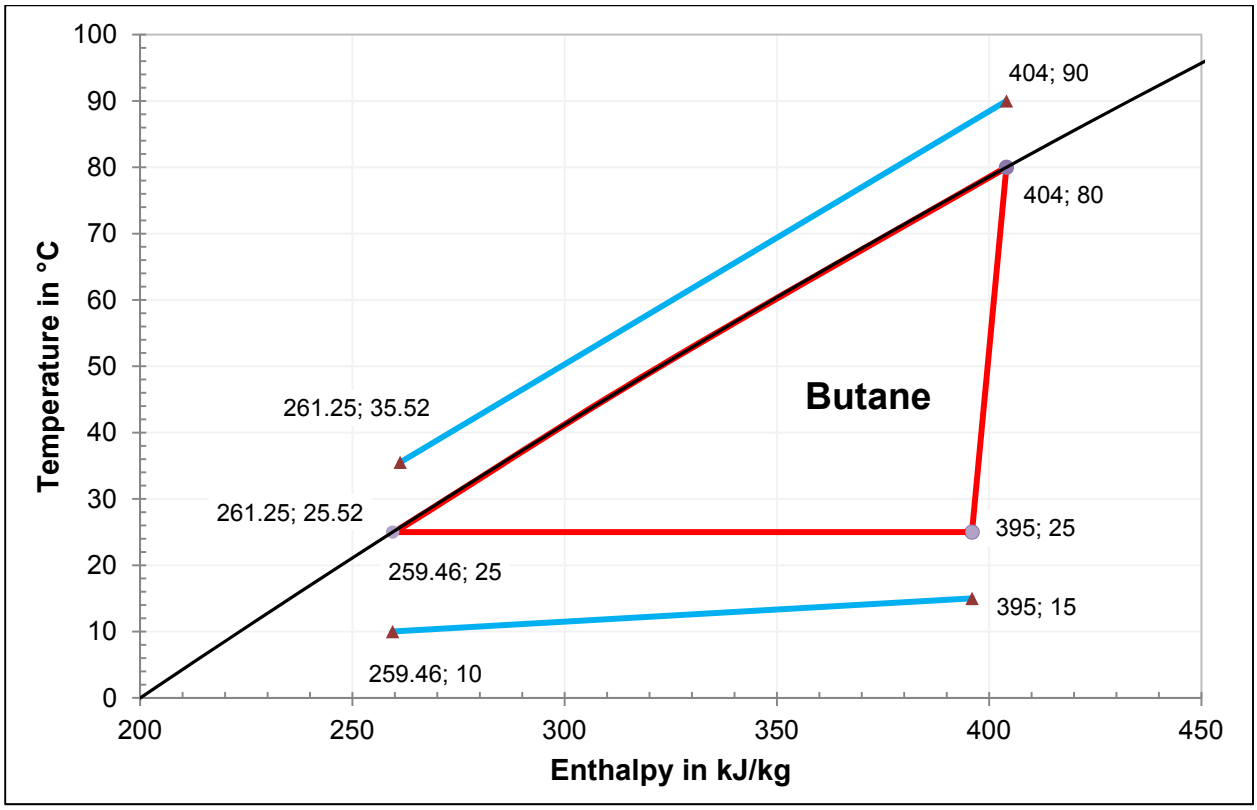

Figure 4.21: T,h-diagram of the short term heat recovery design with R134a as working fluid.

charged due to this effect. It can also be stated that the enthalpy difference of the OFC, which generates the heat into power, is relatively small (9 kJ/kg) compared to those of the ORC application of R 134a (17 kJ/kg), despite a greater pressure drop above of the expander. This is caused by the relatively huge positive gradient of the isotrope in the two-phase area compared to the

superheated area as well as the decreased expander efficiency and effects an increase of the working fluid mass flow as stated in *table 4.4*. The calculation procedure for the OFC has only one run, because the maximal power output is obviously at T_o = 80°C. The results for the short term OFC design are stated in *table 4.4* and show an increased recovery potential for the butane application (31.7 kW) compared to the ORC butane application (29.2 kW). The R 134a OFC application documents a decrease of $P_{\text{max output}}$ (27.7 kW) against the ORC design (30.5 kW).

Table 4.4: Resulting cycle parameter for the short term OFC design at T_c = 80 °C and η_{expander} = 0.6.

	R134a	Butane	Water
$\dot{Q}_{\text{heat source}}$ in kW:	882,8	898,4	906,9
P_{turbine} in kW:	57,0	50,9	44,9
P_{pump} in kW:	22,3	11,2	0,2
$P_{\text{net output}}$ in kW:	27,7	31,7	35,7
η_{OFC} in %:	3,1	3,5	3,9
$\rho_{\text{inlet turbine}}$ in kg/m³:	928,2	500,4	971,8
$\rho_{\text{outlet turbine}}$ in kg/m³:	67,8	16,1	0,3
X_6 in kg/kg:	0,463	0,378	0,090
$\dot{V}_{\text{outlet turbine}}$ in m³/h:	547,4	1410,3	55105,5
$\beta_{\text{ratio }\rho6/\rho5}$ in (kg/m³)/(kg/m³):	0,073	0,032	0,0003
$\dot{V}_{\text{inlet pump}}$ in m³/h:	30,7	39,5	14,2
p_{HP} in MPa:	2,633	1,012	0,047
p_{LP} in MPa:	0,665	0,243	0,003
$\psi_{\text{ratio pHP/pLP}}$ in MPa/MPa:	0,253	0,241	0,067
$\Delta p_{\text{HP-LP}}$ in MPa:	1,968	0,768	0,044
$\dot{m}_{\text{working fluid}}$ in kg/s:	10,304	6,291	3,941

For the OFC water application results the most net power output with $P_{\text{max output}}$= 35.7 kW against $P_{\text{max output}}$ = 28.4 kW at the ORC before. The conversion efficiency of the OFC is generally smaller (app. 3.5 %) than those of the ORC (app. 5.7 %). This is caused by an increase of the charged heat. Here the most promising OFC application, with butane as a working fluid, differs 386.8 kW against the butane ORC application (511.6 kW). A comparison of *table 4.3* and *4.4* indicates further advantages and disadvantages of both solutions. An increase of the density combined with the increased mass flow for butane at the outlet of the turbine leads to a doubling of the volume flow rate at the outlet of the turbine. This is an indication of greater sizing of OFC plants compared to ORC plants which is an important factor if looking for an implementation place. Furthermore, it can be stated that a much higher energy consumption of OFC pumps, than those of ORC pumps, is the result. R 134a and butane show here approximately ten times higher energy consumption. Finally, it should be noted that the pressure levels are two times higher than those of the ORC, regarding R 134a and butane.

For a direct comparison to the ORC *figure 4.22* is generated which depicts the $P_{\text{max output}}$ for prospective expander efficiencies of η_{expander} = 0.9 and existing η_{expander} = 0.6. Therefore the

design potential for the OFC future of this application is given and state that equal expander efficiencies lead to much higher $P_{\text{max output}}$ results (between 50.5 and 53.7 kW, as depicted in *figure 4.22*, left).

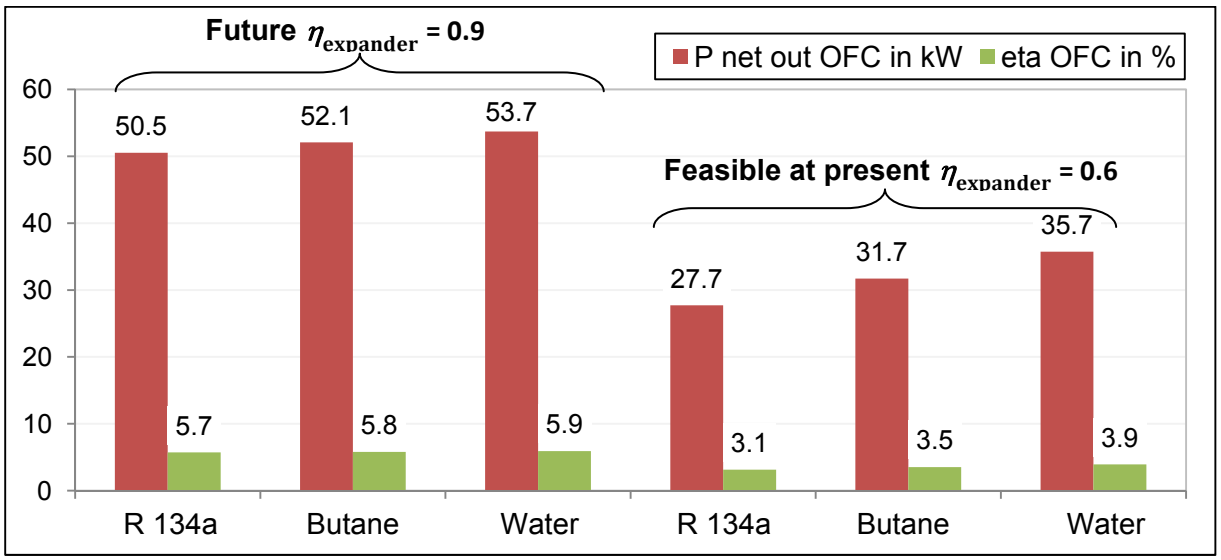

Figure 4.22: Comparison of calculation results for different expander efficiencies (η_{expander} = 0.9 and η_{expander} = 0.6) at the short term OFC design.

4.3.2. Ideal Heat Recovery Design

A further improvement of the cooling loop at the CIM can be established by a closed cooling water loop as depicted in *figure 4.23* and leads to the ideal heat recovery design. This change of layout leads to an avoiding water consumption compared to the short term heat recovery design,

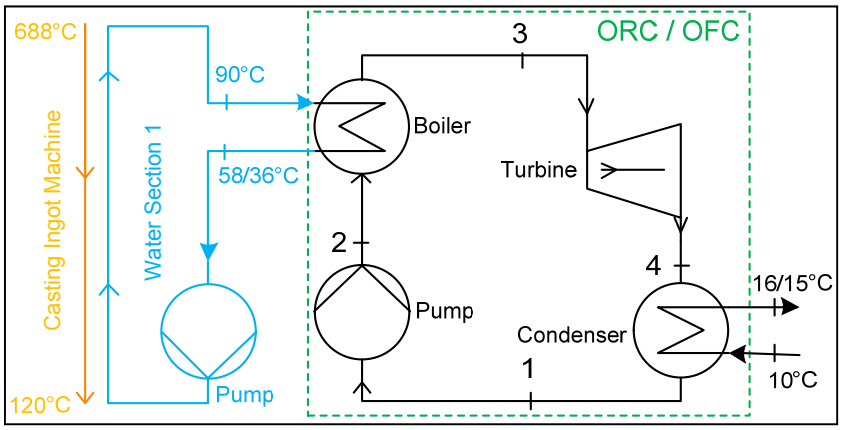

Figure 4.23: Design of the ideal heat recovery system at the CIM.

because the water is cycled and not wasted as before. This effects the implementation of new equipment (pump). Only the water during the maintenance has to be wasted. Furthermore an increase of the water inlet temperature at the CIM has to be considered. For the ORC this temperature results at 57.8°C and for the OFC at 35.52°C, to anciently 10°C. Therefore the temperature spread for each application decreases and effects an increase of the passing cooling water

mass flow at the same heat charge of CIM. The resulting mass flows are the ratios of both changed temperature spreads and the heat charge of the CIM (1,320 kW) and can be expressed by *equation 4.22*.

$$\dot{Q}_{\text{heat charge CIM}} = \dot{m}_{\text{ideal water}} \cdot c_{\text{p,water}} \cdot (T_{\text{outlet CIM}} - T_{\text{inlet CIM}}) \quad (4.22)$$

For the ORC application results $\dot{m}_{\text{ideal water ORC}}$ = 9.78 kg/s (35.21 m³/h) and for the OFC application $\dot{m}_{\text{ideal water OFC}}$ = 5.79 kg/s (20.83 m³/h). In *table 4.1* $\dot{m}_{\text{water}}$ = 3.94 kg/s (14.21 m³/h) for the short term design is stated. Thereby, the heat charge increases at the same given enthalpy states of both power cycles due to *equation 4.23*.

$$\dot{Q}_{\text{heat charge cycle}} = \dot{m}_{\text{ideal water}} \cdot (h_{\text{outlet boiler}} - h_{\text{inlet boiler}}) \quad (4.23)$$

The heat charge of thermodynamic cycles increases by the given mass flow factors of 2.48 for the ORC and 1.47 for the OFC to 1,320 kW. This means the whole heat charge of the CIM has to be absorbed by the thermodynamical cycles and therefore can be used for the heat to power conversion. Therefore, it finally results in an increased net power output for both applications against the short term design. The ideal ORC design generates now 75.7 kW for R 134a and the OFC 46.6 kW for butane, which represent the most promising heat recovery solutions for the CIM. It should be noted that such an ideal design is feasible for the existing plant and is no fictive imagination. The existing water flow rate of 56 m³/h is higher and the plant is therefore constructed. The heat transfer from the casting mould to water would be equal, because the decreased temperature spread will be balanced through an increased heat transfer coefficient, caused by the increased velocity for each water section. It should be also noted that this assumption has to be proven before running such a concept to ensure the essential heat discharge of the casting moulds. A further resulting advantage will be a decrease of pump power consumption for the cooling water supply. This can be simplified expressed by *equation 4.24*.

$$P = \Delta p \cdot \dot{V} \quad (4.24)$$

Caused by the decrease of cool water flow rates, regarding the existing layout, -37 % energy for the ORC and -62.8 % for the OFC application will be consumed, at a constant pressure drop.

4.3.3. Conclusion

This subchapter processed the waste heat recovery at the casting ingot machine of PFA 2. The heat recovery potential is considered for an ORC and OFC application at water section one (see *figure 2.3*). This heat source has a steady heat charge of 1,320 kW at water section one for the whole casting session, which is generally favourable for waste heat recovery systems. The working fluids are R 134a, butane and water. At which water serves as a comparative working fluid that is passed out as solution by specific cycle parameters (like low pressure and high volume flow rates). Two design layouts are considered and calculated. The short term heat recovery design (see *figure 3.6* and *figure 4.16*), describes an easily realisable open loop concept. Here are the most promising calculation results at 30.5 kW for the ORC with R 134a as working fluid and 31.7 kW for the OFC with butane as a working fluid. The subsequent ideal heat recovery design (see *figure 4.23*) is driven by a pump in a closed water loop at the CIM and thus differs from the short term heat recovery design. This concept leads to improved calculation results. For the R 134a ORC design results a net power output of 75.7 kW and for the butane OFC design 46.6 kW. It can therefore be stated that the postulated exergetic advantages in *chapter 4.2.3*, of the OFC against the ORC, are not existent for the ideal heat recovery design. It can be stated that the ideal R 134a ORC design is the most promising waste heat to power conversion processes. The following annual energy recovery potential, depicted in *figure 4.24*, is the result for two casting sessions per day during one year (365 days).

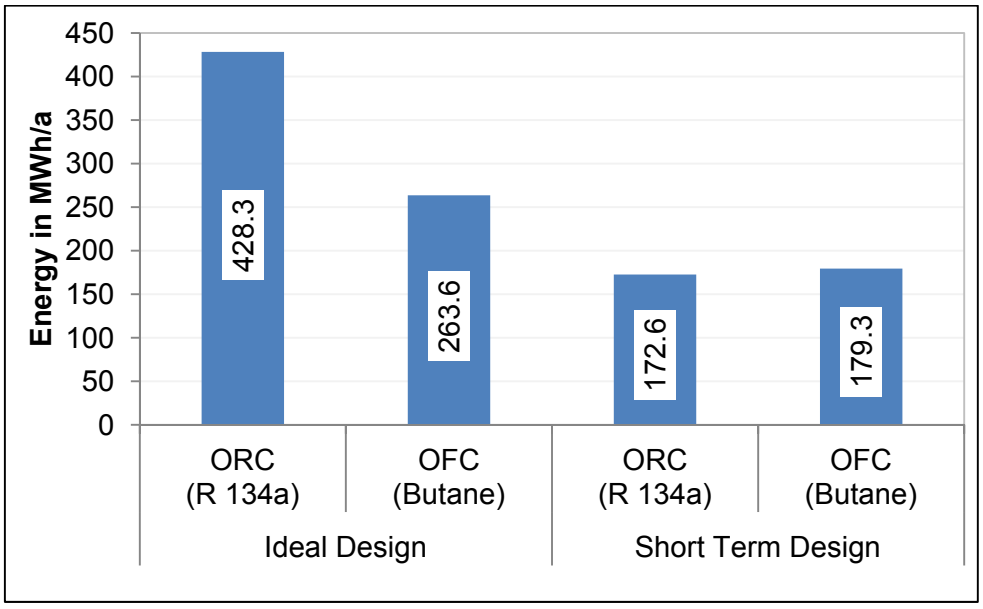

Figure 4.24: Annual energy recovery potential of most promising ORC and OFC designs at the casting ingot machine, PFA 2.

4.4. Potential of Furnace 9

The other promising waste heat source for an improvement of energy efficiency by heat to power at PFA 2 is the mentioned wasted flue heat of furnace 9. This total heat sum of 32,899 MJ is represented by the addition of wasted false air (6,797 MJ) and theoretical combustion gas heat (26,102 MJ), which are stated in *table 3.1*. This means that 26,102 MJ are alternately wasted caused by the theoretical combustion gas while the burner is on and for the rest of process time 6,797 MJ are relative constantly wasted by the insert false air (see *figure 4.25*). The flue waste heat can be time sequenced split, as described in *table 4.5*, into several power ranges of 618 up to 2,060 kW. While the burner is shut down (6h 29min) a heat power range between 136 and 463 kW results, caused by the stack effect. While the burner is running (8h 15min) a heat power

Table 4.5: Listed flue waste heat of Charge 67801 caused by combustion gas and false air, at a reference temperature of 25°C.

Range of waste heat	Time in min	Time in %	$T_{\text{flue gas, arithm.}}$ in °C	$Q_{\text{flue gas}}$ in MJ	$P_{\text{flue gas average}}$ in kW
100 and >90% (2060 and >1854 kW)	78	9%	1,069	9,190	1,964
≤ 90 and >70% (≤ 1854 and >1442 kW)	60	7%	940	6,088	1,691
≤ 70 and >50% (≤ 1442 and >1030 kW)	8	1%	798	638	1,329
≤ 50 and >30% (≤ 1030 and >618 kW)	94	11%	839	4,362	773
≤ 30 % (≤ 618 kW)	644	73%	650	12,621	327

range of 7 to 2060 kW is wasted through flue gas. *Figure 4.25* depicts the evaluated flue waste heat of the furnace in detail. $T_{\text{exhaust measure}}$ indicates the measured temperature in the exhaust pipe during the measure campaign of Charge 67801, located and stated in *figure 3.1*. The flue mass flow $\dot{m}_{\text{flue gas}}$ results by division of the volume flow rate of flue $\dot{V}_{\text{flue gas}}$ and the density of $\rho_{\text{air,25°C}}$. Thereby $\dot{V}_{\text{flue gas}}$ consists of the time sequenced insert false air volume flow rate and the sum of combustion components, the air and natural gas volume flow rates. $\dot{Q}_{\text{flue}}$ results then as the heat power of flue waste heat at the given enthalpy difference of flue Δh_{flue}. The simplified enthalpies of flue are assumed by the enthalpies of air as stated in *equation 4.25*.

$$\dot{Q}_{\text{flue}} = \dot{m}_{\text{flue gas}} \cdot \left(h_{\text{air,T}_{\text{exhaust measure}}} - h_{\text{air,25°C}}\right) = \dot{m}_{\text{flue gas}} \cdot \Delta h_{\text{flue}} \qquad (4.25)$$

This evaluation of discharged flue waste heat, depicted in *figure 4.25,* represents the potential and basis for the following calculations of various heat recovery systems at the furnace. The calculations consider two design layouts, an indirect and direct ORC. The OFC is passed out due to decreased net power output results and decreased thermal match advantages for high temperature applications. The indirect heat recovery design runs with thermal oil as heat transfer fluid and is therefore thermally decoupled from the flue gas in the stack. The direct heat recovery system is directly conducted with the flue gas and therefore has to follow the heat power of flue and creates unsteady operation behaviour of the power plant.

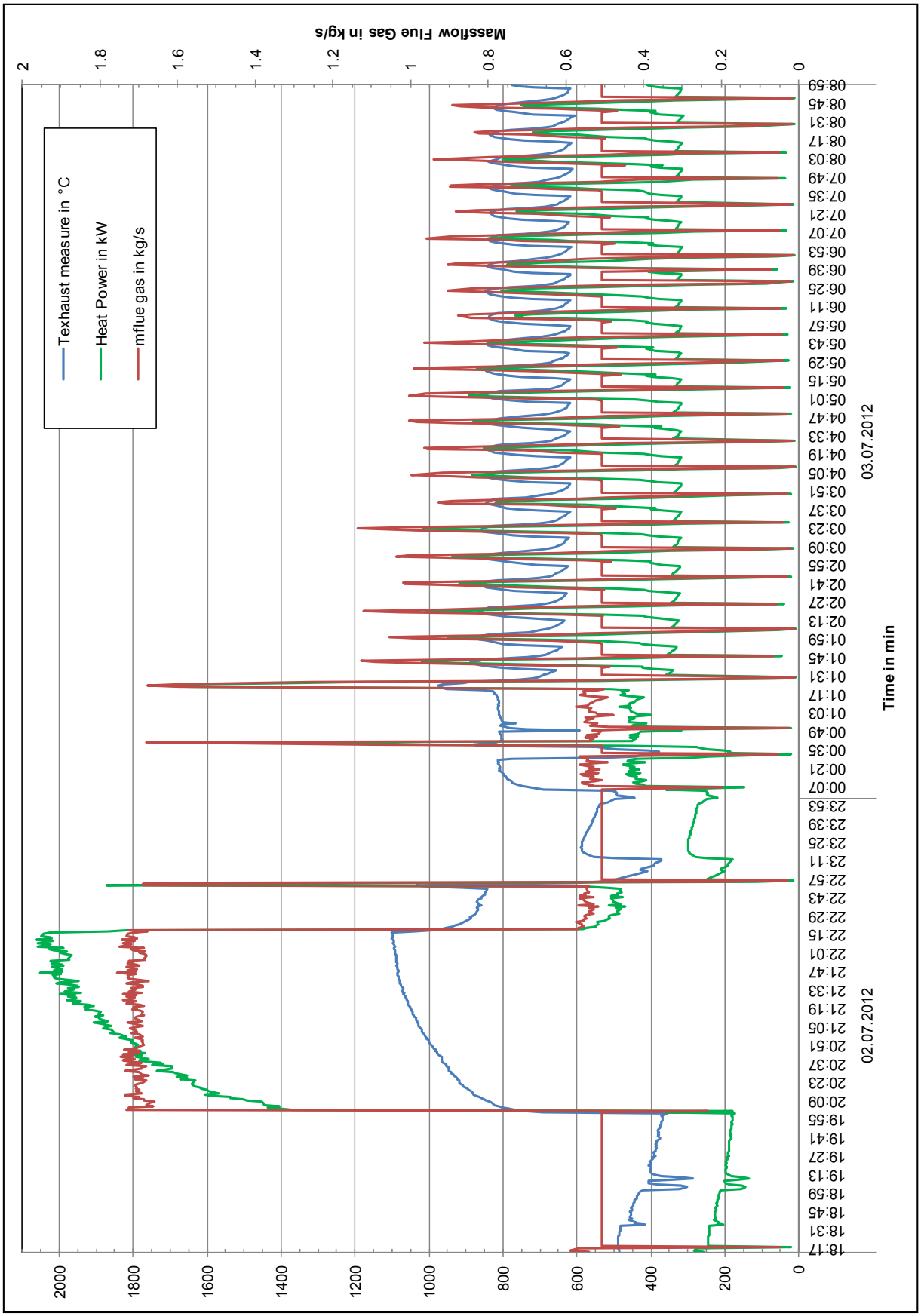

Figure 4.25: Logged temperature, evaluated heat power and mass flow of flue gas as a function of the process time at furnace 9, Charge 67801.

4.4.1. Indirect Heat Recovery Design

The indirect heat recovery design, realised as an ORC, is a basic application for generating flue waste heat into electricity. This is conceptual solved by the depicted scheme in *figure 4.26*. It illustrates the decoupling of heat source and power plant. It has the advantage that the ORC states are fixed magnitudes during the whole run of these thermodynamical cycles. Thereby constant conversion efficiencies can be stated which simplifies the calculation by linear relations.

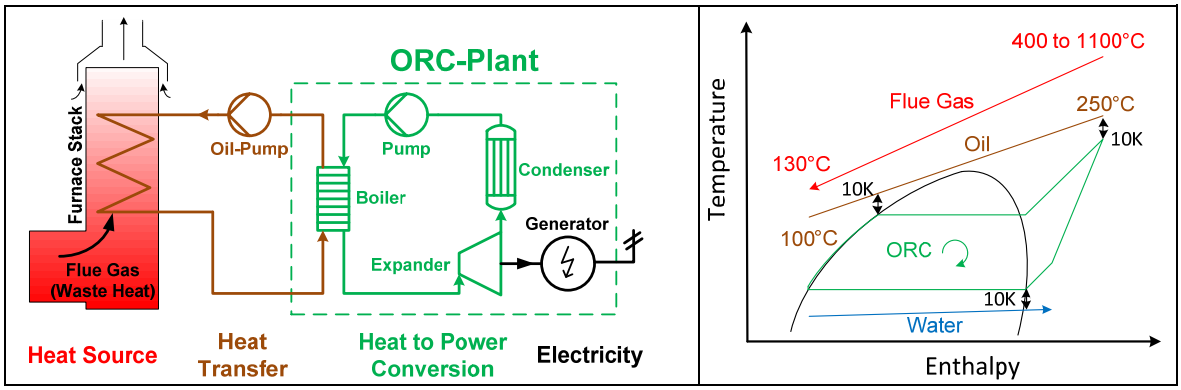

Figure 4.26: Scheme (left) and T,s-diagram (right) of an ORC as indirect heat recovery design.

Thus increased exergy losses have to be accepted caused by the additional temperature spread at the heat exchangers during the heat transformation. The heat of flue is absorbed by a thermal oil loop and runs with a circulation pump. Thereby the heat is transferred from the flue in the furnace stack to the heat exchanger of the power generating plant. This heat exchanger serves as a boiler and heats the working fluid from the saturated liquid to expander inlet state. Then the expansion of the working fluid follows to produce power. The condensation completes the thermodynamical cycle. As working fluids pentane, ammonia, R 245fa and toluene are chosen. Here pentane serves as preferred working fluid and is already applied by ORMAT in this temperature range as stated in [Ladam 12]. R 245fa and toluene are chosen due to their comparable and promising thermo-physical matching. Ammonia serves as a well known working fluid and serves as a reference. [Quoilin 11] and [Tchanche 11] list further possible working fluids. The boiler in- and outlet temperature of thermal oil is set to 250 and 100°C, as depicted in *figure 4.26*. This range is fixed irrespective of the temperature and mass flow of flue gas. However, this requires an adaption of the thermal oil mass flow and finally the ORC working fluid mass flow. The flue gas temperature varies within a temperature range of 288 and 1100 °C at the beginning of the heat transfer. The throughput temperature of stack is defined at 130°C by a pinch of 30K and is fixed for the whole session. As heat sink serves, as stated before, water at 10°C and 5K temperature spread till the saturated vapour enthalpy. Hereby it serves as the lower limitation of the thermodynamical cycle and generates the condensation temperature of 25°C and condenser outlet temperature. The heat source defines the upper limitation by a given pinch of 10K, whereby results the boiler pressure and the inlet state of expander. With respect to further input data, stated in *table 4.6*, results the depicted ORC in *figure 4.27*. It represents the visual calculation results of pentane for the indirect ORC application.

Table 4.6: Input data for the calculation procedure of furnace 9.

Working Fluid:	Pentane, R245fa, toluene and ammonia
Heat Transfer Fluid:	air
η_{pump} :	0.75
$\eta_{expander}$:	0.9
$\eta_{generator}$:	0.9
$T_{2,\ heat\ tranfer\ fluid,\ min}$:	130°C
$T_{1,\ heat\ transfer\ fluid,\ max}$:	1100°C
$p_{\ heat\ source}$:	0.101325 MPa
$\dot{m}_{\ flow\ heat\ source}$:	Unsteady (0.05 to 1.75 kg/s)
Pinch Heat Source :	10K
$\Delta T_{\ sink}$:	5K
Pinch Heat Sink:	10K

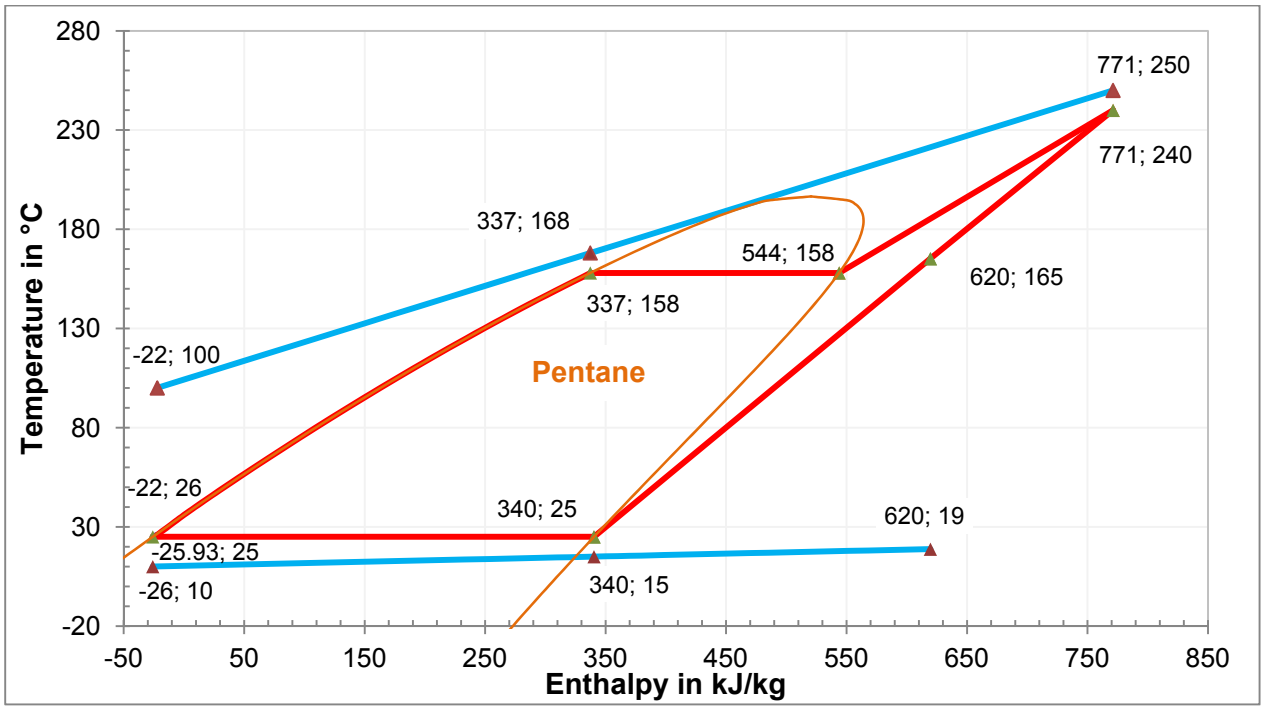

Figure 4.27: T,h-diagram of the indirect heat recovery design with pentane as working fluid.

The detailed calculation results for each working fluid are listed in *table 4.7*. Here has to be noted that R 245fa runs at a supercritical pressure level (p_{boiler} =50 bar and $p_{boiler} > p_{crit}$), as depicted in *figure 4.28*. The results show generally increased conversion efficiencies due to increased heat source temperatures (see *chapter 4.2.1*). Here R 245fa states the highest (17.98 %) and ammonia the lowest (15.23 %) efficiency. A fixed maximal heat charge of 1,875 kW leads to the same order of magnitudes for the net power output $P_{net\ output}$. Here the maximal net power output results for R 245fa at $P_{net\ output}$ = 337.13 kW. Further advantages of this fluid choice can be noted by the sizing factors like in- and outlet densities (relative high) and volume flow rate at the outlet of the turbine (relative low). The high pressure level of R 245fa equals ammonia and is higher than those of toluene and pentane. This can be also stated for the low pressure level where R 245fa has the desirable positive pressure (compared to atmospheric pressure) in the system.

Huge deheating powers between 233.1 and 659.84 kW should be noted. Here the use of a recuperation would be a promising way of optimised calculation.

Table 4.7: Calculation results of the indirect ORC design.

	Pentane	R245fa	Toluene	Ammonia
$\dot{Q}_{\text{heat source}}$ in kW:	1875	1875	1875	1875
P_{turbine} in kW:	358.40	398.32	364.3	327.36
P_{pump} in kW:	8.91	23.73	0.66	10.03
$P_{\text{net output}}$ in kW:	314.54	337.13	327.27	285.60
$\eta_{\text{power cyle}}$ in %:	16.78	17.98	17.45	15.23
$\rho_{\text{inlet turbine}}$ in kg/m³:	36.41	986.83	3.83	21.48
$\rho_{\text{outlet turbine}}$ in kg/m³:	1.365	66.254	0.0981	5.73
x_6 in kg/kg:	1.76	1.46	1.44	1.176
$\dot{V}_{\text{outlet turbine}}$ in m³/h:	6233	267.8	93,306.4	713.6
$\beta_{\text{ratio } \rho 6/\rho 5}$ in (kg/m³)/(kg/m³):	26.67	14.9	39	3.75
$\dot{V}_{\text{inlet pump}}$ in m³/h:	13.7	13.25	10.6	6.79
p_{HP} in MPa:	1.83	5	0.173	5
p_{LP} in MPa:	0.068	0.148	0.004	1.003
$\Psi_{\text{ratio pHP/pLP}}$ in MPa/MPa:	26.71	33.73	45.45	4.98
$\Delta p_{\text{HP-LP}}$ in MPa:	1.75	4.85	0.169	3.99
$\dot{Q}_{\text{recuperation}}$ in kW:	659.84	562.43	461.66	233.1
$\dot{m}_{\text{working fluid}}$ in kg/s:	2.36	4.93	2.54	1.14
$\Delta T_{\text{superheated}}$ in K:	82	supercritical	109.5	151.1

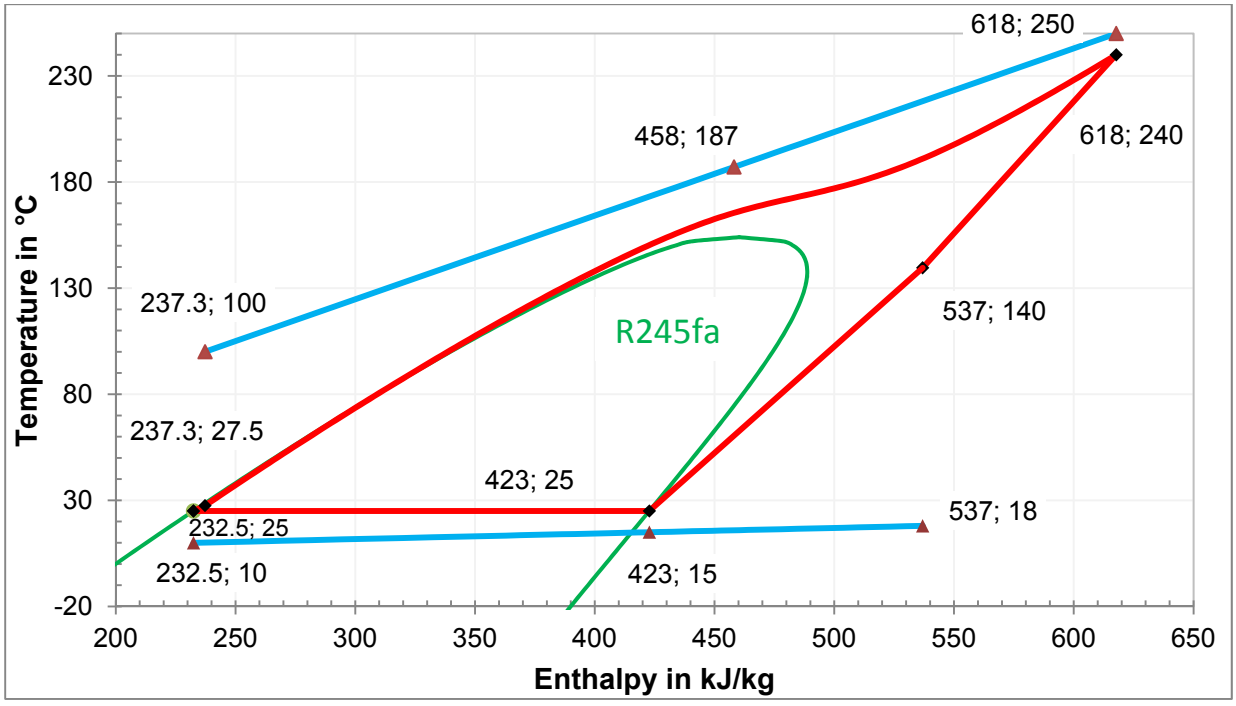

Figure 4.28: T,h-diagram of R 245fa as a supercritical indirect heat recovery system, furnace 9.

The simplification through the decoupled heat transfer states constant heat conversion efficiencies due to constant enthalpies of the thermodynamical cycle. However, the heat charge is unsteady as described before. For the integration of the convertible heat charge *equation 4.26* is used.

$$\dot{Q}_{\text{ORC flue heat charge}} = \eta_{\text{ORC}} \cdot \dot{m}_{\text{flue gas}} \cdot \left(h_{\text{air,T}_{\text{exhaust measure}}} - h_{\text{air,25°C}}\right) \qquad (4.26)$$

Hereby results for $\eta_{\text{ORC pentane}}$ = 16.78 %, the integrated flue mass flow $\dot{m}_{\text{flue gas}}$ and enthalpies h_{air} of Charge 67801 a total net power output of 1,341.8 kWh. Extrapolated for one year (365 days) and daily one casting session, a total recovered energy of 498,76 MWh/a for the indirect pentane ORC application results. The results for each working fluid are depicted in the following *figure 4.29*.

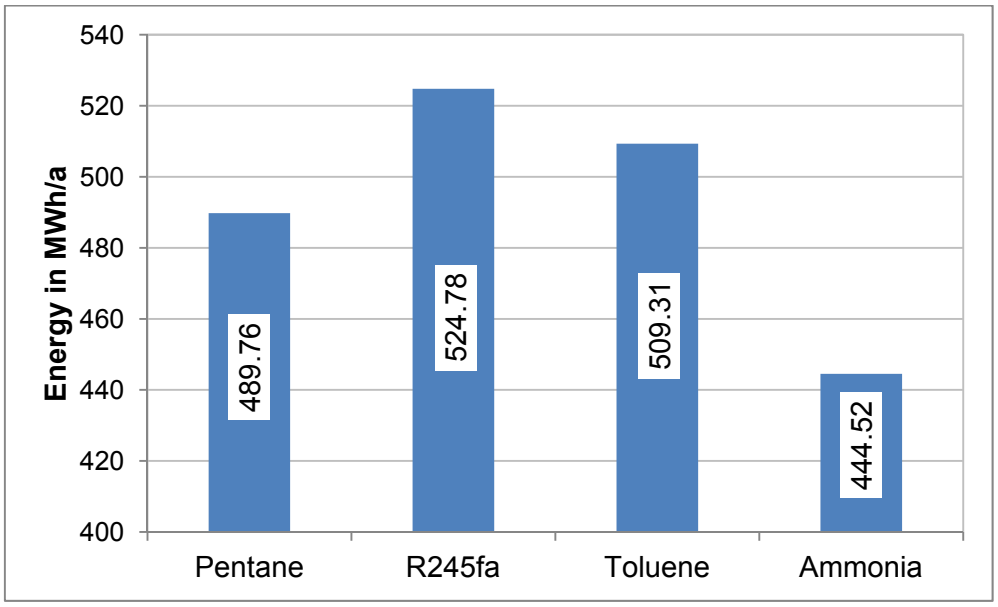

Figure 4.29: Annual energy recovery potential of the direct heat recovery system for each working fluid, Charge 67801.

4.4.2. *Direct Heat Recovery Design*

The direct heat recovery design differs from the indirect by the elimination of the thermal oil heat transfer loop, as depicted in *figure 4.30*. This has the advantage that exergy losses are reduced compared to the indirect heat recovery design and therefore more convertible heat exists. The disadvantage is the alternating and challenging operation behaviour of the power plant due to the directly coupled cycle. This requires the determination of a function which expresses the varying conversion efficiencies with respect to the flue mass flow and temperatures (optimised states, see *figure 4.31*). Water serves as working fluid because it is highly thermally resistant compared to common organic fluids. [Ladam 12] states that ORC do not tolerate temperatures above 250°C. The upper thermal limitation is set to 600°C and 50 bar.

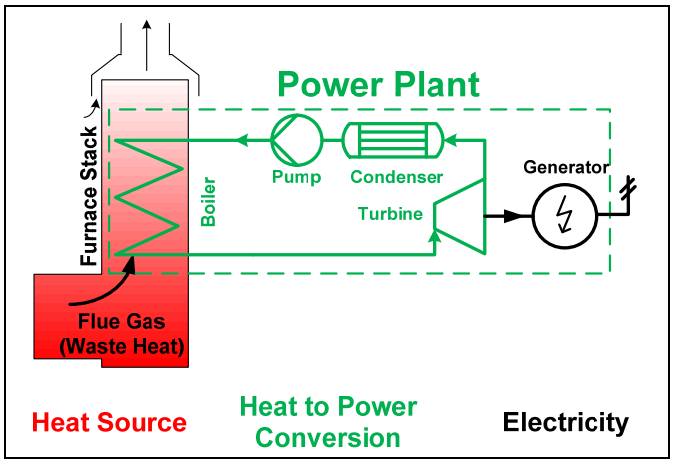

Figure 4.30: Scheme of the direct heat recovery design.

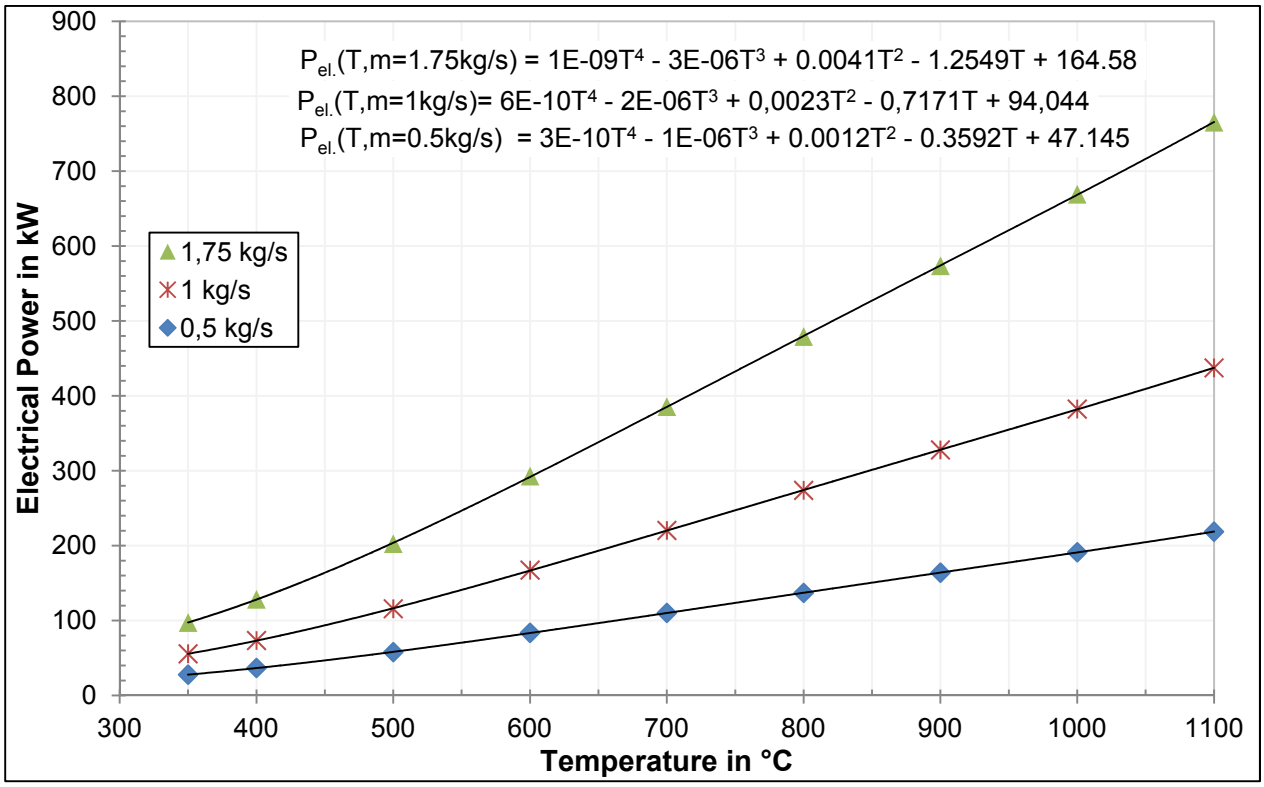

Figure 4.31: Net power output of the direct heat recovery system for various flue mass flow as a function of the exhaust temperature, within the limitations of p_{max} = 50 bar and $T_{inlet\ turbine\ max.}$ = 600°C.

The net power outputs for three typical mass flows of the flue gas are determined within a temperature range of 288 to 1100°C. Therefore the calculation starts at 350°C and considers the optimised operation pressure for a maximal power output of the steam cycle at each time step. The boiler pinch is set to 10K. The calculation results in *figure 4.31* show a linear relation between the different mass flows, which can be expressed by *numerical equation 4.27*.

$$P_{\text{el.steam}} = 6 \cdot 10^{-10} T^4 m - 2 \cdot 10^{-6} T^3 m + 0.0023 T^2 m - 0.7171 T m + 94.044 \quad (4.27)$$

This relation makes the integration of the net power output for each time step possible. Thus the total power output for the flue gas of Charge 67801 can be determined by 3,033.87 kWh/cycle and 1,107.36 MWh/a. *Figure 4.32* illustrates a calculated steam cycle at a given exhaust temperature of 800°C, the upper superheated temperature limit of 600°C and maximal pressure of 50 bar. The pinch results at 274°C and defines the endpoint of heat recovery at 55°C and 112 kJ/kg.

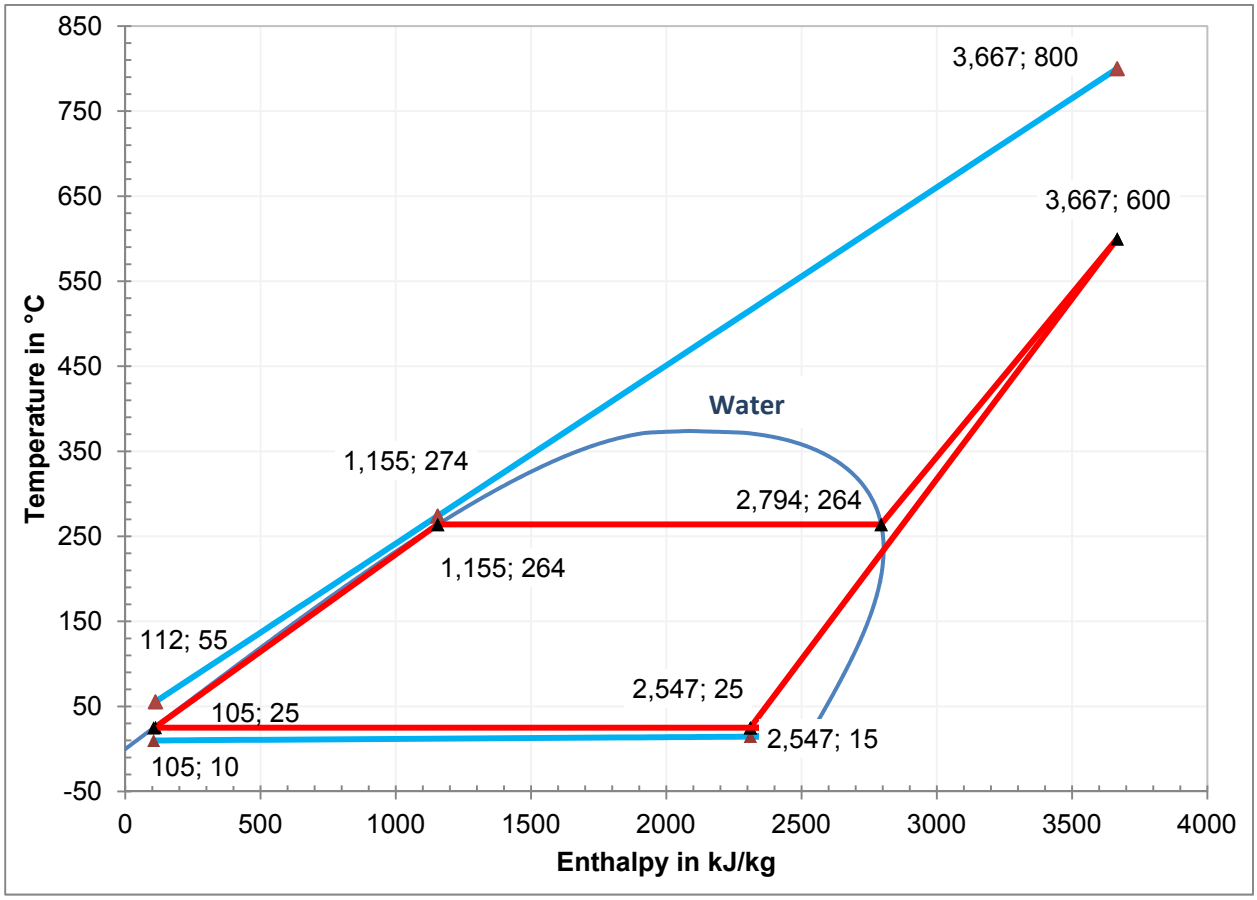

Figure 4.32: T,h-diagram of the direct heat recovery system with water as working fluid.

4.4.3. Conclusion

This subchapter processed the waste heat recovery of flue at the furnace 9 of PFA 2. The heat recovery potential is considered for an ORC and common steam power cycle. This heat source has an unsteady heat charge by varying temperatures from 288 to 1100 °C and flue mass flows from 0.01 to 1.75 kg/s, within a power range of 7 to 2,060 kW, as depicted in *figure 4.25*. The total wasted heat due to flue gas can be stated at 9,139 kWh, for Charge 67801. Accrue alternate flue heat generally challenges waste heat recovery systems. As working fluids are chosen pentane, toluene, ammonia, R245fa and water. Two design layouts are considered and calculated. The indirect heat recovery design, depicted in *figure 4.26*, describes a concept of thermal decoupling by a thermal oil loop. Here the most promising calculation has a conversion efficiency of 17.98% for the R245fa application. This means in total 1,437.76 kWh for Charge 67801, which can be recovered. *Figure 4.30* depicts the subsequent direct heat recovery design which is driven by a thermal coupled and therefore conducted thermodynamical cycle. As working fluid water is chosen due to its thermally resistance compared to commonly used organic fluids. This concept leads to improved calculation result with 3,033.87 kWh which can be recovered. *Appendix-B* (see *appendix*) marks the point of installation for the heat exchanger of each considered heat recovery solution. *Figure 4.33* shows the total energy recovery potential for each heat recovery design at furnace 9. Here the annual basis is set to one cycle per day and 365 days a year. *Appendix-2* lists an overview of the most promising heat to power solutions.

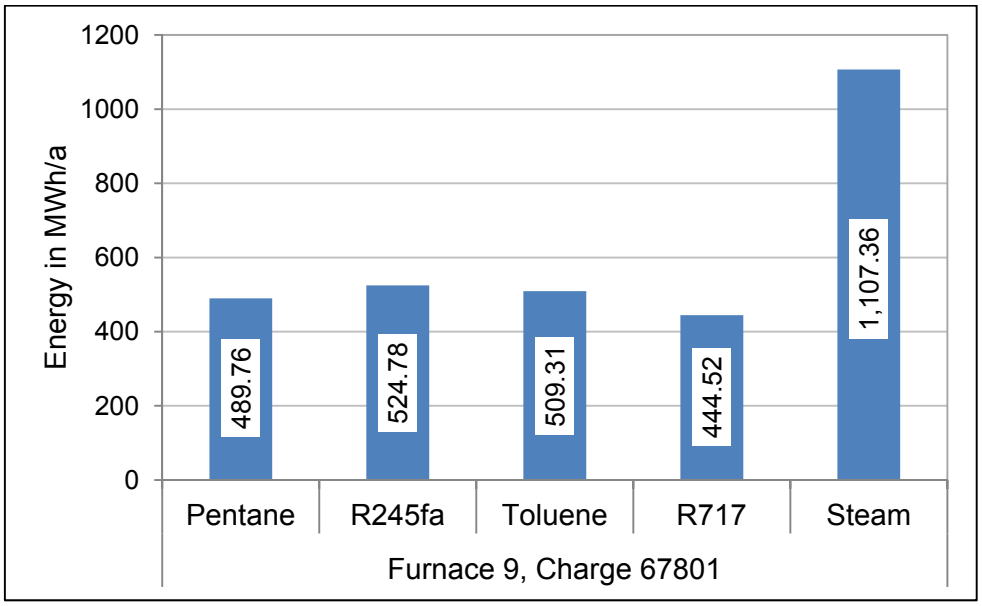

Figure 4.33: Annual energy recovery potential of the flue heat for each working fluid, at furnace 9 and Charge 67801.

5. Further Work

The energy balance development of furnace 9 reveals that the detection of wasted **flue energy** is not possible with the existing equipment. This is caused by the deviation of $T_{\text{furnace roof}}$ and $T_{\text{exhaust measured}}$ in *figure 2.4* as well as by the absence measured and logged flue volume flow rates, respectively. Due to the essential impact of the energy balance (42% of the total energy output), it should be fairly straight forward to implement online measurements. These have to measure the exhaust temperature and volume flow rate of the flue gas. This will give an exact basis for a recommended procedure of the heat recovery technology choice. A recommendation for the location of these measurements is given at *appendix-B*.

Therefore, this monitoring measurement additionally includes the determination of the **burner efficiency** by the exhaust temperature. The burner efficiency is one of the most important factors for energy consumption at PFA 2 (*equation 3.16*) and varies throughout a cycle and with the types of charged metals. Controlling the burner power with the burner efficiency throughout a cycle leads to lower energy consumption without any or only slight disadvantages regarding the process duration.

Furthermore, it has been determined that an extensive influence by false air exists. This source of waste energy can be eliminated by the implementation of a **pressure control system** in the exhaust pipe, as depicted in *figure 4.2* and described in *chapter 4.1.2*. Here should be also the correct installation location of the pressure sensor determined with respect to the pressure distribution in the furnace. The implementation is recommended as soon as possible due to the direct energy saving effect.

An improved control quality of the **melt temperature** in the furnace during the casting session, describes another point of further work in this CastAl project. The existing control quality of $T_{\text{melt}} \pm 26°C$ should be verified by the possibilities of the existing equipment. A decreased control quality to $T_{\text{melt}} \pm 10°C$ should be the target. This avoids energy consumption according to *chapter 4.1.1*.

Monitoring the **tapped molten metal** in the transport vehicle would prevent unnecessary heat charge before, during and after tapping due to the knowledge of charged heat by liquid metal. These temperatures vary within a temperature range of 800 to 860°C, stated by [Sivertsen 12].

The energy improvement through the **preheating of charge metal** should be determined. Applying preheating chambers (see *chapter 4.1.3*) will enhance the process efficiency through a decreasing need of energy preheated metal in the furnace. Here the optimal preheating temperature for both flu inlet and metal has to be determined with respect to the charging requirements of the furnaces.

The impact of improved efficiency by the **preheating of combustion gas** should be determined.

The operation of the **air ventilating system** at the casting ingot machine (above water section 1) should be considered regarding possible shut down times.

An investigation of **methods and operational sequences** could also enhance the process efficiency for the reduction of process or holding times at the furnace.

The evaluation of the measured **exhaust gas constitution** by SINTEF-Materials and Chemistry will lead to a meaningful statement for applicable heat exchanger materials and maintenance expectations for the heat to power solutions.
This disquisition gives simplified results of heat recovery technologies. Various optimisation appendages will lead to improved design layouts and should be investigated in more detail to give a **realistic potential estimation** (e.g. consideration of pressure drop, additional heat load by surrounding, adaption of pressure or temperatures).
Furthermore, it should be determined which **maximal water mass flow** is possible at the casting ingot machine to increase the power output but also confirm a safe heat discharge.
An additional improvement of OFC and ORC can be obtained by using mixtures as **working fluid**s because of their temperature glide in the condenser, which yields a better match for the cooling agent in the T,h-diagram. Therefore, further working fluids should be investigated for each design.
An application for the **heat load accumulation** of the flue gas should be determined. This decrease the operation challenges for such considered power plants and makes them more lasting.
These **operation challenges** of the **heat to power** solutions have to be proofed regarding applicability. It should be determined which alternating power and temperature ranges are manageable and applicable for such ORC, OFC and Rankine cycle and how they influence the conversion efficiency.
A heat recovery system for an aluminium plant will only be built when it is considered economically viable and with a minimum of process disturbance. The **complexity** and **cost** of the heat to power applications must be carefully investigated.
The economical attractiveness could be increased by introducing **other ways of utilising heats** besides electric power production, such as production of cold, drying and desalination. Customers for the recovered heat need to be on the spot.

REFERENCE

[Apelian 09] Apelian, D.: *Aluminum Cast Alloys: Enabling Tools for Improved Performance.* North American Die Casting Association, Wheeling, Illinois (2009), page 7
Access on July 25th, 2012:
http://www.diecasting.org/research/wwr/WWR_AluminumCastAlloys.pdf

[BCS 08] BSC Inc.: *Waste Heat Recovery – Technology and Opportunities in U.S. Industry.* Report (2008), pages 1, 3, 6, 46, 47, 53 and A19-A20

[Chen 10] Chen, H.; Goswami, Y.; Stefanakos, E.K.: *A review of thermodynamic cycles and working fluids for the conversion low-grade waste heat.* Renewable and Sustainable Energy Reviews 14 (2010), page 3062

[De Monte 03] De Monte, M.; Padoano, E.; Pozzetto, D.: *Waste heat recovery in a coffee roasting plant.* Case study, Applied Thermal Engineering 23 (2003), pages 1033-1044

[Duffy 05] Duffy, D.: *Better Cogeneration through Chemistry: the Organic Rankine Cycle*. SOWA and Distributed Energy (2005)

[ENOVA 09] ENOVA Rapport 2009-5: *Potensial for energieeffektivisering i norsk landbasert industry.* (2009), page 4
Access on July 12th, 2012:
https://docs.google.com/viewer?a=v&q=cache:nczQfV9Q7lkJ:www2.enova.no/publikasjonsoversikt/file.axd

[FactSage 12] CRCT – ThermFact Inc. & GTT-Technologies, FactSage™ 6.3 (2012)
Access on July 25th, 2012:
http://www.crct.polymtl.ca/factsage/FactSage_Applications/Workshop_Combustion.pdf

[Fischer 11] Fischer, J.: *Comparison of trilateral cycles and organic Rankine cycles.* Energy 36 (2011), page 6208-6219

[FLIR 12] FLIR Systems Inc., Wilsonville, OR 97070 (2011)
Access on July 15th, 2012:
http://www.flir.com/cs/emea/en/view/?id=41401

[Förster 06] Förster, H.; Schmidt, K.P.: *Kreisprozesse für die maximale Nutzung von Wärmeangeboten im Temperaturbereich von 80 bis 250°C in Industrie, Geothermie und Solarwirtschaft.* VDI-Berichte, Nr. 1924 (2006), page 289-303

[GE 97] GE Measurement & Control
Access on July 15th, 2012:
http://www.pge.com/includes/docs/pdfs/about/edusafety/training/pec/toolbox/tll/appnotes/panametrics_ultrasonic_flowmeter.pdf

[Heidelberg 07] Heidelberg Cement, Organic Rankine Cycle Method, Heidelberg (2007)
Access on July 17th, 2012:
http://www.heidelbergcement.com/global/en/company/products_innovations/innovations/orc.htm

[Huijuian 10] Huijuan, C.: *The Conversion of Low-Grade Heat into Power Using Supercritical Rankine Cycles*. Graduate School Theses and Dissertations, University of South Florida - Department of Chemical & Biomedical Engineering, Tampa (2010), Paper 3447, pages 96 -101
Access on July 13th, 2012:
http://scholarcommons.usf.edu/cgi/viewcontent.cgi?article=4642&context=etd

[Hydro 08.1] Hydro Aluminium Sunndal, Støperi PFA 2, LOTO (Lock out tag out), Lasepunkter Støp og Pakkeanlegg, SU009002, Rev. A

[Hydro 08.2] Hydro Aluminium Sunndal, Støperi PFA 2, LOTO (Lock out tag out), Lasepunkter for Ovner og Renner, SU009025, Rev. A

[Hydro 12.1] Hydro ASA, CastAl project description, July (2012)

[Hydro 12.2] Hydro ASA:
Access on July 13th, 2012:
http://www.hydro.com/en/Products/Casthouse-products/Foundry-alloys/#

[Kliem 05] Kliem, B.P.: *Grundlagen des Zweiphasen-Schraubenmotors.* Dissertation, University Dortmund (2005)

[Ladam 11] Ladam, Y. et al.: *Heat Recovery from Aluminium reduction Cells.* The Minerals, Metals & Materials Society, Trondheim (2011), pages 393-398

[Ladam 12] Personal communication with Yves Ladam (SINTEF), August (2012)

[Löffler 07] Löffler, M.: *Kreisprozess mit Flashverdampfung im Arbeitsraum einer Kolbenmaschine.* VGB PowerTech. Int. J for Electricity Heat Generation (2007), 7:92-7

[Maerz 06] Maerz-Gautschi Industrieofenanlagen GmbH, Documentation TD-05 62 49, Section II, SU-F2-GAU-A04-00002, page 3
Access: P:\05 62 49 Hydro Sunndal\mg Dokumentation\Mechanik\Manuals\F5\SU-F2-GAU-A04-00002_Section-II_1.doc

[Meltech 11] Meltech-CRE Ltd., Blackburn, United Kingdom (2011)
Access on July 13th, 2012:
http://meltech-cre.co.uk/repository/animation/animation_1309509831_Multiport%20aluminium%20extrusions%202.jpg

[Memo 11] Hydro ASA, Mathcad - Model energy requirement charge.pdf (2011)

[Migchielsen 05] Migchielsen, J.; De Groot, J.D.: *Potentials for increasing fuel efficiency for aluminium melting furnaces.* The Minerals, Metals & Materials Society, Annual Meetign ans Exhibiton, San Fransisco (2005), pages 893-898

[Migchielsen 06] Migchielsen, J.; De Groot, J.D.: *Design considerations for charge preheating ovens.* The Minerals, Metals & Materials Society, Annual Meetign ans Exhibiton, San Fransisco (2006), pages 737-740

[Migchielsen 09] Migchielsen, J.; Schmidt, T.: *Waste heat recovery in an aluminium cast house.* The Minerals, Metals & Materials Society, Annual Meetign ans Exhibiton, San Fransisco (2009), ISBN-13: 9780873397353, pages 717-720

[Migchielsen 10] Migchielsen, J.; Gräb, H. W.; Schmidt, T.: *Retrofitting Aluminium Melting Furnaces.* The Minerals, Metals & Materials Society, Annual Meetign ans Exhibiton, San Fransisco (2010), pages 663-668

[Nekså 09] Nekså, P.; Ladam, Y.: *Spillvarme – en kilde til kraftproduksjon, Waste Heat - a source for power production.* ENOVA Industrikonferanse, Trondheim (2009)

[Quoilin 11] Quoilin, S. et al.: *Thermo-economic optimization of waste heat recovery Organic Rankine Cycles.* Applied Thermal Engineering 31 (2011), page 2887

[Rosenkilde 10] Rosenkilde, C.: *Memo - Cast House Furnace Energy Consumption.* Hydro Aluminium, Research & technology Development (2010)
Memo energy model_CR 31.01.doc

[Sivertsen 12] Personal Communication with Jan Sivertsen, Hydro, July (2012)

[Steck 12] Steck, J.: *Leak rate calculation.* Maceas GmbH, Harkebrüge (2012)
Access on August 7th, 2012:
http://www.prosensys.com/pdfs/leak-rate_calculation.pdf

[STOWA 07] STOWA, Organic Rankine Cycle for Electricity Generation, Selected Technologies (2007)
Access on July 17th, 2012:
http://www.stowaselectedtechnologies.nl/Sheets/index.html

[Tabuk 08] Tabuk, M.B.; Børgrund, M.A.: *Energy flow analysis in an aluminium plant and survey of material balance.* Project report, NTNU-Department of Energy and Process Engineering, Trondheim (2008), page B 12-14

[Tchanche 11] Tchanche, B.F. et al.: *Low-grade heat conversion into power using organic Rankine cycles – A review of various applications*. Renewable and Sustainable Energy Reviews 15 (2011), page 3974 -3975

[Testo 11] Testo AG, Type: Testo 435.
Access on July 15th, 2012:
http://www.testo.com/online/embedded/Sites/INT/SharedDocuments/ProductBrochures/MeasurementParameters_velocity_en.pdf;jsessionid=A3AFAD2923E927CCC44F9931F8DE293A

[Vetter 11] Vetter, C.: *Parameterstudie zur Simulation von Niedertemperatur Kreisprozessen.* KIT Scientific Publishing, Karlsruhe (2011), ISBN 978-3-86644-673-1, page 9

[Wang 09] Wang, L.K. et al.: Handbook of Advanced Industrial and Hazardous Wastes Treatment. Edition 2, CRC Press, Boca Raton (2009), p. 198, ISBN 978-1-4200-7219-8

[Wiki 09] Wikipedia, August 25th 2009
Access on August 6th, 2012:
http://upload.wikimedia.org/wikipedia/commons/7/7f/Stack_damper_mechanism.svg&imgrefurl

[XTC 06] Access on July 13th, 2012:
http://www.nh-tuning.de/images/product_images/info_images/OZ/italia150_racesilver.jpg

[Zamfirescu 08] Zamfirescu, C.; Dincer, I.: *Thermodynamic analysis of a novel ammonia-water trilateral Rankine cycle.* Thermochimica Acta (2008), page 7-15

APPENDIX

Appendix-1: Listing of process specific parameters for furnace 9, Charge 67801.

Process start:	02.07.2012	6:17 PM		Process Duration:	14h 43 min		
Process end:	03.07.2012	9:00 AM		Tapping Duration:	45 min		
				Main Door Duratio	21 min		
	Gas flow in m³/h	Furnace Angle in grad	$p_{furnace}$ in Pa	$T_{flue\ gas}$	T_{melt}	$T_{furnace\ roof}$	$T_{exhaust\ measure}$
min.	0	0	-50.8	441.2	31	636.3	287.9
max.	692.5	31	23.1	588.9	756.5	957	1099.8

Appendix-2: Listing of the most promising heat to power solution results.

			Balance Model	Heat to Power			Payback per year in € (for 0.1 €/kWh)
				Heat		Power	
			MJ / kWh for Charge 67801	kWh available	MWh/a available	MWh/a recovered	
Furnace	Pentane		9,139	7,996	2,919	489.76	48,975.82
	R245fa					524.78	52,478.26
	Toluene					509.31	50,931.35
	R717					444.52	44,451.83
	Steam			9,139	3,336	1107.363	110,736.32
CIM (ideal heat recovery design)	ORC	R134a	10,230	10,230	7,468	411.28	41,128.18
		Butane				409.35	40,934.97
		Water				451.09	45,108.87
	OFC ($\eta_{expander}$=0.6)	R134a				221.45	22,145.03
		Butane				253.43	25,342.87
		Water				285.41	28,540.70
	OFC ($\eta_{expander}$=0.9)	R134a				403.73	40,372.70
		Butane				416.52	41,651.84
		Water				429.31	42,930.98

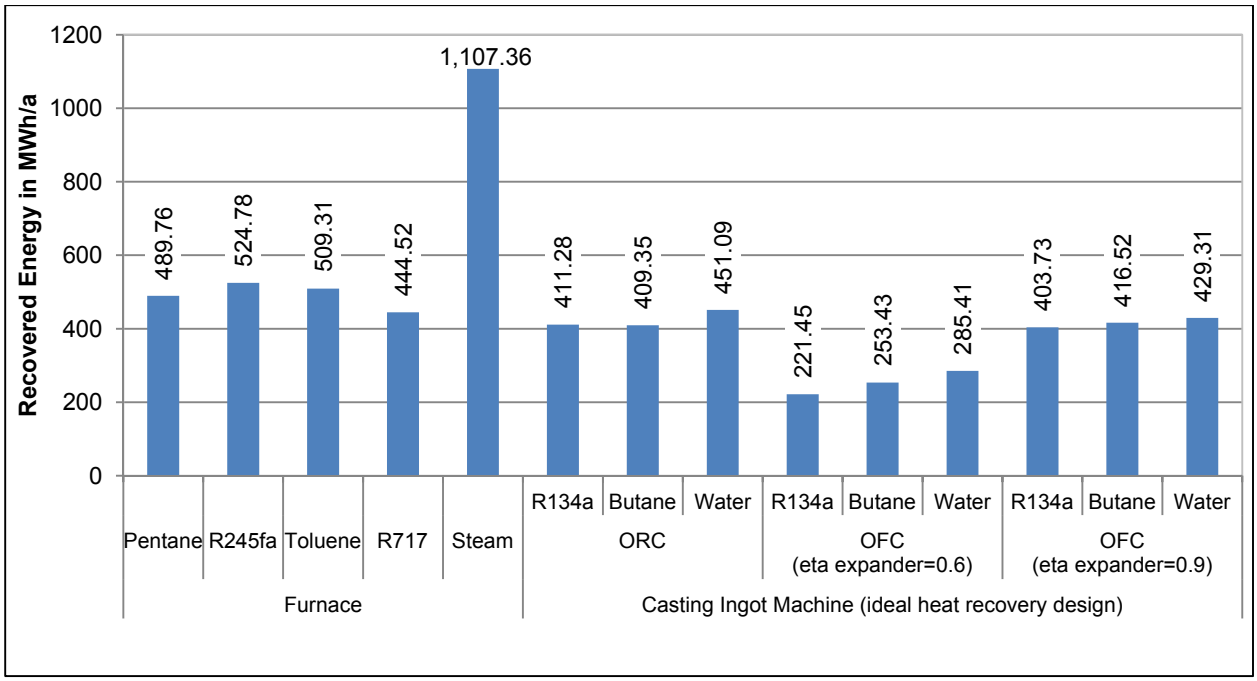

Appendix-A: Illustration of the net power output per year of various heat to power solutions.

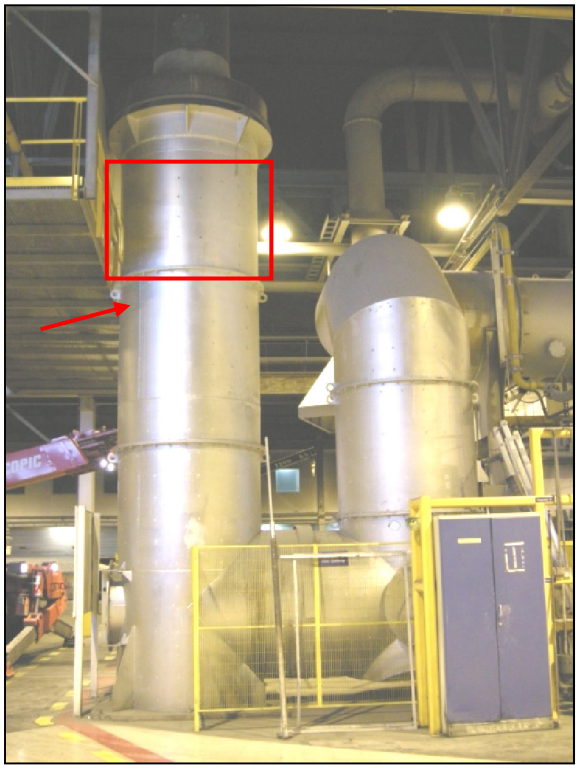

Appendix-B: Illustration of the exhaust pipe at furnace 9. The red rectangle marks the point of installation for a heat exchanger of the considered heat recovery designs at the furnace. The red arrow indicates the recommended measure location of the flue volume flow rate.

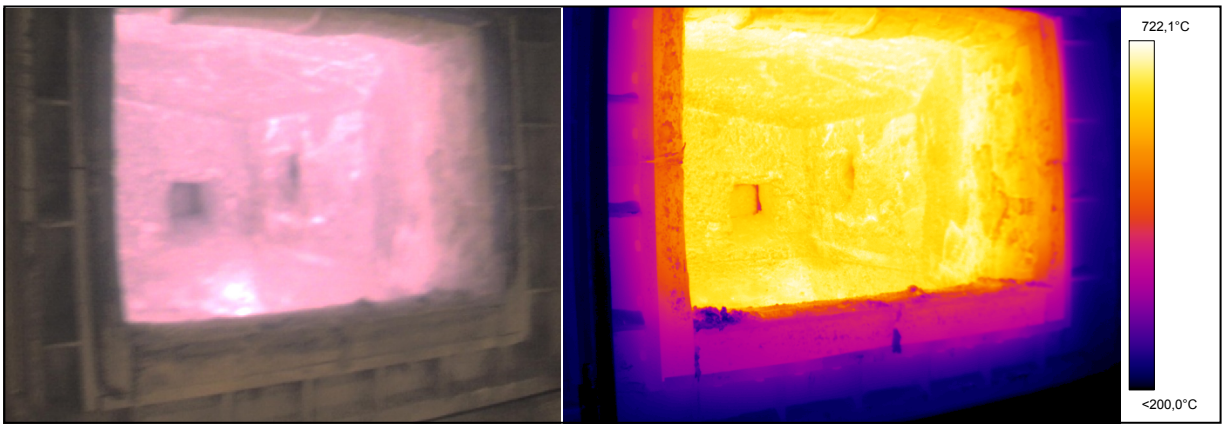

Appendix-C: Heat image of the furnace interior while charging.

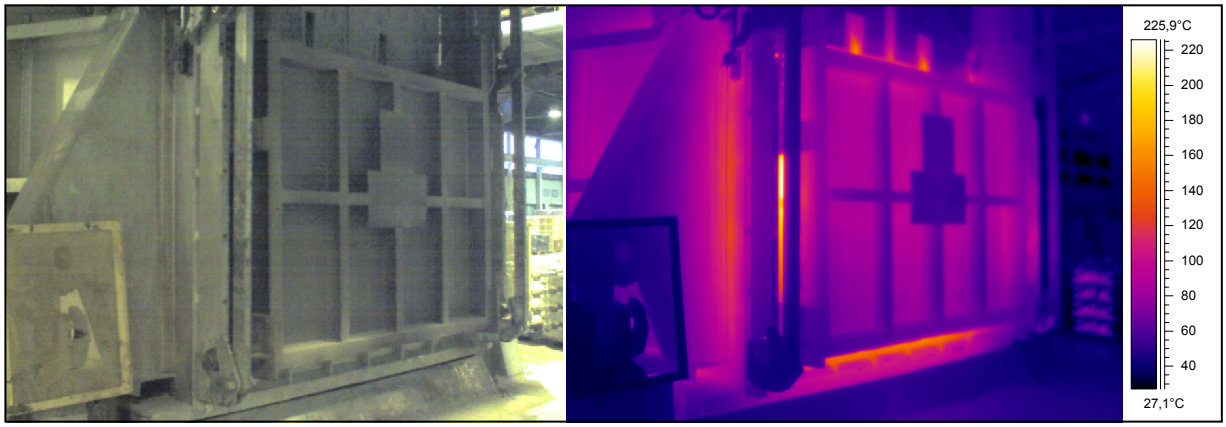

Appendix-D: Heat image of the furnace surface and main door while holding.

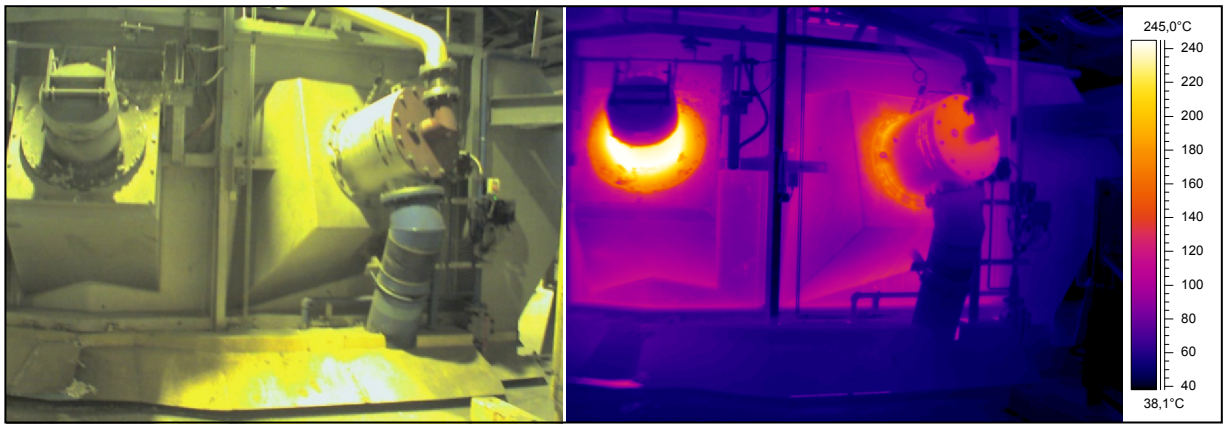

Appendix-E: Heat image of the burner and tapping port at the furnace 9 while preheating.

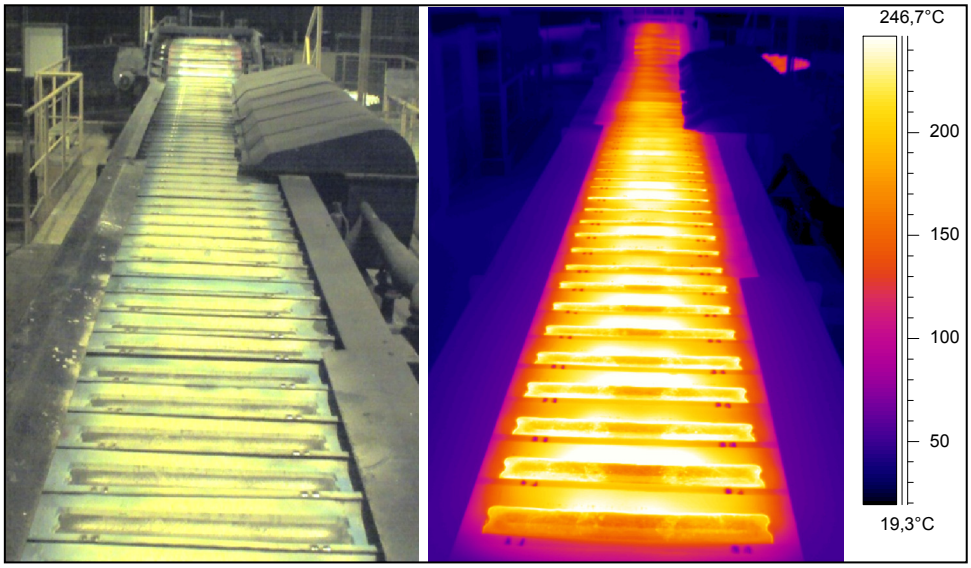

Appendix-F: Heat image of the casting ingot machine while casting.

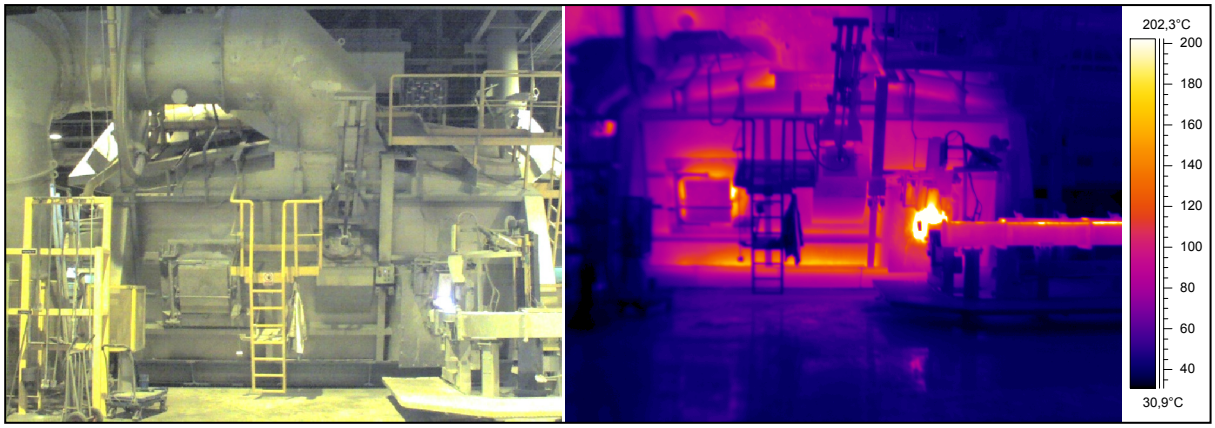

Appendix-G: Back view of the furnace 9 while casting.

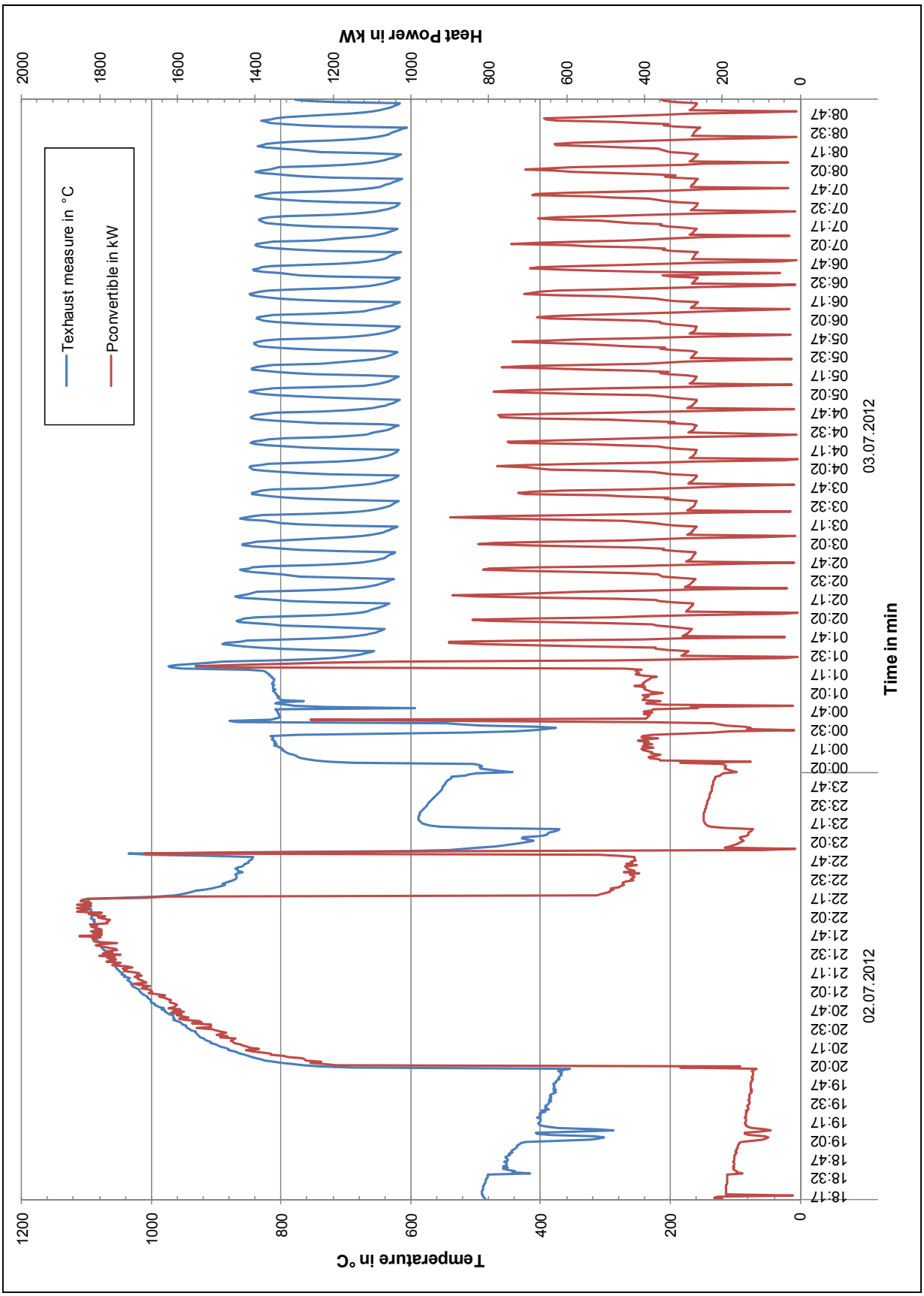

Appendix-H: Integration of convertible flue heat power as a function of process time at furnace 9,Charge 67801. Expressed by *equation 4.26.*

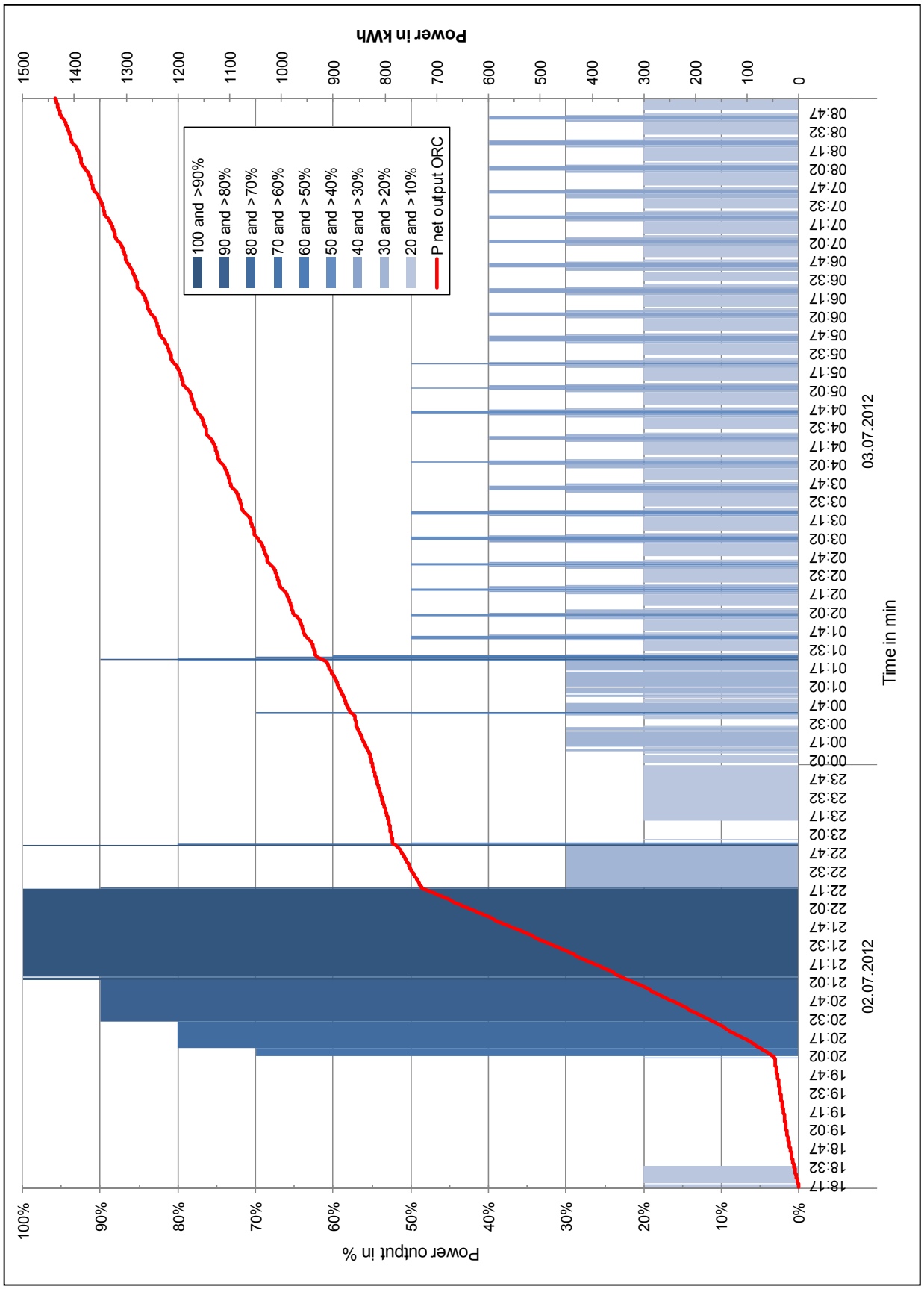

Appendix-I: Operation behaviour of the pentane ORC charged by flue heat as a function of process time at furnace 9, Charge 67801.

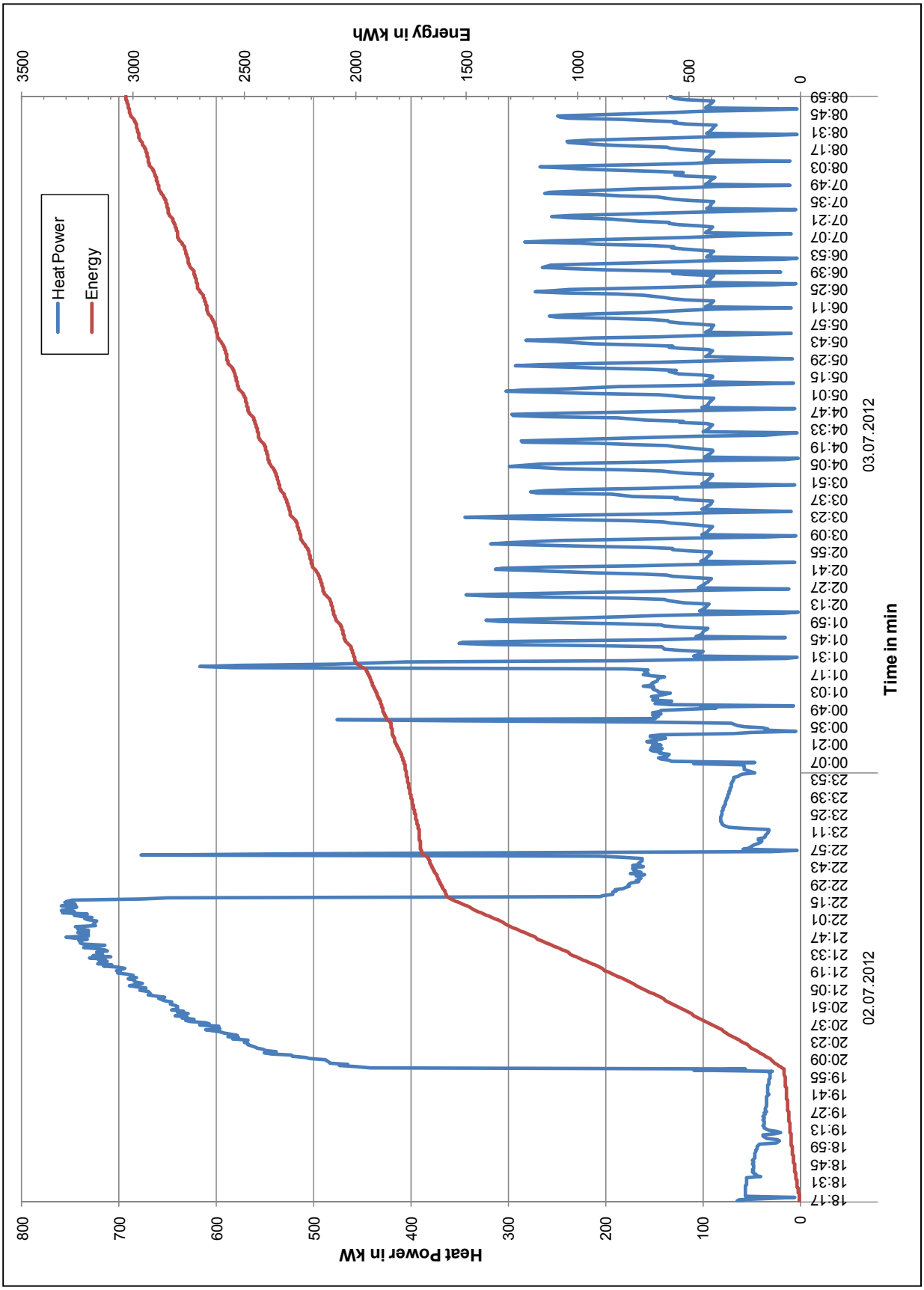

Appendix-J: Heat power and net power output of the direct coupled steam power cycle as a function of process time at furnace 9,Charge 67801.

Furnace			
Timeline	$t_{Main\ Door}$:	2,700	in sec.
	t_{Port}:	1,260	in sec.
	t_{total}:	52,980	in sec.
Calculation Parameter	Natural Gas Factor:	0.97	
	Air Excess:	0.03	
	$T_{Exhaust\ gas}$:	570.21	in °C (average)
	$T_{Casting}$:	730	in °C
	$T_{Ambient}$:	20	in °C
	$T_{Cast\ House}$:	28	in °C
	$c_{p,Al,solid}$:	1.05	in kJ/(kgK)
	$c_{p,Al,liquid}$:	1.18	in kJ/(kgK)
	$\Delta h_{fusion,\ Al}$:	397.08	in kJ/kg
	$T_{fusion,\ Al}$:	660	in °C
	$c_{p,Si,liquid}$:	0.94	in kJ/(kgK)
	$\Delta h_{fusion,\ Si}$:	1,800	in kJ/kg
			in kJ/kg
	$\Delta h_{Si,\ add.}$:	2,088	(add $Si_{20°C}$ to $Al_{(750°C)}$)
	$\Delta h_{Natural\ Gas}$:	-37,101.52	in kJ/kg (varies by $T_{exhaust}$)
	ε:	0.95	
	σ:	5.67E-08	in W/(m²K)
	$A_{main\ door}$:	3.50	in m²
	A_{ports}:	0.70	in m²
	$A_{furnace}$:	1,500	in m²
	$\alpha_{Furnace}$:	5	in W/(m²K)
	f_{Dross}:	0.01	
	f_{Oxide}:	0.30	
	Δh_{Dross}:	-16,596	in kJ/kg

Casting Ingot Machine			
Timeline	$t_{Street\ 1,\ water}$:	80	in sec.
	$t_{Street\ 1,\ air}$:	25	in sec.
	$t_{Way\ to\ street\ 2}$:	30	in sec.
	$t_{Street\ 2}$:	80	in sec.
	$t_{Section}$:	190	in sec.
	t_{total}:	27,900	in sec.
Calculation Parameter	$T_{Cast\ House}$:	25	in °C
	$T_{Casting}$:	750	in °C
	$c_{p,Al,solid}$:	1.05	in kJ/(kgK)
	$c_{p,Al,liquid}$:	1.18	in kJ/(kgK)
	$\Delta h_{fusion,\ Al}$:	397.08	in kJ/kg
	$T_{fusion,\ Al}$:	660	in °C
	ε:	0.80	
	σ:	5.1E-08	in W/(m²K)
	$A_{parts,\ in\ mould}$:	0.20	in m²
	$A_{parts,\ out\ of\ mould}$:	0.50	in m²
	$\alpha_{Furnace}$:	40	in W/(m²K)
	T_{w2}:	30	in °C

Appendix-K: Listing of the energy balance input parameters for furnace 9 and CIM.